MACHINE PERCEPTION
OF
PARTIALLY SPECIFIED PLANAR SHAPES

by

Paul Frank Singer

A Dissertation Presented to the
FACULTY OF THE GRADUATE SCHOOL
UNIVERSITY OF SOUTHERN CALIFORNIA
In Partial Fulfillment of the
Requirements for the Degree
DOCTOR OF PHILOSOPHY
(Electrical Engineering)

May 1985

ACKNOWLEDGMENTS

I wish to gratefully acknowledge the constant support and encouragement given to me by all of my family, especially my wife Maria, my daughter Megan, and both of my parents.

I have been very fortunate to have Dr. Rama Chellappa as the chairman of my dissertation committee. His advice and guidance have been invaluable and he has provided a high standard of excellence. I have thoroughly enjoyed our many conversations and I look forward to a lasting friendship. I am also appreciative of the other members of my committee, Dr. A.A. Sawchuk, Dr. D.R. Estes and Dr. K.S. McCurley who have also contributed to my academic success. I have enjoyed the friendship of the faculty, staff, and students at U.S.C. and I wish them all well.

A special note of gratitude goes to the Hughes Aircraft Co. doctoral fellowship program which has supported all of my graduate studies, thank you.

TABLE OF CONTENTS

TABLE OF CONTENTS (Continued)

LIST OF ILLUSTRATIONS

LIST OF TABLES

ABSTRACT

A new set of global shape descriptors is defined which is useful in the machine perception of planar shapes from their partially specified boundaries. These shape descriptors are estimated from the observed portions of the boundary, thus obviating the need for boundary reconstruction. The boundary is modeled as a circular autoregressive (CAR) process. The CAR descriptors are defined from the coefficients of this model. The CAR descriptors preserve class shape information and are shown to be insensitive to within class variations. The maximum likelihood (ML) estimator of the CAR descriptors is derived from the CAR model. Obscured boundaries are modeled as the product of the complete boundary and a binary valued obscuring process. This model of obscuration is general enough to include both occlusion and segmentation errors. The ML estimator is extended to include obscured boundaries by retaining the form of the original ML estimator and rederiving its component parts. This derivation is dependent upon the asymptotic stationarity of the obscured boundary process. The asymptotic properties of the extended ML estimator and its estimates are established. These properties are used to derive a tight *analytic* upper bound on classification performance. A classifier is designed from the asymptotic distribution of the estimates and two classification experiments are performed using partially obscured boundaries. The first experiment uses four synthetic shape classes and establishes the dependence of classification accuracy upon the stationarity of the boundary process. The extended ML estimates are shown to perform better than the least squares (LS) estimates computed from the reconstructed boundary. The second experiment uses real aircraft boundaries and *all* model parameters are estimated from the observed boundary. An experimental classification accuracy of 91% is achieved using the extended ML estimator on boundaries which are 30% obscured.

1.0 INTRODUCTION

The basic tenets which justify the use of shape in the perception of an object by a machine are the importance of shape to the human visual system and the invariance of shape with respect to environmental conditions. Zusne [1] pointed out the dependence of the human visual system upon shape for the perception of objects. The fact that an object's shape is independent of its environment (e.g., lighting conditions such as sun angle) is important in limiting the number of parameters involved in the process of recognition. The shape of an object is also invariant to changes in sensor characteristics such as resolution, sensitivity, signal-to-noise ratio (SNR) or dynamic range. Because of these invariant properties, shape classification has been applied in the fields of genetics [2], radiology [3], scene analysis [4], robotics [5], and target recognition [6].

The shape of an object manifests itself in the boundary of an object's image. Even though shape is insensitive to changes in the environment or sensor characteristics, the boundary is not. The process of extracting the boundary from the image of an object is called segmentation. The desire to extract boundaries which retain the invariant properties of shape has made segmentation one of the most difficult tasks in machine perception. Consequently, almost all developments of shape descriptors (see Chapter 2) explicitly assume that the complete boundary has been segmented. This is an unrealistic assumption if the object is in an uncontrolled environment. The result of this assumption is that a disproportionate share of the burden is placed upon the segmentor. Even if the segmentor is able to perfectly extract complete boundaries, there is still the implicit assumption that no occlusion exists between the sensor and the object. Therefore, it is very likely that the segmentor will, for one reason or another, extract a boundary which is only partially specified.

The philosophy adopted in this dissertation on shape descriptors is one of a more equitable distribution of the burden associated with the fidelity of the boundary. The shape descriptors are defined from a boundary model which explicitly accommodates imperfect boundary segmentation. The problem of partially specified boundaries is addressed by deriving an estimator of the shape descriptors which includes a model

of the obscuring process. The model of the obscuring process embodies many of the phenomena which result in missing boundary points. These phenomena include segmentation errors as well as occlusion.

1.1 OVERVIEW

Chapter 2 reviews the definitions of other shape descriptors which have appeared in the literature. Special attention is paid to the boundary representation schemes which have been used. The way in which invariance to rotation, translation, and scaling is achieved is also examined. When available, experimental results are discussed. Several approaches which have been applied to partially occluded shapes are also examined.

Chapter 3 begins by defining the mathematical representation which is used to represent the boundary process. The boundary process is then modeled as a CAR process. The CAR descriptors are defined as a set of shape descriptors from this model and their attributes are discussed. A technique for generating closed boundary sequences from a CAR model is presented. In deriving this technique for generating boundary sequences, insights are gained which lead to the development of CAR diagrams. CAR diagrams provide a two dimensional graphic representation of the m dimensional feature space of the CAR descriptors. The statistics of the CAR boundary processes which are needed in later chapters are derived in the final section of this chapter.

The ML estimator of the CAR descriptors is derived in Chapter 4. Since the analytic minimization of the negative log-likelihood function is intractable, several numerical algorithms for function minimization are discussed. All of these algorithms iterate on the solution and require a set of initial values to begin. The LS estimator is derived to provide the initial estimates of the CAR descriptors. Estimators are also derived for the other model parameters which appear in the negative log-likelihood function.

A model of the observed (possibly obscured) boundary process is established in Chapter 5. Inherent in this model is the definition of the obscuring process. A statistical model of the obscuring process is specified which is representative of obscuration due to segmentation error. The mean, autocorrelation, and power spectral density of the obscuring process are derived from its probability density function. The

ML estimator of the CAR descriptors is then extended to include the case of partially specified boundaries. The form of the negative log-likelihood function is retained, but the eigenvalues which totally comprise this function, except for the periodogram of the observed boundary sequence, are rederived. This derivation is based upon the asymptotic stationarity of the observed boundary process. The LS estimates computed from the linearly interpolated observed boundary sequence are used as initial values for the numerical minimization algorithms. Estimators are also derived for the parameters of the CAR model and the model of the obscuring process since they appear in the extended negative log-likelihood function. The asymptotic properties of the extended ML estimator and its estimates are established and the Cramer-Rao lower bound is derived. An approximation to the extended negative log-likelihood function is derived which can be used when the statistical model of the obscuring process is unknown.

In Chapter 6 the extended ML estimator is tested on both real and synthetic boundary data with varying amounts of obscuration. The experiment using synthetic boundary data tested the estimator under favorable conditions. The experiment which used real boundary data was performed under very realistic conditions. *All* parameters which characterize the CAR process or the obscuring process were estimated from the observed boundary data. The real data experiment was structured to demonstrate the insensitivity of the CAR descriptors to within class variations. These results are analyzed using CAR diagrams. CAR diagrams are constructed for each shape class in both experiments.

A discriminant function classifier is derived in Chapter 7 using Bayes decision theory and the asymptotic properties of the extended ML estimator and its estimates. This classifier is used to classify the four synthetic shape classes defined in Chapter 6. The LS estimates are also tested in this experiment. The results are analyzed using CAR diagrams and a link is established between classification accuracy and the stationarity of the CAR model. A classification experiment is then performed using real aircraft shapes. These results are combined with those of Chapter 6 and some general conclusions are drawn. The asymptotic properties of the extended ML estimator are then used to derive a tight analytic upper bound on classification performance.

The conclusions of the research results presented in this dissertation are summarized in Chapter 8. Future research topics which will extend these results are suggested.

1.2 TECHNICAL CONTRIBUTIONS

This dissertation presents three significant contributions to the body of engineering knowledge on machine perception. These contributions are developed from the CAR model of the boundary and the CAR descriptors which represent the shape of the boundary. The initial contribution is the extension of the ML estimator of the CAR discriptors to include the case of partially occluded boundaries. This extension of the ML estimator is accomplished by introducing a statistical model of the obscuring process into the derivation of the ML estimator. This approach requires no reconstruction of the obscured portions of the boundary. The use of LS estimates computed from linearly interpolated boundaries is shown to produce less favorable classification results. The classification accuracy of the extended ML estimates is experimentally demonstrated in two experiments using real and synthetic shape classes respectively. General conclusions regarding the classification accuracy of real shapes are deduced from these results.

The second contribution provides, for the first time, an analytic means of tightly bounding the classification performance of the classic pattern recognition paradigm shown in Figure 1.2-1.

Figure 1.2–1. Classic Pattern Recognition System

The asymptotic properties of the extended ML estimator and its estimates are combined with the theory of Bayesian classifiers to derive this performance bound. This bound on classification performance is computed from parameters which can be related to the performance of the segmentor and the CAR descriptors of the shape

classes. The ability to analytically compute this bound obviates the need to repeatedly perform classification experiments to determine the effects that segmentation errors have on classification performance. This allows system engineering trade-off studies to be done more conveniently during the design phase of a machine perception system.

The third contribution is an engineering tool which aids in the design and analysis of the class feature sets and the classifier. This tool provides a means of viewing the m dimensional feature space defined by the CAR descriptors in two dimensions. This technique is not based upon projections or approximations; rather a one-to-one onto mapping is established between the points in the m dimensional feature space and sets of points in the complex plane. This graphic representation of the feature space is called a CAR diagram. It can be used to display the relative locations of the shape classes, the dispersion of the class estimates, and the decision boundaries of the classifier. For example, a CAR diagram may be used as a guide in selecting the order of the CAR model. The model order only needs to be large enough to provide adequate separation of the shape classes. This separation can be inferred from the CAR diagram. The results of the classification experiments are qualitatively discussed using a CAR diagram. It is shown how shapes may be characterized by their locations in these diagrams.

These three contributions provide the complete theory and methodology necessary to design and evaluate a machine perception system capable of recognizing partially specified planar projections of object shapes.

2.0 AN OVERVIEW OF THE SHAPE DESCRIPTORS USED FOR MACHINE PERCEPTION

The perception of an object from its shape has been the subject of many shape analysis studies during the past several decades. A thorough review of this literature has been published by Pavlidis [7] which examines many of the techniques that have been developed. The shape descriptors defined by these techniques are considered to be either global or local depending upon the way in which the boundary is characterized. The global shape descriptors are computed from all the points along the boundary. The two most popular sets of global shape descriptors, the method of moments and Fourier descriptors, are reviewed in Section 2.1. The definitions of global shape descriptors usually require that complete boundary information be available. A global technique which computes the shape descriptors from a reconstructed boundary is also reviewed.

Local shape descriptors, as their name implies, represent the local characteristics of the boundary. The syntactic relationships among these local features are used to identify the shape. The process of identifying these relationships requires grammars which contain a large amount of knowledge about the shape classes. Attributed grammars are used when attributes of a shape are associated with the local shape descriptors. Several papers on the syntactic approach to shape recognition are reviewed in Section 2.2. Two approaches are also reviewed on the use of local features to recognize boundaries which are only partially specified.

2.1 GLOBAL SHAPE DESCRIPTORS

The definitions of the method of moments and the Fourier descriptors are reviewed in this section. The salient characteristic of these global shape descriptors is their invariance to translation, rotation, and scaling of the boundary within the image plane. There is only one definition of the method of moments and it may be implemented on either the boundary or silhouette of a planar shape. Several sets of Fourier descriptors have been defined for various boundary representations. Different means of obtaining invariance to translation, rotation, and scaling are reviewed. One implementation obtains target orientation by retaining the variation of the descriptors to rotation.

The Method of Moments

The method of moments defines a set of shape features which are nonlinear functions of the geometric central moments of an object's boundary or silhouette. These features were derived by Hu [8] to be invariant to translation, rotation, scaling, and reflection of the boundary or silhouette in the image plane. They are frequently referred to as the moment invariants. The property of translation invariance is derived from the use of central moments which are computed relative to the centroid of the boundary $(\tilde{x}_0, \tilde{y}_0)$ or silhouette (x_0, y_0). The pq-th central moment of the boundary $\tilde{\mu}_{pq}$ and silhouette μ_{pq} are defined below.

$$\tilde{\mu}_{pq} = \oint_c (x - \tilde{x}_0)^p (y - \tilde{y}_0)^q \, dl \tag{2.1-1}$$

$$\mu_{pq} = \int\int_{-\infty}^{\infty} (x - x_0)^p (y - y_0)^q f(x,y) \, dx \, dy \tag{2.1-2}$$

C is the closed boundary curve of the object and the silhouette function f(x,y) takes on the value one for all points (x,y) on or within the boundary curve C. The integral in (2.1-1) is a line integral along the boundary curve C and the differential dl is equal to the magnitude of the differential vector (dx, dy) along the boundary curve.

$$dl = \sqrt{(dx)^2 + (dy)^2} \tag{2.1-3}$$

Since the differential dl retains only the magnitude of the differential vector, all directional information about the boundary curve is lost. Consequently, the boundary curve C cannot be reconstructed from the complete set of boundary moments. The silhouette moments do preserve all of the information in the silhouette. The boundary moments are sensitive to minor variations in the boundary which may be due to segmentation error. The contrary is true for the silhouette moments. They are very insenstive to the finer details of the shape. This is because the interior of the silhouette dominates the value of the double integral in (2.1-2). Consequently, very high order silhouette moments must be used to achieve any fidelity in reconstruction.

The digital computation of the higher order silhouette moments requires a large dynamic range (word size) because the distance from the centroid to the more remote pixels on the silhouette must be raised to a high exponential power (see equation 2.1-2). The silhouette moments may be generalized by allowing the silhouette function f(x,y) to take on the intensity value of the image at the point (x,y). This generalization is only useful if the intensity profile of the object does not vary with time. This condition may be satisfied in a manufacturing environment where lighting may be accurately controlled. The moment invariants have been successfully used by Dudani [6] in the experimental recognition of six aircraft silhouettes.

Fourier Descriptors

Since an object's boundary is closed, it may be repeatedly traced to produce a periodic boundary sequence. The Fourier descriptors are derived from the coefficients of the Fourier series expansion of this periodic boundary sequence. The Fourier descriptors are defined so that they are invariant to translation, rotation, and scaling. Several sets of Fourier descriptors have been defined. The primary differences among these definitions are due to the use of different boundary representations. Other differences are due to the way in which their invariant properties are derived.

Granlund [9] represents the boundary as a closed contour in the complex plane. A complex function u(t) is defined to represent this contour where the parameter t is proportional to the length along the contour. This complex boundary function is expanded as a Fourier series. A set of Fourier descriptors are then defined from the Fourier series coefficients which are invariant to rotation (starting point on the contour), scaling, and translation of the contour in the complex plane. Translation invariance is achieved by not using the DC term of the Fourier series expansion. This term is equivalent to the centroid of the boundary defined in the method of moments. A character recognition experiment was performed using seven of the defined Fourier descriptors. A total of 175 handwritten characters from a 25 character alphabet were classified. A 2% error rate was achieved, but the results are optimistic because the training set was used as the test set.

Zahn and Roskies [10] used the cumulative change in angular direction of the boundary curve in the x,y plane to represent the boundary. This function is parameterized by the distance along the boundary curve. The Fourier series coefficients of this function are used to define a set of Fourier descriptors which are invariant to translation, scaling, and rotation of the boundary curve. The rotation invariance was attained by using the magnitudes of the Fourier series coefficients. Additional descriptors were defined from the phase angles of these coefficients. The cumulative change in angular direction was used instead of the curvature function of the boundary curve so that polygonal boundaries could be represented. The reconstruction of the boundaries was also considered and this set of Fourier descriptors was shown to be information preserving.

Persoon and Fu [11] used a variation of the boundary representation scheme developed by Zahn and Roskies, but the Fourier series coefficients were not combined to achieve the invariant properties. Instead, the optimal rotation, translation, and scaling of each member of the training set is determined which best matches it to the boundary to be classified. The Euclidian distance is used as the metric to establish the best match. Since the process of determining the optimal rotation, translation, and scaling of each member of the training is very time consuming, a suboptimal search was also developed. The classification of the numerals in the Munson data set of characters [12] resulted in an error rate of 10.6% for the optimal method and 15.4% for the suboptimal method. Unlike Granlund, separate training and test sets were used.

Richard and Hemami [13] used four classes of three-dimensional aircraft shapes to test the Fourier descriptors. The complex boundary representation developed by Granlund was used. Since the aircraft's type, position, and orientation were to be determined by the classifier, the Fourier series coefficients were not made into invariant descriptors. The training set database was computed from 2664 projections of the four aircraft classes taken at 5° intervals. The test set was derived from the training set by the addition of Gaussian white noise to the boundaries. The classification experiment was repeated for different amounts of noise. A set of leave-one-out or jackknife experiments was also performed. The experimental results are good or bad depending upon the desired accuracy with which the orientation of the aircraft is to be tracked.

Wallace and Mitchell [14] computed the Fourier series coefficients from the chain code of the boundary curve. The Fourier descriptors were used to identify and track the orientation of aircraft in three dimensions. Unlike Richard and Hemami, the orientations were interpolated in the feature space to either reduce the number of projections in the training set or to increase the accuracy of the orientation measurement. Good identification results were obtained on the higher resolution images, but the tracking accuracy was considered good by the authors if it was within plus or minus half a radian, which is a considerable amount of error.

Grogan [15] attempted to reconstruct the occluded portions of the boundary by fitting a right angle between the endpoints of the missing segment. Shape descriptors were then computed from this reconstructed boundary using the Fourier Mellin transform. A classification experiment was performed using this technique on aircraft shapes. The classification results are inconclusive because a very small test set was used. This type of reconstruction is not expected to perform well because the shape descriptors extracted from the reconstructed boundary will in general not be consistent with those which represent the shape class.

2.2 LOCAL SHAPE DESCRIPTORS

Local shape descriptors, frequently referred to as primitives, are extracted from portions of the boundary. This is in contrast to the definitions of the global shape descriptors such as moment invariants or Fourier descriptors which are computed from the entire boundary. The primitives are processed by a syntax analyzer which has a knowledge of the shape grammars. Fu [16] has obtained promising results with this approach, but the grammar of each shape class has to be defined manually. The defining of the grammars for each shape class is a difficult job, particularly when a large number of shape classes are involved. This aspect of the syntactic approach to shape recognition is expected to limit its general use until the grammar can be inferred automatically from a set of training shapes. Pavlidis and Ali [17] developed a hierarchical approach to the syntactic analysis of shape. This resulted in the use of local grammars which are easier to define.

Attributed grammars were used by You and Fu [18] to combine both semantic and syntactic information about the shape. These grammars associate an attribute with the primitives and production rules are defined to process these attributes. Tsai and Fu [19] combined the attributed grammars used in the syntactic approach to shape recognition with the statistical decision theory of mathematical pattern recognition. This hybrid approach attempts to achieve a synergistic combination of these two predominant approaches to shape recognition.

Segment matching may be used to classify shapes whose boundaries are only partially specified. Davis [20] used a relaxation labeling algorithm to combine the matches of the observed boundary segments to polygonal approximations of the shapes. This algorithm was demonstrated on digitized island coastlines. Bhanu and Faugeras [21] have extended this technique by using a stochastic relaxation algorithm which seeks to minimize a penalty function as the matches are assigned.

3.0 THE CAR DESCRIPTORS

The CAR descriptors are a vector of parameters which specify the CAR model of a boundary process. They are used in Chapter 7 as a feature vector to classify the shape represented by the boundary. The definition of the CAR descriptors begins by representing the boundary as a sample sequence of an underlying boundary process. The boundary process is modeled as a CAR process which is completely specified by the CAR descriptors. The information preserving properties of the CAR descriptors are then examined and a technique is presented which generates additional boundary sequences belonging to the same shape class. A two-dimensional graphical representation of the m dimensional feature space of the CAR descriptors is presented. This representation provides insights into the characteristics of the shape classes based upon their graphical location. The statistical properties of the boundary process, including its probability density function, are then derived from its CAR model.

3.1 BOUNDARY REPRESENTATION

The boundary representation scheme described below was chosen because any arbitrary planar boundary can be easily represented as a one-dimensional boundary sequence which is translation invariant. It is assumed that the boundary is a closed four connected curve specified by the set of N ordered pairs (x(n), y(n)). The centroid of the boundary is located at the point (x_0, y_0) defined below.

$$x_0 = \frac{1}{N} \sum_{n=0}^{N-1} x(n) \tag{3.1-1}$$

$$y_0 = \frac{1}{N} \sum_{n=0}^{N-1} y(n) \tag{3.1-2}$$

The sequence of N radial distances r(n) measured from the boundary centroid to the points on the boundary, defined as

$$r(n) = [(x(n) - x_0)^2 + (y(n) - y_0)^2]^{1/2} \tag{3.1-3}$$

will be used to represent the boundary. Since the boundary is closed, the sequence r(n) is circular and satisfies the following equality.

$$r(n + kN) = r(n) \quad \forall \; k \in \{\text{integers}\} \tag{3.1-4}$$

This is equivalent to the boundary sequence being periodic with period N. This periodicity of the boundary sequence provides partial motivation for the development of circular AR boundary models which are the topic of the next section.

Each increment of the index n represents a step along the boundary. Since the boundary sequence r(n) was derived from a set of four connected boundary coordinates, all steps along the boundary are equal in length. Because the boundary is parameterized along its length, this boundary representation scheme can be used to represent any arbitrarily complex planar boundary which can be traced in an unambiguous manner. No exceptions or special rules are required to handle concavities or straight radial segments. This form of boundary representation is easily extracted from the original set of boundary coordinates. It does not require the evaluation of any trigonometric functions and it is not dependent upon the disposition of neighboring boundary points.

The boundary sequence r(n) is invariant to translations of the boundary within the image plane. This is because the radial distances which represent the boundary are measured from the centroid of the boundary. A consequence of the boundary sequence being translation invariant is that any quantity derived from this boundary sequence (eg., the CAR descriptors) and not dependent upon the boundary centroid will also be invariant to translations of the boundary within the image plane. This is identically equivalent to defining the moment invariants [8] in terms of the central moments of an object to obtain invariance to translation. It is also equivalent to removing the DC term from the set of Fourier coefficients before defining the Fourier descriptors [9], so even though the CAR descriptors presented in the next section are not implicitly translation invariant, they can be made explicitly so by representing the boundary relative to its centroid. This is no less general than, and requires no more information than those techniques by which Fourier descriptors and moment invariants are made invariant to translation. An example of an implicitly translation invariant boundary representation is a chain code [22].

3.2 THE CAR MODEL

The periodic boundary process r(n) developed in the previous section will be modeled as an m-th order CAR process. The CAR model of the boundary process r(n) is defined below.

$$r(n) = \sum_{k=1}^{m} a_k \, r(n-k) + \epsilon(n) \tag{3.2-1}$$

The a_i's are the m CAR coefficients which form the m-vector $\vec{a}$ that denotes the CAR descriptors. The error process $\epsilon(n)$ is a stationary Gaussian distributed white noise process with the following statistics.

$$\mu_\epsilon = E\{\epsilon(n)\} = \alpha \tag{3.2-2}$$

$$R_\epsilon(k) = E\{\epsilon(n)\,\epsilon(n+k)\} \tag{3.2-3}$$

$$= \alpha^2 + \beta\,\delta(k) \quad , \quad 0 \leq k \leq N-1 \tag{3.2-4}$$

The circularity of the boundary process r(n) can be shown to impose a similar condition upon the error process $\epsilon(n)$. The following expression for the error process is obtained from (3.2-1).

$$\epsilon(n) = r(n) - \sum_{k=1}^{m} a_k \, r(n-k) \tag{3.2-5}$$

The (n+N) th value of the error process is then equal to

$$\epsilon(n+N) = r(n+N) - \sum_{k=1}^{m} a_k \, r(n+N-k) \tag{3.2-6}$$

which can be simplified using the circularity condition on r(n) given by (3.1-4).

$$\epsilon(n+N) = r(n) - \sum_{k=1}^{m} a_k \, r(n-k) \tag{3.2-7}$$

$$= \epsilon(n) \tag{3.2-8}$$

The last equality follows from (3.2–5). The above derivation could be repeated for any integer multiple of N. This leads to the following conclusion.

$$\epsilon(n + kN) = \epsilon(n) \quad \forall \; k \; \epsilon \; \{\text{integers}\} \tag{3.2–9}$$

A class of shapes is identified by a specific set of CAR descriptors $\vec{a}$. There is no variation of $\vec{a}$ within this class. The differences between shapes in this class manifest themselves as different sample sequences of the error process. Each shape has associated with it the CAR descriptors $\vec{a}$ of the class it belongs to and a specific sample sequence of the error process. The CAR descriptors embody the shape information common to all members of the class. The error sequence contains the shape information unique to a particular member of the class. This is the reason CAR descriptors are tolerant of within class variations. These variations do not affect the values of the CAR descriptors but rather are reflected in the sample error sequences.

The CAR descriptors preserve class shape information in the following sense. Given the CAR descriptors of a class of shapes and the values of α and β, a boundary sequence r(n) can be generated which is associated with a boundary of that class. The particular boundary with which r(n) is associated is unspecified. Such a sequence, r(n), can be generated directly from the defining relationship given in (3.2–1) if the m initial conditions are known. If arbitrary initial conditions are used the boundary sequence r(n) in general will not close. That is,

$$r(n+N) \neq r(n) \tag{3.2–10}$$

and since r(n) is not circular it is not associated with any closed boundary. Further insight into the cause of this difficulty can be obtained by viewing the CAR model as a discrete, linear, constant coefficient (the CAR descriptors) filter. The input to this filter is the error process and its output is the boundary process. The wrong set of initial conditions causes a transient response at the beginning of the filter's output. Since the transient response due to the initial conditions decays with increasing n, assuming a stable filter, it is unlikely that the N-th output will in general equal the initial value. What is desired is the steady state response of this filter. The steady state response of the filter can be obtained through the frequency domain using the transfer function of the filter.

The transfer function of the filter associated with the CAR model is derived from the Z-transform of (3.2-1). The Z-transform of a sequence r(n) is denoted $Z\{r(n)\}$ and defined as follows [23].

$$Z\{r(n)\} = \sum_{n=0}^{N-1} r(n)z^{-n} \tag{3.2-11}$$

The Z-transform of (3.2-1) is

$$R(z) = R(z)\sum_{k=1}^{m} a_k z^{-k} + E(z) \tag{3.2-12}$$

where the linearity and shift properties of the Z-transform have been used. R(z) and E(z) denote the Z-transform of the sample boundary and error sequences respectively. The transfer function H(z) of the filter is defined as

$$H(z) \triangleq \frac{R(z)}{E(z)} \tag{3.2-13}$$

and from (3.2-12) is equal to the following.

$$H(z) = \frac{1}{1 - \sum_{k=1}^{m} a_k z^{-k}} \tag{3.2-14}$$

The transfer function H(z) shapes the spectrum of the sample boundary sequences. Since the input and output processes are periodic and have the same period, their frequency spectrums are composed of discrete line spectra located at the following set of frequencies.

$$\omega_n = \frac{2\pi}{N} n \; ; 0 \leq n \leq N - 1 \tag{3.2-15}$$

The spectrum of the filter associated with the CAR model is obtained by evaluating the transfer function H(z) on the unit circle. The unit cirlce in the Z-plane is defined below.

$$z = e^{j\omega} \tag{3.2-16}$$

Since only the discrete set of frequencies specified in (3.2-15) are of interest only the following set of samples on the unit circle need to be considered.

$$z_n = e^{j\omega_n} \tag{3.2-17}$$

$$= e^{j\,2\pi/N\,n} \tag{3.2-18}$$

The frequency response of the filter at the frequencies specified in (3.2-15) is equal to the transfer function of (3.2-14) evaluated at the values of z given in (3.2-18).

$$H(z_n) = \frac{1}{1 - \sum_{k=1}^{m} a_k\, z_n^{-k}} \tag{3.2-19}$$

For the sake of convenience, the notation for the values of the transfer function H(z) evaluated at the points given in (3.2-18) will be changed to that shown below, directly reflecting the dependence upon the frequency index n.

$$H(n) = \frac{1}{1 - \sum_{k=1}^{m} a_k\, e^{j\,2\pi/N\,nk}} \tag{3.2-20}$$

The steady state response of the filter to a given sample sequence of the error process will now be obtained. Let E(k) and R(k) be the discrete Fourier transforms (DFT) of sample sequences of the input error process and the output boundary process respectively. The DFT of these processes is defined below.

$$E(k) = \sum_{n=0}^{N-1} \epsilon(n)\, e^{-j\,2\pi/N\,nk} \tag{3.2-21}$$

$$R(k) = \sum_{n=0}^{N-1} r(n)\, e^{-j\,2\pi/N\,nk} \tag{3.2-22}$$

Since the input process is circular, see (3.2-9), the circular convolution theorem [23] can be used to obtain the following relationship between E(k), R(k), and the transfer function of the filter H(k) specified in (3.2-20).

$$R(k) = H(k)\, E(k) \tag{3.2-23}$$

The sample boundary sequence r(n) generated from the sample error process is equal to the inverse DFT (IDFT) of R(k). The IDFT of R(k), defined below, is the steady state output of the filter and is equal to the sample boundary sequence r(n).

$$r(n) = \frac{1}{N} \sum_{k=0}^{N-1} R(k) e^{j\,2\pi/N\,nk} \tag{3.2-24}$$

Since r(n) is the steady state response of the filter, it satisfies the circularity constraint (3.1-4) on the boundary sequence. This procedure was originally demonstrated by Kashyap and Chellappa [24] and will be used later to generate sample boundary sequences which belong to a class of shapes specified by a selected set of CAR descriptors.

Even though the CAR descriptors preserve class shape information and are able to generate a sample boundary sequence associated with a given class of shapes, they are unable to generate the boundary sequence associated with a particular member of that shape class. This is because a particular member of a shape class is completely specified by both the CAR descriptors of that class and the sample error sequence associated with that particular member. If both of these are known, then the desired boundary may be generated using the procedure described above.

The CAR descriptors have been shown to be invariant to those linear transformations which affect a rotation or scaling upon the boundary without changing its shape [24]. It was further shown therein that the ratio $\alpha/\sqrt{\beta}$ derived from the error process of the CAR model is also invariant to these linear transformations. An augmented set of CAR descriptors may be defined which includes this ratio as an additional descriptor. This additional descriptor is expected to improve classification performance and it would be a desirable descriptor to include in a practical application of the CAR descriptors. The use of a similarily defined feature has been shown to improve performance in speech recognition experiments [25]. This ratio was not used as a feature in the boundary classification experiments presented in Chapter 7. The boundaries generated for the classification experiment which used synthetic boundaries all had the same value of $\alpha/\sqrt{\beta}$. Consequently, in this rather special (synthetic)

case, the ratio $\alpha/\sqrt{\beta}$ possessed no information which could be used to discriminate between the boundaries of the different shape classes. The next section presents a two dimensional graphical representation of the m dimensional feature space of the CAR descriptors. This graphical representation provides a means of viewing the separation of the shape classes when high order (m>3) CAR processes are used to model the boundary.

3.3 A GRAPHIC REPRESENTATION OF FEATURE SPACE

The development of a machine perception system capable of recognizing object shapes includes the tasks of feature selection and classifier design. The selection of a set of features defines the feature space and each shape class is identified by its location in this feature space. In selecting the features it is helpful to know the location and extent of the shape classes in the resulting feature space. This information is also useful in the design and analysis of the classifier. This information can best be portrayed by a graphic representation of the shape classes in feature space. Such a graphic representation is easy to produce for feature spaces of dimension two or less, since simple plots can be made on paper. If the feature space is of dimension three, then 3-D plotting routines may be helpful but the perspective must be carefully specified. The direct viewing of higher dimensional (>3) feature spaces is in general very difficult. The use of projections may provide some insights, but their usefulness quickly decreases with increasing dimensionality. In this section a two-dimensional graphic representation of an arbitrarily dimensioned CAR feature space is presented which does not depend upon projections or approximations. The characteristics of shape classes are then discussed relative to their location in feature space.

The CAR descriptors were defined from an m-th order CAR model and they completely specify the transfer function H(z) (see equation 3.2-14) associated with this CAR model. This transfer function is also completely specified by its m poles which are denoted by the p_i's. These poles are the roots of the m-th degree polynomial Q(z) in the denominator of the transfer function H(z). By definition, Q(z) is equal to the following.

$$Q(z) = \prod_{k=1}^{m} (z - p_k) \qquad (3.3\text{-}1)$$

These poles can be related to the CAR descriptors by multiplying both the numerator and denominator of H(z) by z^m

$$H(z) = \frac{z^m}{z^m - \sum_{k=1}^{m} a_k z^{m-k}} \tag{3.3-2}$$

and equating the resulting experession for Q(z) in the denominator of (3.3-2) to the one in (3.3-1).

$$z^m - \sum_{k=1}^{m} a_k z^{m-k} = \prod_{k=1}^{m} (z - p_k) \tag{3.3-3}$$

The expressions for the CAR descriptors in terms of the poles are obtained by expanding the right side of (3.3-3) and equating the coefficients of like powers in z. For example, consider a third order (m=3) CAR model. Equation (3.3-3) is then equal to

$$z^3 - a_1 z^2 - a_2 z - a_3 = (z - p_1)(z - p_2)(z - p_3) \tag{3.3-4}$$

$$= z^3 - (p_1 + p_2 + p_3) z^2 + (p_1 p_2 + p_1 p_3 + p_2 p_3) z - p_1 p_2 p_3 \tag{3.3-5}$$

which yields the following set of expressions for the CAR descriptors in terms of the poles.

$$a_1 = p_1 + p_2 + p_3 \tag{3.3-6}$$

$$a_2 = -(p_1 p_2 + p_1 p_3 + p_2 p_3) \tag{3.3-7}$$

$$a_3 = p_1 p_2 p_3 \tag{3.3-8}$$

The poles in general will be complex and can be plotted in the complex z-plane. A plot of the poles in the complex z-plane with the unit circle included for reference will be called a CAR diagram. Since there exist a one-to-one onto mapping between the coefficients of a polynomial (the CAR descriptors) and its roots (poles), there exist a similar mapping between the points in the feature space of the CAR descriptors and the associated sets of poles in the z-plane. The CAR diagram therefore provides a two-dimensional graphic representation of an m dimensional CAR feature space. If the poles associated with different shape classes are plotted in the same CAR diagram, the relative locations of the shape classes may be viewed in two dimensions.

The poles of each member of a training set may be plotted to give an indication of the extent of a shape class. The decision boundaries of a classifier may also be plotted in the CAR diagram. However, since a point in the feature space of the CAR descriptors is mapped onto a set of m points in the CAR diagram, care must be used in interpreting these decision boundaries. A CAR diagram may also be used to plot the trajectory of the CAR descriptors as the boundary changes due to three dimensional rotation of the object.

A one-to-one correspondence also exist between the stationarity of a CAR process and the stability of the filter associated with it. If all the poles in the CAR diagram are within the unit circle then the filter is stable and the associated CAR process is stationary. If any of the poles lie outside the unit circle, or if any multiple of poles lie on the unit circle, then the filter is unstable and the process is not stationary. Just as varying degress of filter stability exist, varying degrees of process stationarity may be defined. The closer the poles are located to the unit circle in the CAR diagram, the less stationary the associated CAR process is. Since the boundary sequences close, only stable filters and, consequently, stationary processes will be considered.

3.4 STATISTICS OF THE CAR MODEL

The CAR model defined by (3.2-1) is a statistical model of the boundary process r(n). This model can be viewed as a discrete linear filter (see Section 3.2) which relates the input error process $\epsilon(n)$ to the output boundary process r(n). This view of the CAR model as a discrete linear filter will be combined with the statistical properties of the error process given in Section 3.2 to derive the probability density function of the boundary process [26]. Since the filter is linear and the input error process is stationary and Gaussian distributed, the output boundary process will also be stationary and Gaussian distributed. The Gaussian distribution of the output boundary process r(n) is completely specified in terms of its first and second order statistics.

The first order statistic of the boundary process is its mean μ_r which can be derived from the mean of the error process (see equation 3.2-2) and the transfer function H(k) of the filter associated with the CAR model.

$$\mu_r = \alpha\, H(o) \qquad (3.4\text{-}1)$$

$$= \frac{\alpha}{1 - \sum_{k=1}^{m} a_k} \tag{3.4-2}$$

The second order statistics of the boundary process have more interesting properties and can be specified in both the time (autocorrelation function $R_r(k)$) and frequency domain (power spectral density $S_r(n)$). The autocorrelation function $R_r(k)$ of the boundary process defined as

$$R_r(k) = E\{r(n)\, r(n + k)\} \tag{3.4-3}$$

is shown below to be periodic with period N. By definition

$$R_r(k + mN) = E\{r(n)\, r(n + k + mN)\} \tag{3.4-4}$$

then, because of the periodicity of r(n) (see equation 3.1-4), it follows that

$$R_r(k + mN) = E\{r(n)\, r(n + k)\} \tag{3.4-5}$$

which is recognized from the definition in (3.4-3) to be the value of the autocorrelation function at k.

$$R_r(k + mN) = R_r(k) \qquad \forall \quad m \in \{\text{integers}\} \tag{3.4-6}$$

The covariance function of the boundary process r(n) is denoted by $C_r(k)$ and is related to the autocorrelation and mean of this process as shown below.

$$C_r(k) = R_r(k) - \mu_r^2 \tag{3.4-7}$$

It can be seen from (3.4-7) that the covariance function of r(n) will have the same periodic properties that its autocorrelation function has (see equation 3.4-6).

A vector process $\vec{r}$ will now be defined from the boundary sequence r(n). The j-th element of this vector is equal to the j-th value of the boundary sequence.

$$(\vec{r})_j = r(j) \tag{3.4-8}$$

Since the boundary process is stationary, the mean of $\vec{r}$ is the constant vector given below,

$$(\vec{\mu}_r)_j = \mu_r \tag{3.4-9}$$

where μ_r is as determined in (3.4-2). The covariance matrix Σ_r of the vector process is defined as

$$\Sigma_r = E\{(\vec{r} - \vec{\mu}_r)\,(\vec{r} - \vec{\mu}_r)^t\} \tag{3.4-10}$$

and the i, j-th element is equal to the following.

$$(\Sigma_r)_{ij} = E\{(\vec{r} - \vec{\mu}_r)_i\,(\vec{r} - \vec{\mu}_r)_j\} \tag{3.4-11}$$

$$= E\{(r(i) - \mu_r)\,(r(j) - \mu_r)\} \tag{3.4-12}$$

$$= E\{r(i)\,r(j)\} - E\{r(i)\}\,\mu_r - \mu_r\,E\{r(j)\} + \mu_r^2 \tag{3.4-13}$$

$$= R_r(i - j) - \mu_r^2 \tag{3.4-14}$$

$$= C_r(i - j) \tag{3.4-15}$$

The last equality follows from (3.4-7). Since the covariance function $C_r(k)$ is periodic and the i, j-th element of the covariance matrix Σ_r depends only upon the difference $i - j$, Σ_r is a circulant matrix [27].

The second order properties of the boundary process can be obtained more explicitly in the frequency domain. The power spectral density of a discrete process is equal to the DFT of its autocorrelation function. For example, the power spectral density $S_\epsilon(n)$ of the error process is

$$S_\epsilon(n) = \sum_{k=0}^{N-1} R_\epsilon(k)\, e^{-j\,2\pi/N\,nk} \tag{3.4-16}$$

substituting (3.2-4) yields

$$S_\epsilon(n) = \sum_{k=0}^{N-1} [\alpha^2 + \beta\,\delta(k)]\, e^{-j\,2\pi/N\,nk} \tag{3.4-17}$$

$$= \sum_{k=0}^{N-1} \alpha^2 e^{-j 2\pi/N\, nk} + \beta \sum_{k=0}^{N-1} \delta(k)\, e^{-j 2\pi/N\, nk} \tag{3.4-18}$$

$$= \alpha^2 N\, \delta(n) + \beta \tag{3.4-19}$$

where the following identity has been used.

$$\sum_{k=0}^{N-1} e^{-j 2\pi/N\, nk} = N\, \delta(n) \tag{3.4-20}$$

The transfer function H(k) of the filter associated with the CAR model can be used to relate the power spectral densities of the error and boundary processes. Let $S_r(n)$ be the power spectral density of the boundary process, then

$$S_r(n) = |H(n)|^2\, S_e(n) \tag{3.4-21}$$

$$= |H(n)|^2\, [\alpha^2\, N\, \delta(n) + \beta] \tag{3.4-22}$$

$$= \alpha^2\, H^2(o)\, N\, \delta(n) + \beta |H(n)|^2 \tag{3.4-23}$$

$$= \mu_r^2\, N\, \delta(n) + \beta |H(n)|^2 \tag{3.4-24}$$

where the last equality follows from (3.4-1).

The autocorrelation function $R_r(k)$ of the boundary process can also be obtained by evaluating the IDFT of the power spectral density $S_r(n)$ given in (3.4-24).

$$R_r(k) = \frac{1}{N} \sum_{n=0}^{N-1} S_r(n)\, e^{j 2\pi/N\, nk} \tag{3.4-25}$$

The only specific value of $R_r(k)$ which will be of interest in the future is for $k = 0$. This is computed below.

$$R_r(0) = \frac{1}{N} \sum_{n=0}^{N-1} S_r(n) \tag{3.4-26}$$

$$= \frac{1}{N} \sum_{n=0}^{N-1} [\mu_r^2\, N\, \delta(n) + \beta |H(n)|^2] \tag{3.4-27}$$

$$= \mu_r^2 + \frac{\beta}{N} \sum_{n=0}^{N-1} |H(n)|^2 \qquad (3.4\text{–}28)$$

The dependence of the mean μ_r of the boundary process upon the CAR descriptors is evident from (3.4–2). Similarily, the dependence of the covariance matrix Σ_r upon the CAR descriptors can be traced back from (3.4–14), (3.4–25), and (3.4–23) which contains the transfer function H(n) specified by the CAR descriptors. This dependence upon the CAR descriptors is made notationally explicit below in the expression for the probability density function of the boundary process.

$$p_r(\vec{r}\,;\vec{a}) = \frac{1}{(2\pi)^{N/2}\,|\Sigma_r(\vec{a})|^{1/2}}\; e^{-1/2\,(\vec{r}-\vec{\mu_r}(\vec{a}))^t\,\Sigma_r^{-1}(\vec{a})\,(\vec{r}-\vec{\mu_r}(\vec{a}))} \qquad (3.4\text{–}29)$$

This probability density function provides complete statistical information about the boundary process.

4.0 THE MAXIMUM LIKELIHOOD ESTIMATOR OF THE CAR DESCRIPTORS

In this chapter the ML estimates of the CAR descriptors are derived from a given sample boundary sequence $\vec{r}$. They define the CAR model which is most likely to generate this sample sequence. The ML estimates $\hat{\vec{a}}$ are obtained by searching the m-dimensional space of CAR descriptors to find the set of CAR descriptors which maximizes the probability density function $p_r(\vec{r}\,;\vec{a})$ (see equation 3.4-29), given the sample boundary sequence $\vec{r}$. In the absence of a closed form solution for $\hat{\vec{a}}$, several algorithms are presented which numerically find the value $\hat{\vec{a}}$. This is a difficult problem to solve even numerically and the difficulties which arise are discussed. Successive improvements in the algorithms are noted and a final algorithm is chosen which produces consistent results in a reasonable amount of time. All of these algorithms iterate on the solution and require an initial value of the CAR descriptors to begin the iterations. These initial values are provided by the least squares estimator which is derived from the CAR model. Additionally, an estimate of β (see equation 3.2-4) is required which corresponds to the values of the CAR descriptors at each iteration. Such an estimator is derived and all of the requirements to initialize and run the algorithm are satisfied.

4.1 THE ML ESTIMATOR

Let $\vec{r}$ be a sample sequence of a boundary process as defined in Section 3.4. The probability of observing this particular sample sequence is equal to (3.4-29) evaluated at $\vec{r}$. Equation (3.4-29) is repeated below for reference, but the explicit dependence upon the CAR descriptors $\vec{a}$ has been suppressed for notational convenience. This dependence upon the CAR descriptors is contained in the statistics $\vec{\mu}_r$ and Σ_r.

$$p_r(\vec{r}\,;\vec{a}) = \frac{1}{(2\pi)^{N/2}\,|\Sigma_r|^{1/2}}\, e^{-1/2(\vec{r}-\vec{\mu}_r)^t \Sigma_r^{-1}(\vec{r}-\vec{\mu}_r)} \tag{4.1-1}$$

Given the specific value of $\vec{r}$ provided by the sample boundary sequence, (4.1-1) becomes a function of the CAR descriptors. This function is known as the likelihood function of the CAR descriptors. The set of CAR descriptors $\hat{\vec{a}}$ which maximize the likelihood function are the ML estimates of the CAR descriptors and specify the CAR

model most likely to generate the given sample sequence of the boundary. Since the natural logarithm is a monotonically increasing function, the set of CAR descriptors $\hat{\vec{a}}$ which maximize the likelihood function also maximize the log-likelihood function defined below.

$$L(\vec{a}) = \ln [p_r(\vec{r}; \vec{a})] \tag{4.1-2}$$

$$= -\frac{1}{2}(\vec{r} - \vec{\mu}_r)^t \Sigma_r^{-1} (\vec{r} - \vec{\mu}_r) - \frac{1}{2}\ln|\Sigma_r| - \frac{N}{2}\ln(2\pi) \tag{4.1-3}$$

The value $\hat{\vec{a}}$ which maximizes the log-likelihood function is unaffected by the third term of (4.1-3) since that term is independent of the CAR descriptors. Similarily, the value of $\hat{\vec{a}}$ is independent of any positive multiplier of the log-likelihood function. If the log-likelihood function is multiplied by a negative constant, the ML estimate $\hat{\vec{a}}$ of the CAR descriptors is then located at the minimum of this new function. All of these properties have been combined together below in deriving the negative log-likelihood function $L^-(\vec{a})$ from (4.1-3).

$$L^-(\vec{a}) = -2\left[L(\vec{a}) + \frac{N}{2}\ln(2\pi)\right] \tag{4.1-4}$$

$$= (\vec{r} - \vec{\mu}_r)^t \Sigma_r^{-1} (\vec{r} - \vec{\mu}_r) + \ln|\Sigma_r| \tag{4.1-5}$$

The ML estimate $\hat{\vec{a}}$ of the CAR descriptors is the value of $\vec{a}$ which minimizes the negative log-likelihood function shown above. The dependence of the negative log-likelihood function upon the CAR descriptors is contained in the statistics $\vec{\mu}_r$ and Σ_r. The results of Section 3.4 will be used to make that dependence more explicit.

It was shown in Section 3.4 that the covariance matrix Σ_r is circulant and as such may be expressed in the following form [27].

$$\Sigma_r = \frac{1}{N} U \Lambda U^* \tag{4.1-6}$$

The matrix U is the unitary Fourier matrix defined below and Λ is the diagonal eigenvector matrix also defined below.

$$(U)_{nk} = e^{-j\,2\pi/N\,nk} \tag{4.1-7}$$

$$(\Lambda)_{nk} = \lambda_n\,\delta(n-k) \tag{4.1-8}$$

A further consequence of Σ_r being circulant is that its eigenvalues are given by the DFT of the associated convariance function $C_r(k)$ (see equation 3.4-15).

$$\lambda_n = \sum_{k=0}^{N-1} C_r(k)\, e^{-j\,2\pi/N\,nk} \tag{4.1-9}$$

By substituting the result of (3.4-7) into the above and separating the difference

$$\lambda_n = \sum_{k=0}^{N-1} R_r(k)\, e^{-j\,2\pi/N\,nk} - \sum_{k=0}^{N-1} \mu_r^2\, e^{-j\,2\pi/N\,nk} \tag{4.1-10}$$

the first term is recognized to be the definition of the power spectral density $S_r(n)$ and the second term can be simplified using the identity given in (3.4-20).

$$\lambda_n = S_r(n) - \mu_r^2\, N\, \delta(n) \tag{4.1-11}$$

The derived result for the power spectral density $S_r(n)$ given in (3.4-24) can be used to simplify the above expression for λ_n. This yields the following result for the eigenvalues of the convariance matrix Σ_r.

$$\lambda_n = \beta\, |H(n)|^2 \tag{4.1-12}$$

Recall that H(n) is the transfer function of the discrete linear filter (see equation 3.2-20) specified by the CAR model associated with the underlying boundary process.

Return now to the expression for the negative log-likelihood function (see equation 4.1-5) and let

$$\vec{\rho} = \vec{r} - \vec{\mu}_r \tag{4.1-13}$$

then

$$L^-(\vec{a}) = \frac{1}{N}\,[\vec{\rho}^{\,t}\, U^*\, \Lambda^{-1}\, U\, \vec{\rho}\,] + \ln\left[\prod_{n=0}^{N-1} \lambda_n\right] \tag{4.1-14}$$

where the properties of unitary matrices have been used to compute the inverse of Σ_r and its determinant has been expressed as the product of its eigenvalues. The vector

matrix products in (4.1-14) can be grouped together as follows and the principle property of logarithms can be used to simplify the last term.

$$L^{-}(\vec{a}) = \frac{1}{N}(U\vec{\rho})^{*}\,\Lambda^{-1}\,(U\vec{\rho}) + \sum_{n=0}^{N-1} \ln \lambda_n \tag{4.1-15}$$

Define the vector

$$\vec{P}_{\rho} = U\vec{\rho} \tag{4.1-16}$$

then the first term of (4.1-15) can be expanded as shown below.

$$\frac{1}{N}(U\vec{\rho})^{*}\,\Lambda^{-1}\,(U\vec{\rho}) = \frac{1}{N}\,\vec{P}_{\rho}{}^{*}\,\Lambda^{-1}\,\vec{P}_{\rho} \tag{4.1-17}$$

$$= \frac{1}{N}\sum_{n=0}^{N-1} P_{\rho}^{*}(n)\,(\Lambda^{-1}\vec{P}_{\rho})_n \tag{4.1-18}$$

$$= \frac{1}{N}\sum_{n=0}^{N-1} P_{\rho}^{*}(n)\left[\sum_{k=0}^{N-1} (\Lambda^{-1})_{nk}\,P_{\rho}(k)\right] \tag{4.1-19}$$

$$= \frac{1}{N}\sum_{n=0}^{N-1} P_{\rho}^{*}(n)\left[\sum_{k=0}^{N-1} \lambda_n^{-1}\,\delta(n-k)\,P_{\rho}(k)\right] \tag{4.1-20}$$

$$= \frac{1}{N}\sum_{n=0}^{N-1} P_{\rho}^{*}(n)\,\lambda_n^{-1}\,P_{\rho}(n) \tag{4.1-21}$$

$$= \sum_{n=0}^{N-1} \frac{|P_{\rho}(n)|^2}{N}\frac{1}{\lambda_n} \tag{4.1-22}$$

The negative log-likelihood function has been reduced to the following form where the dependence upon the CAR descriptors is clear from (4.1-12).

$$L^{-}(\vec{a}) = \sum_{n=0}^{N-1} \frac{|P_{\rho}(n)|^2}{N}\frac{1}{\lambda_n} + \ln \lambda_n \tag{4.1-23}$$

Further insight into this negative log-likelihood function can be obtained by expanding the vector matrix product which defines the vector $\vec{P}_\rho$ (see equation 4.1-16).

$$P_\rho(n) = (U\vec{\rho})_n \tag{4.1-24}$$

$$= \sum_{k=0}^{N-1} \rho(k)\, e^{-j\,2\pi/N\,nk} \tag{4.1-25}$$

The vector $\vec{P}_\rho$ is seen to be equal to the vector formed from the DFT of the sequence represented by the vector $\vec{\rho}$. From this follows the observation that the sequence

$$\frac{|P_\rho(n)|^2}{N} \tag{4.1-26}$$

which appears in the negative log-likelihood function is the periodogram of the sequence $\vec{\rho}$. By substituting the definition of $\rho(n)$ (see equation 4.1-13) into (4.1-25), a relationship to the given sample boundary sequence r(n) can be established.

$$P_\rho(n) = \sum_{k=0}^{N-1} [r(k) - \mu_r]\, e^{-j\,2\pi/N\,nk} \tag{4.1-27}$$

$$= \sum_{k=0}^{N-1} r(k)\, e^{-j\,2\pi/N\,nk} - \mu_r N\delta(n) \tag{4.1-28}$$

Denote the DFT of the sample boundary sequence r(k) by the sequence $P_r(n)$.

$$P_r(n) = \sum_{k=0}^{N-1} r(k)\, e^{-j\,2\pi/N\,nk} \tag{4.1-29}$$

The sequence $P_\rho(n)$ can now be expressed as

$$P_\rho(n) = P_r(n) - \mu_r N\, \delta(n) \tag{4.1-30}$$

and the periodogram of $\rho(k)$ defined in (4.1-26) is equal to the following.

$$\frac{|P_\rho(n)|^2}{N} = \frac{|P_r(n) - \mu_r N\, \delta(n)|^2}{N} \tag{4.1-31}$$

Notice that

$$\frac{|P_\rho(n)|^2}{N} = \frac{|P_r(n)|^2}{N} \quad \vee n \neq 0 \tag{4.1-32}$$

which means the periodogram of the sequence $\rho(n)$ is equal to the periodogram of the sample boundary sequence except at $n=0$. The value of $P_\rho(0)$ can be evaluated from (4.1-25) and (4.1-13).

$$P_\rho(0) = \sum_{k=0}^{N-1} \rho(k) \tag{4.1-33}$$

$$= \sum_{k=0}^{N-1} [r(k) - \mu_r] \tag{4.1-34}$$

$$= \sum_{k=0}^{N-1} r(k) - N\mu_r \tag{4.1-35}$$

$$= N\left[\left(\frac{1}{N} \sum_{k=0}^{N-1} r(k)\right) - \mu_r\right] \tag{4.1-36}$$

The term in parenthesis in (4.1-36) is, by definition, the sample mean of the given boundary process r(n) and is denoted as $\hat{\mu}_r$ below.

$$\hat{\mu}_r = \frac{1}{N} \sum_{k=0}^{N-1} r(k) \tag{4.1-37}$$

$P_\rho(0)$ is equal to the following where (4.1-37) has been substituted into (4.1-36).

$$P_\rho(0) = N[\hat{\mu}_r - \mu_r] \tag{4.1-38}$$

There are two important cases in which (4.1-38) becomes equal to zero. The first case involves practical applications of the negative log-likelihood function in which μ_r will be approximated by the sample mean of the given boundary process $\hat{\mu}_r$. Obviously, in this case $P_\rho(0)$ will be equal to zero. The second case of interest will occur in Section

5.4 where the asymptotic properties ($N \to \infty$) of the ML estimator are examined. Since $\hat{\mu}_r$ is an unbiased estimator of μ_r [28] the following limit exists

$$\lim_{N\to\infty} \hat{\mu}_r = \lim_{N\to\infty} \frac{1}{N} \sum_{k=0}^{N-1} r(k) \tag{4.1-39}$$

$$= \mu_r \tag{4.1-40}$$

and is equal to μ_r. Consequently, $P_\rho(0)$ is asymptotically equal to zero. Since these are the only cases which will be of interest it will be assumed that

$$P_\rho(0) = 0 \tag{4.1-41}$$

and the negative log-likelihood function can be simplified accordingly.

$$L^-(\vec{a}) = \ln \lambda_0 + \sum_{n=1}^{N-1} \frac{|P_\rho(n)|^2}{N} \frac{1}{\lambda_n} + \ln \lambda_n \tag{4.1-42}$$

The dependence of the negative log-likelihood function upon the sample sequence of the boundary r(n) can be made more obvious by substituting (4.1-32) into the above equation for $L^-(\vec{a})$.

$$L^-(\vec{a}) = \ln \lambda_0 + \sum_{n=1}^{N-1} \frac{|P_r(n)|^2}{N} \frac{1}{\lambda_n} + \ln \lambda_n \tag{4.1-43}$$

The two following equations are included below to summarize the negative log-likelihood function of the CAR descriptors. They are repeated from (4.1-12) and (3.2-20) respectively.

$$\lambda_n = \beta |H(n)|^2 \tag{4.1-44}$$

$$H(n) = \frac{1}{1 - \sum_{k=1}^{m} a_k e^{-j2\pi/N\, nk}} \tag{4.1-45}$$

The data dependence of the negative log-likelihood function is completely contained in the periodogram term. Likewise, the dependence of the negative log-likelihood function upon the CAR descriptors is contained in the eigenvalues.

4.2 MINIMIZING THE NEGATIVE LOG–LIKELIHOOD FUNCTION

The ML estimates $\hat{\vec{a}}$ of the CAR descriptors are obtained by minimizing the negative log-likelihood function of the CAR descriptors which was derived in the previous section (see equation 4.1-43). This is an increasingly difficult problem as the order of the CAR model, m, increases because an m + 1 dimensional surface must be searched for its global minimum. Closed form solutions for $\hat{\vec{a}}$ which require the solution of the following equation

$$\nabla L^{-}(\vec{a}) = 0 \tag{4.2-1}$$

are made untenable by the complex form of the above gradient. The gradient of the negative log-likelihood function is given in Appendix A. Since closed form solutions are not available, numerical algorithms must be considered. A series of algorithms were investigated until consistently accurate results were obtained. The level of sophistication of the required algorithm grew, as might be expected, with increases in the order of the CAR model. The simplest algorithms will be reviewed first with a steady progression towards the more powerful ones. All of these algorithms assume that an initial estimate of $\hat{\vec{a}}$ is available to start the algorithm. This availability will be assumed in this section and methods of obtaining an initial value of $\hat{\vec{a}}$ will be addressed in Section 4.3.

The Method of Steepest Descent [29]

The method of steepest descent, also known as the gradient method, is the fundamental algorithm for minimizing a differentiable function of m variables. As its name implies, this algorithm performs a line search for the minimum of $L^{-}(\vec{a})$ in the direction of steepest descent. This direction is the negative gradient of $L^{-}(\vec{a})$. The algorithmic steps are given below.

Step 1: Let n = 1 and choose an initial value $\hat{\vec{a}}_1$ and a stopping parameter $\epsilon > 0$.

Step 2: Let $\vec{d} = -\nabla L^{-}(\vec{a}_n)$ and stop if $|\vec{d}| < \epsilon$, otherwise find the value of h which minimizes $L^{-}(\vec{a}_n + h\vec{d})$.

Step 3: Let $\vec{a}_{n+1} = \vec{a}_n + h\vec{d}$, increment the index n = n + 1 and repeat Step 2.

The steepest descent algorithm will converge and usually works quite well during the initial descent towards the minimum. As the minimum is approached the rate of convergence can become painfully slow. Short orthogonal zig-zag steps are taken. This is because the steepest descent algorithm depends upon a linear approximation to $L^{-}(\vec{a})$ to guide its direction of movement and this approximation is not always accurate. The following algorithms attempt to ameliorate this difficulty by deflecting the direction of the gradient.

Newton's Method [29]

Newton's method is an improvement over the steepest descent algorithm in that it uses a quadratic rather than linear approximation to the negative log-likelihood function. The resulting algorithm is presented below.

Step 1: Let $n = 1$ and choose an initial value $\vec{a}_1$ and a stopping parameter $\epsilon > 0$.

Step 2: Let $\vec{a}_{n+1} = \vec{a}_n - H^{-1}(\vec{a}_n) \nabla L^{-}(\vec{a}_n)$ where

$$(H(\vec{a}))_{ij} = \frac{\partial^2 H(\vec{a})}{\partial a_i \, \partial a_j} \tag{4.2-2}$$

is the Hessian of the negative log-likelihood function and is given in Appendix B. Increment the index $n = n + 1$.

Step 3: If $|\nabla L^{-}(\vec{a}_n)| < \epsilon$ stop, otherwise repeat Step 2.

Notice that the parameter h of the steepest descent algorithm has been replaced by the inverse of the Hessian matrix of the negative log-likelihood function. Premultiplying the gradient by the inverse Hessian has the effect of deflecting the direction of the gradient.

Convergence of Newton's method is not assured since the Hessian may become singular at some point $\vec{a}_n$ during the iteration making $\vec{a}_{n+1}$ undefined. However, if the starting point is close enough to $\hat{a}$, then the inverse of the Hessian should continue to exist and Newton's method will then converge. The combined convergence characteristics of the method of steepest descent and Newton's method suggest that a possible synergistic combination of the two algorithms may exist. The method of steepest descent converges well at the beginning where the Hessian may be singular, and Newton's method converges well near $\hat{a}$ where the method of steepest descent tends to zig-zag. Another possible solution is to use a matrix other than the Hessian to deflect the gradient. This is the approach taken by the method of Davidon, Fletcher, and Powell, which is presented next.

Method of Davidon, Fletcher and Powell (DFP)

The method of DFP was originally proposed by Davidon in 1959 [30], and later developed by Fletcher and Powell in 1963 [31]. This method deflects the gradient through a sequence of directions which are conjugate with respect to the Hessian matrix. A set of direction vectors $\vec{d}_i$ are conjugate with respect to the matrix H if the following equality is satisfied for all i.

$$\vec{d}_i^{\,t} H \vec{d}_j = 0 \quad \forall\, j \neq i \tag{4.2-3}$$

It has been shown that an n-dimensional quadratic function will be minimized in n steps if it is searched along the directions conjugate to its Hessian matrix [29]. This is the basis for the development of the method of DFP which, like Newton's method, uses a quadratic approximation to the negative log-likelihood function. The algorithmic steps of the method of DFP are presented below.

Step 1: Let $k = 1$ and choose an initial value $\vec{a}_1$, a stopping parameter $\epsilon > 0$ and an $n \times n$ positive definite symmetric matrix D_1.

Step 2: Let $j = 1$ and set $\vec{x}_k = \vec{a}_k$.

Step 3: If $|\nabla L^-(\vec{x}_j)| < \epsilon$ stop, otherwise let $\vec{d}_j = -D_j \nabla L^-(\vec{x}_j)$ and find the value of h which minimizes $L^-(\vec{x}_j + h\vec{d}_j)$. Let $\vec{x}_{j+1} = \vec{x}_j + h\vec{d}_j$ then if $j < n$ go to Step 4, otherwise ($j = n$) let $\vec{a}_{k+1} = \vec{x}_{n+1}$ and increment $k = k + 1$. Go to Step 2.

Step 4: Let

$$D_{j+1} = D_j + \frac{\vec{p}\,\vec{p}^{\,t}}{\vec{p}^{\,t}\vec{q}} - \frac{D_j \vec{q}\,\vec{q}^{\,t} D_j}{\vec{q}^{\,t} D_j \vec{q}} \tag{4.2-4}$$

where $\vec{p} = h\vec{d}_j$ and $\vec{q} = \nabla L^-(\vec{x}_{j+1}) - \nabla L^-(\vec{x}_j)$, increment $j = j + 1$ and repeat Step 3.

If the function being minimized is quadratic, then in addition to stopping after one iteration on k as previously mentioned, the direction vectors $\vec{d}_i$ will be conjugate and D_{n+1} will equal the inverse of the Hessian at $\vec{a}_k$. This is why the method of DFP is sometimes called a quasi-Newton method.

The method of DFP was used exclusively in obtaining the experimental results presented in later chapters for the following reasons. There is no requirement to derive and then evaluate the Hessian of the negative log-likelihood function at each iteration. There are no problems with singularities. The method converges well to the very end and provides consistent results.

4.3 INITIALIZING AND RUNNING THE MINIMIZATION ALGORITHM

The DFP algorithm discussed in Section 4.2 requires an initial estimate of the CAR descriptors to begin. Obviously the closer this initial value is to $\hat{a}$ the fewer the number of required iterations will be. The least squares estimator of the CAR descriptors will be used to provide the initial values because it is a self starting algorithm which is easy to compute and no iterations are required.

The least squares estimator of the CAR descriptors minimizes the total energy in the error process $\epsilon(n)$ of the CAR model. Let E be the total energy of the error process, then

$$E = \sum_{n=0}^{N-1} \epsilon^2(n) \tag{4.3-1}$$

$$= \sum_{n=0}^{N-1} \left[r(n) - \sum_{k=1}^{m} a_k \, r(n-k) \right]^2 \tag{4.3-2}$$

the last equality follows from substitution of (3.2-5) into (4.3-1). The CAR descriptors $\tilde{a}$ which minimize E are found by solving the following system of equations.

$$\frac{\partial E}{\partial a_i} = 0 \quad \forall \; i = 1(1)m \tag{4.3-3}$$

The partial derivative of E with respect to a_i is easily shown to be the following.

$$\frac{\partial E}{\partial a_i} = -2 \sum_{n=0}^{N-1} \left[r(n) - \sum_{k=1}^{m} a_k \, r(n-k) \right] r(n-i) \tag{4.3-4}$$

Setting the above result equal to zero yields the following system of linear equations.

$$\sum_{n=0}^{N-1} \left[r(n) - \sum_{k=1}^{m} \tilde{a}_k \, r(n-k) \right] r(n-i) = 0 \qquad \forall \; i = 1(1)m \tag{4.3-5}$$

$$\sum_{n=0}^{N-1} \left[\sum_{k=1}^{m} \tilde{a}_k \, r(n-k) \right] r(n-i) = \sum_{n=0}^{N-1} r(n) \, r(n-i) \tag{4.3-6}$$

$$\sum_{k=1}^{m} \tilde{a}_k \left[\sum_{n=0}^{N-1} r(n-k) \, r(n-i) \right] = \sum_{n=0}^{N-1} r(n) \, r(n-i) \tag{4.3-7}$$

The least squares estimates $\tilde{a}$ can generally be used to start the DFP algorithm but some problems can arise. The solution of the m equations in (4.3-7) requires the inversion of an m $\times$ m matrix which can become numerically difficult as m becomes large.

The stationarity of the CAR model defined by the LS estimates of the CAR descriptors must be checked before they are used to initialize the DFP algorithm. This may be done by using a CAR diagram. If a pole p is outside the unit circle in the CAR diagram, it is reflected about the unit circle to its reciprocal conjugate position; that is:

$$p \rightarrow \frac{1}{p^*} \tag{4.3-8}$$

The magnitude spectrum of the resulting filter is the same as the original except it now defines a stationary CAR model. This is demonstrated below, let H(z) be a filter with an unstable pole p, then H(z) can be written as follows

$$H(z) = \frac{H_1(z)}{(1 - pz^{-1})} \; ; \; |p| > 1 \tag{4.3-9}$$

where $H_1(z)$ is the stable part of the filter. The above equation can be algebraically manipulated as follows.

$$H(z) = \frac{H_1(z)}{(1 - p\,z^{-1})} \; \frac{z^{-1} - p^*}{z^{-1} - p^*} \tag{4.3-10}$$

$$= \frac{H_1(z)}{z^{-1} - p^*} \; \frac{z^{-1} - p^*}{1 - p\,z^{-1}} \tag{4.3-11}$$

The second term of (4.3-11) is an all pass filter [23] and does not affect the magnitude of H(z); therefore the following relationship holds.

$$|H(z)| = \left| \frac{H_1(z)}{z^{-1} - p^*} \right| \tag{4.3-12}$$

The magnitude of H(z) may also be calculated from (4.3-9) and equated to (4.3-12).

$$\left| \frac{H_1(z)}{1 - p\,z^{-1}} \right| = \left| \frac{H_1(z)}{z^{-1} - p^*} \right| \tag{4.3-13}$$

Notice that the transfer function on the right has a pole at $1/p^*$ which is inside the unit circle since $|p|>1$ (see equation 4.3-9). Consequently, reflecting an unstable pole about the unit circle, as in (4.3-8), produces a stable filter with no change in the magnitude of the transfer function. The stationary set of CAR descriptors is then recovered by reexpanding the denominator polynomial. The relationship between the roots of the denominator polynomial and the CAR descriptors was previously discussed in detail in Section 3.3.

It is evident from the equations defining the negative log-likelihood function, (4.1-43) to (4.1-45), that in addition to an initial value of $\vec{a}$, a corresponding value of β is required to evaluate (4.1-44). An estimate of β can be obtained from the given sample boundary sequence r(n) and the least squares estimates $\tilde{a}$ of the CAR descriptors which were just derived. Equation (3.4-28) can be solved for β as shown below.

$$R_r(0) = \mu_r^2 + \frac{\beta}{N} \sum_{n=0}^{N-1} |H(n)|^2 \tag{4.3-14}$$

$$\beta = \frac{R_r(0) - \mu_r^2}{\frac{1}{N}\sum_{n=0}^{N-1} |H(n)|^2} \tag{4.3-15}$$

The following estimates for μ_r and $R_r(0)$ can be computed directly from the given sample sequence of the boundary r(n).

$$\hat{\mu}_r = \frac{1}{N}\sum_{n=0}^{N-1} r(n) \tag{4.3-16}$$

$$\hat{R}_r(0) = \frac{1}{N}\sum_{n=0}^{N-1} r^2(n) \tag{4.3-17}$$

These estimates are used to evaluate (4.3-15) to obtain an estimate of β.

$$\hat{\beta} = \frac{\hat{R}_r(0) - \hat{\mu}_r^2}{\frac{1}{N}\sum_{n=0}^{N-1} |H(n)|^2} \tag{4.3-18}$$

The transfer function H(n) appearing in the above estimator for β is evaluated using the least squares estimates of the CAR descriptors $\tilde{a}$ which were previously derived.

$$H(n) = \frac{1}{1 - \sum_{k=1}^{m} \tilde{a}_k e^{-j 2\pi/N\, nk}} \tag{4.3-19}$$

The least squares estimates of the CAR descriptors and the above estimate of β provide sufficient information to initialize the DFP algorithm. At each iteration of the algorithm, the negative log-likelihood function must be evaluated for a new set of CAR descriptors. This requires that a corresponding value of β be available. This value of β can be obtained from the estimator in (4.3-18) by evaluating the transfer function H(n) at the new set of CAR descriptors.

5.0 ESTIMATION OF THE CAR DESCRIPTORS FROM PARTIALLY OBSCURED BOUNDARIES

The ML estimator of the CAR descriptors which was derived in Section 4.1 is extended in this chapter to include partially obscured boundaries. This is accomplished by including a model of the obscuring process in the boundary model. The form of the negative log-likelihood function is retained so that it is only necessary to derive the relationship between the CAR descriptors and the eigenvalues of the covariance matrix of the partially obscured boundary process. The extended ML estimates of the CAR descriptors derived from a partially obscured boundary are intuitively appealing for the following reason. The ML estimates of the CAR descriptors identify the CAR model most likely to generate the observed portions of the boundary. The values of the CAR descriptors are estimated from just the observed portions of the boundary. No attempt is made to reconstruct the unobserved portions of the boundary. The asymptotic properties of the extended ML estimator of the CAR descriptors are then investigated and the Cramer-Rao lower bound on the variance of the estimates is derived. The last section presents an approximation to the extended negative log-likelihood function which can be used when a model of the obscuring process is unavailable.

5.1 THE OBSCURING PROCESS

The obscuring process embodies a large number of phenomena capable of partially obscuring an object's boundary. An obstruction between the sensor and object is the obvious cause of partial obscuration, but the obscuring process also includes partial obscuration due to shadowing, low contrast between the object and its background, inadequate sensor resolution, and noise. These later possibilities all give rise to difficulties in segmentation. The obscuring process can be used to model these segmentation errors as well as true obstructions. As a result of this, the requirement that the segmentor extract complete boundaries may be relaxed. The segmentor need only identify those boundary points it is sure of. It will be shown that this approach shifts some of the stress from the segmentor to the features and classifier.

Let $\rho(n)$ be the observed boundary sequence which is a partially obscured version of the complete boundary sequence r(n). The observed boundary sequence $\rho(n)$ is related to the complete boundary sequence r(n) by the obscuring sequence $\gamma(n)$ as shown below.

$$\rho(n) = \gamma(n)\, r(n) \tag{5.1-1}$$

The obscuring sequence $\gamma(n)$ is a sample sequence of a binary valued obscuring process. As might be imagined, if the n-th boundary point is observed, then $\gamma(n) = 1$, otherwise it is obscured and $\gamma(n) = 0$. The obscuring process $\gamma(n)$ is independent of the boundary process r(n), but in order to retain the circularity of the observed boundary process $\rho(n)$, the obscuring process $\gamma(n)$ must also be circular.

$$\gamma(n + kN) = \gamma(n) \quad \forall\ k \in \{\text{integers}\} \tag{5.1-2}$$

The distribution of the obscured boundary points around the boundary may take on many forms and dependencies. The statistical model of the obscuring process developed in this section is for segmentation error which may result from simple thresholding of the gradient image. Other models may be developed using similar techniques. An approximation technique is presented in Section 5.5 which can be used when the underlying statistical model is unknown.

Assuming that the obscured points are distributed around the boundary independent of whether the neighboring points are observed or not, the obscuring process can be modeled as a binary valued Bernoulli process. The probability distribution function of such a process is given below.

$$P(\gamma(n) = 1) = p \tag{5.1-3}$$

$$P(\gamma(n) = 0) = 1 - p = q \tag{5.1-4}$$

The value of q is the average fraction of the boundary sequence which will be obscured. The first and second order statistics of the obscuring process are computed below from their respective definitions. The mean μ_γ is defined below

$$\mu_\gamma = E\{\gamma(n)\} \tag{5.1-5}$$

$$= 1 \cdot P(\gamma(n) = 1) + 0 \cdot P(\gamma(n) = 0) \tag{5.1-6}$$

$$= p \tag{5.1-7}$$

and is equal to the probabliity of observing a sample point of the boundary. The autocorrelation function $R_\gamma(k)$ of the obscuring process is derived from its definition as follows.

$$R_\gamma(k) = E\{\gamma(n)\,\gamma(n+k)\} \tag{5.1-8}$$

$$= 1 \cdot P(\gamma(n) = 1, \gamma(n+k) = 1) \tag{5.1-9}$$

Since $\gamma(n)$ and $\gamma(n+k)$ are independent, the above probability distribution separates as shown below.

$$R_\gamma(k) = P(\gamma(n) = 1) \cdot P(\gamma(n+k) = 1) \tag{5.1-10}$$

$$= \begin{cases} p\,; k = 0 \\ p^2\,; k \neq 0 \end{cases} \tag{5.1-11}$$

This result can be rewritten using the Kronecker delta notation.

$$R_\gamma(k) = p^2 - (p^2 - p)\,\delta(k) \tag{5.1-12}$$

$$= p^2 + p\,(1 - p)\,\delta(k) \tag{5.1-13}$$

$$= p^2 + pq\,\delta(k) \tag{5.1-14}$$

Since the obscuring process has a constant mean μ_γ and an autocorrelation function $R_\gamma(k)$ which only depends upon the difference k and not upon n, it is at least wide sense (second order) stationary.

The power spectral density $S_\gamma(n)$ of the obscuring process is by definition equal to the DFT of the autocorrelation function of that process.

$$S_\gamma(n) = \sum_{k=0}^{N-1} R_\gamma(k)\, e^{-j\,2\pi/N\,nk} \tag{5.1-15}$$

Substituting (5.1-14) into the above equation results in

$$S_\gamma(n) = \sum_{k=0}^{N-1} [p^2 + pq\,\delta(k)]\, e^{-j2\pi/N\, nk} \tag{5.1-16}$$

and using the identity of (3.4-20) yields the following result.

$$S_\gamma(n) = p^2 N\,\delta(n) + pq \tag{5.1-17}$$

Since the boundary representation defined in Section 3.1 is computed relative to the centroid of the boundary, the problem of estimating the centroid from a partially specified boundary will be examined. Consider the point (x_0', y_0') computed from the N ordered pairs $(\gamma(n)\,x(n),\ \gamma(n)\,y(n))$ defined by the partially specified boundary curve.

$$x_0' = \frac{1}{pN} \sum_{n=0}^{N-1} \gamma(n)\,x(n) \tag{5.1-18}$$

$$y_0' = \frac{1}{pN} \sum_{n=0}^{N-1} \gamma(n)\,y(n) \tag{5.1-19}$$

Notice that on average only pN of these points will contribute to the summations. Given a sample boundary curve, the expected value of x_0' can be evaluated as follows, using the result of (5.1-7).

$$E\{x_0'\} = \frac{1}{pN} \sum_{n=0}^{N-1} E\{\gamma(n)\}\,x(n) \tag{5.1-20}$$

$$= \frac{1}{pN} \sum_{n=0}^{N-1} p\,x(n) \tag{5.1-21}$$

$$= \frac{1}{N} \sum_{n=0}^{N-1} x(n) \tag{5.1-22}$$

$$= x_0 \tag{5.1-23}$$

The last equality follows from the definition of the boundary centroid given in Section 3.1 (see equation 3.1-1). An analogous result may be derived between the point y'_0 and the centroid coordinate y_0 of the complete boundary sequence. Since the expected value of the point (x'_0, y'_0) is the centroid (x_0, y_0) of the complete boundary curve, it can be used in (3.1-3) to compute the boundary representation of a partially specified boundary.

5.2 THE EXTENDED ML ESTIMATOR OF THE CAR DESCRIPTORS

The ML estimator of the CAR descriptors which was derived in Chapter 4 will be extended in this section to include the case of partially obscured boundaries. The partially obscured boundaries will be represented by the observed boundary process $\rho(n)$ defined in the previous section. As in the work of Dunsmuir and Robinson [32], it will be assumed that the negative log-likelihood function of the CAR descriptors derived from the observed boundary process $\rho(n)$ has the same form as the negative log-likelihood function prevously derived (see equation 4.1-43) from the complete boundary process. The extended negative log-likelihood function which results from this assumption is given below.

$$L^{-}(\vec{a}) = \ln \lambda_0 + \sum_{n=1}^{N-1} \frac{|P_\rho(n)|^2}{N} \frac{1}{\lambda_n} + \ln \lambda_n \qquad (5.2\text{-}1)$$

The periodogram of the complete boundary sequence r(n) has been replaced by the periodogram of the observed boundary sequence and the eigenvalues are now those of the covariance matrix Σ_ρ associated with the observed boundary process.

The periodogram of the observed boundary sequence is defined as follows. Let $P_\rho(n)$ be the DFT of the observed boundary sequence $\rho(k)$,†

$$P_\rho(n) = \sum_{k=0}^{N-1} \rho(k)\, e^{-j\,2\pi/N\,nk} \qquad (5.2\text{-}2)$$

---

† The notation $\rho(n)$ and $P_\rho(n)$ used in this section should not be confused with similar notation used previously in Section 4.1

then the periodogram of $\rho(k)$ is equal to the following.

$$\frac{|P_\rho(n)|^2}{N} \tag{5.2-3}$$

The mean of the observed boundary process can be derived from its definition

$$\mu_\rho = E\{\rho(n)\} \tag{5.2-4}$$

and the definition of $\rho(n)$ (see equation 5.1-1).

$$\mu_\rho = E\{\gamma(n)\, r(n)\} \tag{5.2-5}$$

Since the obscuring process is independent of the boundary process, the above expectation may be separated.

$$\mu_\rho = E\{\gamma(n)\}\, E\{r(n)\} \tag{5.2-6}$$

$$= \mu_\gamma\, \mu_r \tag{5.2-7}$$

$$= p\, \alpha\, H(0) \tag{5.2-8}$$

The last equality follows from (5.1-7) and (3.4-1). Notice that the mean μ_ρ of the observed boundary process is a constant.

The definition of the covariance matrix Σ_ρ associated with the observed boundary process is given below

$$\Sigma_\rho = E\{(\vec{\rho} - \vec{\mu}_\rho)(\vec{\rho} - \vec{\mu}_\rho)^t\} \tag{5.2-9}$$

where $\vec{\rho}$ is the N dimensional vector process formed from the observed boundary process $\rho(n)$. The i, j-th element of this covariance matrix is given by the following.

$$(\Sigma_\rho)_{ij} = E\{(\rho(i) - \mu_\rho)(\rho(j) - \mu_\rho)\} \tag{5.2-10}$$

$$= E\{\rho(i)\, \rho(j) - \mu_\rho\, \rho(i) - \mu_\rho\, \rho(j) + \mu_\rho^2\} \tag{5.2-11}$$

$$= E\{\rho(i)\, \rho(j)\} - \mu_\rho^2 \tag{5.2-12}$$

Recall the definition of the observed boundary process $\rho(n)$ given in (5.1-1) in terms of the obscuring process $\gamma(n)$ and the complete boundary process r(n). Parzen [33] specified the conditions under which a process such as the observed boundary process $\rho(n)$ is asymptotically stationary. These conditions are:

1. The complete boundary process r(n) must be at least wide sense (second order) stationary. This was shown to be the case for CAR processes in Section 3.4.
2. The complete boundary process r(n) and the obscuring process $\gamma(n)$ must be independent. This was specified as part of the definition of the obscuring process in Section 5.1.
3. The obscuring process must be bounded. This condition is satisfied by virtue of defining the obscuring process to be a binary valued 0, 1 process.
4. The obscuring process must possess a generalized harmonic analysis. Since the obscuring process is periodic (see equation 5.1-2), it necessarily admits a generalized harmonic analysis.

Since all of the above conditions have been satisfied, the observed boundary process is asymptotically stationary and in the limit (5.2-12) reduces to

$$(\Sigma_\rho)_{ij} = R_\rho(i - j) - \mu_\rho^2 \tag{5.2-13}$$

where $R_\rho(k)$ is the asymptotic autocorrelation function of $\rho(n)$. Let $C_\rho(k)$ be the covariance function of this same process, then by (3.4-7) the above equation simplifies to the following.

$$(\Sigma_\rho)_{ij} = C_\rho(i - j) \tag{5.2-14}$$

Since $\rho(n)$ is periodic and the elements of the above covariance matrix depend only upon the difference of the indices, the covariance matrix Σ_ρ is circulant. Thus, the covariance matrix of the observed boundary process retains the circulant property of the covariance matrix of the complete boundary process (see equation 3.4-15) and its eigenvalues may be similarily evaluated (see equation 4.1-9).

$$\lambda_n = \sum_{k=0}^{N-1} C_\rho(k)\, e^{-j\,2\pi/N\,nk} \tag{5.2-15}$$

$$= \sum_{k=0}^{N-1} \left[R_\rho(k) - \mu_\rho^2 \right] e^{-j\,2\pi/N\,nk} \tag{5.2-16}$$

$$= \sum_{k=0}^{N-1} R_\rho(k)\, e^{-j\,2\pi/N\,nk} - \mu_\rho^2 \sum_{k=0}^{N-1} e^{-j\,2\pi/N\,nk} \tag{5.2-17}$$

The first term in the above equation is recognized as the definition of the power spectral density $S_\rho(n)$ of the observed boundary process $\rho(n)$. The second term in (5.2-17) may be reduced using the identity given in (3.4-20).

$$\lambda_n = S_\rho(n) - \mu_\rho^2\, N\, \delta(n) \tag{5.2-18}$$

Substituting the result of (5.2-8) into the above gives the following expression for the eigenvalues.

$$\lambda_n = S_\rho(n) - p^2\, \alpha^2\, H^2(0)\, N\, \delta(n) \tag{5.2-19}$$

In order to evaluate the power spectral density $S_\rho(n)$ of the observed boundary process, the autocorrelation function $R_\rho(k)$ of this process will first be evaluated. The definition of this autocorrelation function is given below.

$$R_\rho(k) = E\,\{\rho(n)\,\rho(n+k)\} \tag{5.2-20}$$

Substituting the definition of $\rho(n)$ (see equation 5.1-1) into the above equation yields

$$R_\rho(k) = E\,\{\gamma(n)\,\gamma(n+k)\,r(n)\,r(n+k)\} \tag{5.2-21}$$

which may be separated due to the independence of the obscuring process and the complete boundary process.

$$R_\rho(k) = E\,\{\gamma(n)\,\delta(n+k)\}\,E\,\{r(n)\,r(n+k)\} \tag{5.2-22}$$

$$= R_\gamma(k)\,R_r(k) \tag{5.2-23}$$

The circular convolution theorem [23] of discrete Fourier transform theory can be used to evaluate the DFT of (5.2-23). This yields the following result for the power spectral density $S_\rho(n)$ of the obscured boundary process.

$$S_\rho(n) = S_\gamma(n) * S_r(n) \tag{5.2-24}$$

$$= \frac{1}{N} \sum_{k=0}^{N-1} S_\gamma(n-k)\, S_r(k) \tag{5.2-25}$$

The results of (5.1-17) and (3.4-23) can be substituted into the above equation so that the convolution may be evaluated.

$$S_\rho(n) = \frac{1}{N} \sum_{k=0}^{N-1} [p^2 N \delta(n-k) + pq][\alpha^2 H^2(0) N \delta(k) + \beta |H(k)|^2] \tag{5.2-26}$$

$$\begin{aligned} = \frac{1}{N} \sum_{k=0}^{N-1} & [p^2 \alpha^2 H^2(0) N^2 \delta(n-k)\, \delta(k) \\ & + p^2 \beta N |H(k)|^2 \delta(n-k) \\ & + pq\, \alpha^2 H^2(0) N \delta(k) \\ & + pq\, \beta |H(k)|^2] \end{aligned} \tag{5.2-27}$$

$$\begin{aligned} S_\rho(n) = {} & p^2 \alpha^2 H^2(0) N \delta(n) \\ & + p^2 \beta |H(n)|^2 \\ & + pq\, \alpha^2 H^2(0) \\ & + pq \frac{\beta}{N} \sum_{k=0}^{N-1} |H(k)|^2 \end{aligned} \tag{5.2-28}$$

Substitution of the above result into (5.2-19) produces the following expression for the eigenvalues of the covariance matrix associated with the observed boundary process.

$$\lambda_n = p^2 \beta |H(n)|^2 + pq \left[\alpha^2 H^2(0) + \frac{\beta}{N} \sum_{k=0}^{N-1} |H(k)|^2 \right] \tag{5.2-29}$$

This expression, together with the periodogram of the observed boundary process (see equation 5.2-3), are used to evaluate the negative log-likelihood function (see equation 5.2-1) associated with the observed boundary process. The dependence of (5.2-29) and hence (5.2-1) upon the CAR descriptors is contained in the transfer function H(n)

given in (3.2-20). It is interesting to note that if there is no obscuration of the boundary (q = 0), the above expression for the eigenvalues reduces to that originally derived for the complete boundary case (see equation 4.1-12).

The equations which defined the extended negative log-likelihood function for the ML estimator of the CAR descriptors which includes the case of a partially obscured boundary are summarized below.

$$L^{-}(\vec{a}) = \ln \lambda_0 + \sum_{n=0}^{N-1} \frac{|P_\rho(n)|^2}{N} \frac{1}{\lambda_n} + \ln \lambda_n \tag{5.2-30}$$

$$\lambda_n = p^2 \beta |H(n)|^2 + pq \left[\alpha^2 H^2(0) + \frac{\beta}{N} \sum_{k=0}^{N-1} |H(k)|^2 \right] \tag{5.2-31}$$

$$H(n) = \frac{1}{1 - \sum_{k=1}^{m} a_k e^{-j 2\pi/N\, nk}} \tag{5.2-32}$$

5.3 INITIAL VALUES AND ESTIMATES OF p, q, α and β

The ML estimates of the CAR descriptors are obtained from a partially obscured boundary by minimizing the extended negative log-likelihood function derived in the previous section. To minimize the extended negative log-likelihood function using the method of DFP presented in Section 4.2 requires an initial value of the CAR descriptors. The least squares estimator of the CAR descriptors derived in Section 4.3 can again be used to obtain the initial values required by the DFP algorithm. The obscured boundary points can be treated in two ways. Either they can be set to zero, in which case the least squares estimates are computed from the observed boundary sequence $\rho(n)$, or the obscured boundary points can be interpolated. Since the amount of time required by the DFP algorithm to converge depends upon the accuracy of the initial values, the use of linearly interpolated boundary values was chosen. After the obscured boundary values are linearly interpolated from their neighbors, the least squares estimates of the CAR descriptors are computed using the results of Section 4.3.

Examination of the expression for the eigenvalues in the negative log-likelihood function (see equation 5.2-31) reveals that in addition to requiring initial values of the CAR descriptors, values of p, q, α and β associated with the CAR descriptors are also required. In fact, the evaluation of the extended negative log-likelihood function at each iteration requires estimates of p, q, α, and β associated with the then current values of the CAR descriptors. Let $\rho(n)$ be the observed sample boundary sequence and let $\gamma(n)$ and r(n) be the sample sequences of the obscuring process and complete boundary process respectively which define $\rho(n)$ (see equation 5.1-1). The expression for the mean of the obscuring process μ_γ (see equation 5.1-7) suggest the use of the sample mean of the obscuring sequence $\gamma(n)$ as an estimate of p. This estimate of p denoted $\hat{p}$ is given below

$$\hat{p} = \frac{1}{N} \sum_{n=0}^{N-1} \gamma(n) \tag{5.3-1}$$

from which the corresponding estimate of q, denoted $\hat{q}$, follows from (5.1-4).

$$\hat{q} = 1 - \hat{p} \tag{5.3-2}$$

The estimate $\hat{\alpha}$ of the value α can be derived by solving (5.2-8) for α

$$\alpha = \frac{\mu_\rho}{pH(0)} \tag{5.3-3}$$

and replacing p with the estimate $\hat{p}$ and μ_ρ with the sample mean of the observed boundary sequence $\hat{\mu}_\rho$ given below.

$$\hat{\mu}_\rho = \frac{1}{N} \sum_{n=0}^{N-1} \rho(n) \tag{5.3-4}$$

The estimator for α then becomes

$$\hat{\alpha} = \frac{\hat{\mu}_\rho}{\hat{p}\, H(0)} \tag{5.3-5}$$

where H(0) is the DC value of the transfer function (see equation 3.2-20) defined by the then current set of CAR descriptors. The estimator for β is derived by evaluating (5.2-23) at k = 0.

$$R_\rho(0) = R_\gamma(0)\, R_r(0) \tag{5.3-6}$$

This expression can be further evaluated by substituting the results of (5.1-11) at k = 0 and (3.4-28) for $R_\gamma(0)$ and $R_r(0)$ respectively.

$$R_\rho(0) = p[\mu_r^2 + \frac{\beta}{N} \sum_{n=0}^{N-1} |H(n)|^2] \tag{5.3-7}$$

The above equation is solved for β

$$\beta = \frac{R_\rho(0) - p\,\mu_r^2}{\frac{p}{N} \sum_{n=0}^{N-1} |H(n)|^2} \tag{5.3-8}$$

and (3.4-1) is substituted for μ_r.

$$\beta = \frac{R_\rho(0) - p\,\alpha^2\, H^2(0)}{\frac{p}{N} \sum_{n=0}^{N-1} |H(n)|^2} \tag{5.3-9}$$

Sample estimates are available for all the parameters on the right-hand side of (5.3-9) except $R_\rho(0)$, which is given below and denoted $\hat{R}_\rho(0)$.

$$\hat{R}_\rho(0) = \frac{1}{N} \sum_{n=0}^{N-1} \rho^2(n) \tag{5.3-10}$$

The estimator for β is obtained by substituting (5.3-1), (5.3-5) and (5.3-10) into (5.3-9).

$$\hat{\beta} = \frac{\hat{R}_\rho(0) - \hat{p}\,\hat{\alpha} H^2(0)}{\frac{\hat{p}}{N} \sum_{n=0}^{N-1} |H(n)|^2} \tag{5.3-11}$$

As with the estimate $\hat{\alpha}$ above (see equation 5.3-5), the transfer function H(n) is evaluated using the then current set of CAR descriptors.

The minimization algorithm of DFP can now be initialized using the least squares estimates of the linearly interpolated sample boundary sequence $\rho(n)$ and the estimates $\hat{p}$, $\hat{q}$, $\hat{\alpha}$, and $\hat{\beta}$. At each iteration a new set of CAR descriptors are obtained and the estimates of $\hat{\alpha}$, and $\hat{\beta}$ are updated using the new values of the CAR descriptors.

5.4 ASYMPTOTIC PROPERTIES OF THE EXTENDED ML ESTIMATOR

The extended ML estimator derived in Section 5.2 is a member of the general class of estimators of finite parameter models of asymptotically stationary time series. Furthermore, the asymptotically stationary time series considered in the above class of estimators include more general (obscuring) functions $\gamma(n)$. These functions are able to take on values other than zero and one. They are capable of modeling amplitude modulation of the time series. Dunsmuir and Robinson [32] have established the asymptotic consistency of these estimators. This means that the extended ML estimator of the CAR descriptors converges in probability to the actual values. That is, the bias (if there is any) and the variance of the estimator go to zero as the number of samples N increases. They also demonstrate that the estimates are asymptotically efficient and that the estimation error is asymptotically Gaussian distributed with zero mean. Consequently, the asymptotic distribution of the estimation error is completely specified by its mean and covariance. As was just mentioned, the mean has been shown to be zero, and since the estimates are asymptotically efficient, the covariance matrix is given by the Cramer-Rao lower bound. This lower bound, and hence the covariance matrix Σ_a of the asymptotic error, will be derived for the extended ML estimates of the CAR descriptors.

The asymptotic error covariance matrix Σ_a is defined to be

$$\Sigma_a = E\{(\hat{\vec{a}} - \vec{a})(\hat{\vec{a}} - \vec{a})'\} \tag{5.4-1}$$

where $\vec{a}$ is the actual set of CAR descriptors. This covariance matrix is also equal to the Cramer-Rao lower bound given below.

$$\Sigma_a = \left[-E\left\{ \frac{\partial^2 L(\vec{a})}{\partial a_i \, \partial a_j} \right\} \right]^{-1} \tag{5.4-2}$$

The above equality is replaced by the 'greater than or equal to' inequality for a finite number of samples. The likelikhood function $L(\vec{a})$ was previously defined in Section 4.1 and is repeated below for reference.

$$L(\vec{a}) = -\frac{1}{2}(\vec{r} - \vec{\mu}_r)' \Sigma_r^{-1} (\vec{r} - \vec{\mu}_r) - \frac{1}{2}\ln|\Sigma_r| - \frac{N}{2}\ln(2\pi) \tag{5.4-3}$$

During the derivation of the negative log-likelihood function, it was shown (see equation 4.1-23) that the first two terms of the above equation could be simplified to yield the following result

$$L(\vec{a}) = -\frac{1}{2}\sum_{n=0}^{N-1} \frac{|P_\rho(n)|^2}{N}\frac{1}{\lambda_n} + \ln\lambda_n - \frac{N}{2}\ln(2\pi) \tag{5.4-4}$$

where λ_n is given by (5.2-31) and the definition in (5.2-3) is used. The first and second order partial derivatives are evaluated below.

$$\frac{\partial L(\vec{a})}{\partial a_i} = -\frac{1}{2}\sum_{n=0}^{N-1} \frac{|P_\rho(n)|^2}{N}\left(\frac{-1}{\lambda_n^2}\right)\frac{\partial\lambda_n}{\partial a_i} + \frac{1}{\lambda_n}\frac{\partial\lambda_n}{\partial a_i} \tag{5.4-5}$$

$$\frac{\partial^2 L(\vec{a})}{\partial a_i\,\partial a_j} = -\frac{1}{2}\sum_{n=0}^{N-1} \frac{|P_\rho(n)|^2}{N}\left[\left(\frac{-1}{\lambda_n^2}\frac{\partial^2\lambda_n}{\partial a_i\,\partial a_j} + \frac{2}{\lambda_n^3}\frac{\partial\lambda_n}{\partial a_i}\frac{\partial\lambda_n}{\partial a_j}\right]\right. \tag{5.4-6}$$

$$\left. + \left[\frac{1}{\lambda_n}\frac{\partial^2\lambda_n}{\partial a_i\,\partial a_j} - \frac{1}{\lambda_n^2}\frac{\partial\lambda_n}{\partial a_i}\frac{\partial\lambda_n}{\partial a_j}\right]\right.$$

Since the periodogram of a sample sequence of a process is an asymptotically unbiased estimate of the power spectral density of the process [34], it follows that

$$E\left\{\frac{|P_\rho(n)|^2}{N}\right\} = \lambda_n \tag{5.4-7}$$

which can be used to evaluate the negative expectation in (5.4-2).

$$-E\left\{\frac{\partial^2 L(\vec{a})}{\partial a_i\,\partial a_j}\right\} = \frac{1}{2}\sum_{n=0}^{N-1}\frac{1}{\lambda_n^2}\frac{\partial\lambda_n}{\partial a_i}\frac{\partial\lambda_n}{\partial a_j} \tag{5.4-8}$$

The partial derivatives of the eigenvalues are given in Appendix A. The covariance matrix Σ_a of the asymptotic error is equal to the inverse of the m $\times$ m matrix whose i, j-th element is given by the above equation.

5.5 THE PERIODOGRAM APPROXIMATION

If the statistical model of the obscuring process $\gamma(n)$ is unknown, then the eigenvalues of the covariance matrix Σ_ρ of the observed boundary process $\rho(n)$ cannot be evaluated analytically. In this case an approximate form of the extended negative log-likelihood function can be used. Since conditions for asymptotic stationarity of the observed boundary process did not depend upon the statistical model of the obscuring process, the results of (5.2-18) and (5.2-25) are still valid. Substituting (5.2-25) into (5.2-18) produces the following result

$$\lambda_n = \frac{1}{N} \sum_{k=0}^{N-1} S_\gamma(k)\, S_r(n-k) - \mu_\rho^2\, N\, \delta(n) \tag{5.5-1}$$

where the convolution sum of (5.2-25) has been rearranged. The expression for the power spectral density $S_r(n)$ of the complete boundary process r(n) given in (3.4-24) can be substituted into the above equation.

$$\lambda_n = \frac{1}{N} \sum_{k=0}^{N-1} S_\gamma(k)\, [\mu_r^2\, N\, \delta(n-k) + \beta\, |H(n-k)|^2] - \mu_\rho^2\, N\, \delta(n) \tag{5.5-2}$$

The above convolution sum can be expanded and evaluated.

$$\lambda_n = \mu_r^2\, S_\gamma(n) + \frac{\beta}{N} \sum_{k=0}^{N-1} S_\gamma(k)\, |H(n-k)|^2 - \mu_\rho^2\, N\, \delta(n) \tag{5.5-3}$$

Since the statistical model for the obscuring process is unknown, the power spectral density $S_\gamma(n)$ cannot be determined analytically. Since a sample sequence $\gamma(n)$ of the obscuring process is available, the periodogram of this sample sequence can be used as an estimate of the power spectral density $S_\gamma(n)$ in the above equation. Let $P_\gamma(n)$ be the DFT of the sample sequence of the obscuring process,

$$P_\gamma(n) = \sum_{k=0}^{N-1} \gamma(k)\, e^{-j\, 2\pi/N\, nk} \tag{5.5-4}$$

then the periodogram is defined as follows.

$$\frac{|P_\gamma(n)|^2}{N} \tag{5.5-5}$$

Substitution of the above periodogram of $\gamma(n)$ for the power spectral density $S_\gamma(n)$ in (5.5-3) produces the following estimates of the eigenvalues.

$$\hat{\lambda}_n = \mu_r^2 \frac{|P_\gamma(n)|^2}{N} + \frac{\beta}{N} \sum_{k=0}^{N-1} \frac{|P_\gamma(k)|^2}{N} |H(n-k)|^2 - \mu_\rho^2 N \delta(n) \tag{5.5-6}$$

$$= \mu_r^2 \frac{|P_\gamma(n)|^2}{N} + \frac{\beta}{N^2} \sum_{k=0}^{N-1} |P_\gamma(k)\, H(n-k)|^2 - \mu_\rho^2 N \delta(n) \tag{5.5-7}$$

It has been shown [32] that the use of the above estimates of the eigenvalues in the extended negative log-likelihood function (see equation 5.2-30) produces estimates of the CAR descriptors which are both asymptotically consistent and efficient.

Actual implementation of this approximation to the extended negative log-likelihood function requires estimates of μ_ρ, μ_r and β which do not depend upon the statistical model of the obscuring process. The sample mean $\hat{\mu}_\rho$ of the observed sample boundary sequence $\rho(n)$ can be used as an estimate of μ_ρ.

$$\hat{\mu}_\rho = \frac{1}{N} \sum_{n=0}^{N-1} \rho(n) \tag{5.5-8}$$

An estimate of the mean μ_r of the complete boundary process can be obtained by solving (5.2-7) for μ_r

$$\mu_r = \frac{\mu_\rho}{\mu_\gamma} \tag{5.5-9}$$

and using $\hat{\mu}_\rho$ of (5.5-8) and the sample mean $\hat{\mu}_\gamma$ of the sample obscuring sequence defined below

$$\hat{\mu}_\gamma = \frac{1}{N} \sum_{n=0}^{N-1} \gamma(n) \tag{5.5-10}$$

in (5.5-9) for μ_ρ and μ_γ respectively.

$$\hat{\mu}_r = \frac{\hat{\mu}_\rho}{\hat{\mu}_\gamma} \tag{5.5-11}$$

Since the obscuring process $\gamma(n)$ is stationary its mean is a constant. If a frequency of occurance interpretation is given to (5.5-10), that constant can be associated with the parameter p with the following result independent of the statistical model of the obscuring process.

$$\mu_\gamma = p \tag{5.5-12}$$

Therefore an estimate $\hat{p}$ of p can be obtained as follows from (5.5-10).

$$\hat{p} = \hat{\mu}_\gamma \tag{5.5-13}$$

An estimate of β can now be obtained from (5.3-8) by substituting the estimates for $R_\rho(0)$, p and μ_r given in (5.3-10), (5.5-13) and (5.5-11) respectively into (5.3-8).

$$\hat{\beta} = \frac{\hat{R}_\rho(0) - \hat{p}\,\hat{\mu}_r^2}{\frac{\hat{p}}{N} \sum_{n=0}^{N-1} |H(n)|^2} \tag{5.5-14}$$

These estimates of μ_ρ, μ_r and β do not depend upon the statistical model of the obscuring process and can be used with the method of DFP to obtain estimates of the CAR descriptors.

6.0 EXPERIMENTAL ESTIMATION RESULTS FOR THE EXTENDED ML ESTIMATOR

The purpose of the two experiments performed in this chapter is to demonstrate that the extended ML estimator can provide estimates of the CAR descriptors which have sufficiently small variance to be useful in classifying the shapes they are derived from. These experiments also provide insights which will be helpful in understanding and analyzing the classification results obtained in Chapter 7. In the first experiment, synthetically generated boundary data is used to test the performance of the estimator on four different shape classes. In this experiment the model is perfectly fit to the boundary process and all parameters are known. Real aircraft boundary sequences are used in the second experiment which results in a model fit which is less than perfect and all parameters are estimated from the observed boundary sequence. In both experiments the performance of the extended ML estimator is observed as the amount of boundary obscuration is increased. The second experiment which uses the real boundary data is structured to demonstrate the invariance of the CAR descriptors to within class variations.

6.1 ESTIMATES FROM SYNTHETIC BOUNDARY DATA

The purpose of these experiments is to measure the performance of the extended ML estimator under ideal conditions as the amount of obscuration q is increased. By ideal conditions it is meant that the boundary process is in fact a CAR process of known order m and that the statistical model of the obscuring process is known. Four third order (m = 3) CAR processes were chosen to be the boundary processes associated with the shape classes. The CAR diagrams of these shape classes are shown in Figures 6.1-1 to 6.1-4. The pole shown in the CAR diagram of each shape class has multiplicity three. For example, shape class 1 has all three poles located at .6. The same is true for shape classes 2, 3, and 4, which have poles of multiplicity three located at .7, .8, and .9 respectively. The CAR descriptors which identify these shape classes were computed from the poles of each class using (3.3-6), (3.3-7), and (3.3-8). These results are reported in Table 6.1-1 below.

One hundred sample boundaries were generated for each shape class using the DFT technique presented in Section 3.2. The parameters α and β were assigned the values of zero and one respectively.The number of boundary samples N was chosen to

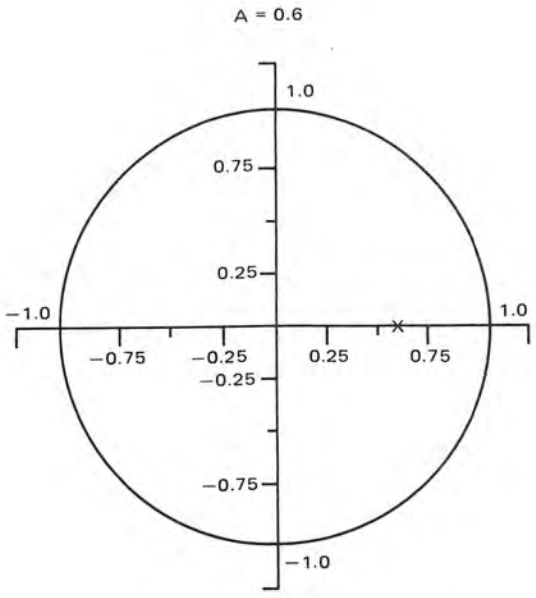

Figure 6.1–1. CAR Diagram of Shape Class 1

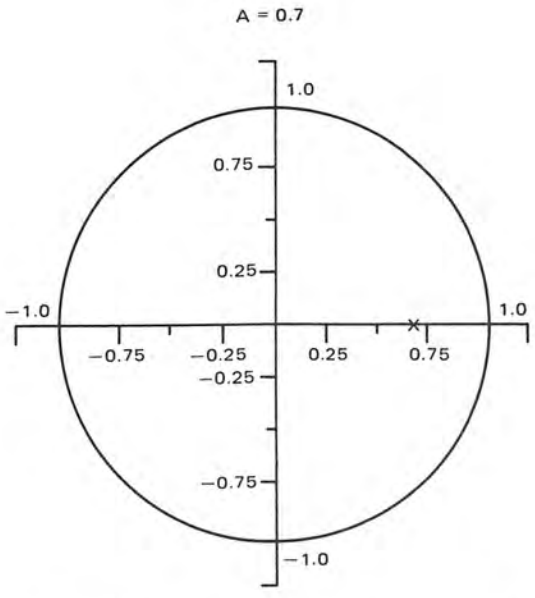

Figure 6.1–2. CAR Diagram of Shape Class 2

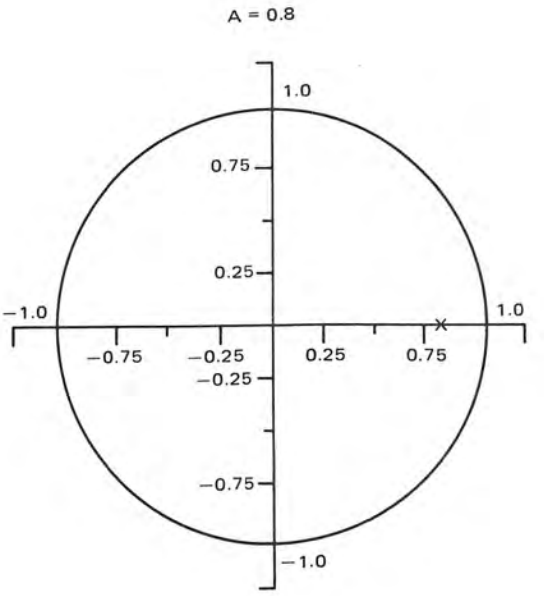

Figure 6.1–3. CAR Diagram of Shape Class 3

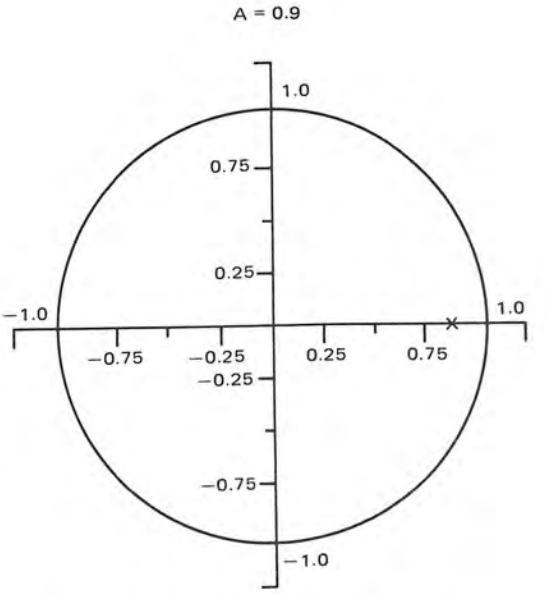

Figure 6.1–4. CAR Diagram of Shape Class 4

TABLE 6.1–1. CAR DESCRIPTORS OF THE FOUR SHAPE CLASSES

	1	2	3	4
a_1	1.80	2.10	2.40	2.70
a_2	−1.08	−1.47	−1.92	−2.43
a_3	.22	.34	.51	.73

be 256 so that the efficiencies of the FFT algorithm could be realized in computing the periodogram of the observed boundary sequences. The observed sample boundary sequences $\rho(n)$ were generated from the complete boundary sequences r(n) using the Bernoulli model of the obscuring process presented in Section 5.1. The obscuration parameter q was varied from zero up to 70% obscuration in increments of 10%.

The sample covariance matrices of the extended ML estimates were computed for each of the shape classes used in the experiment. These results are reported in Tables 6.1–2 to 6.1–5 for all eight values of q which were used. Since the boundary data were synthetically generated, all of the experimental parameters are known. The values of these parameters were used to evaluate the Cramer-Rao lower bound on the covariance of the extend ML estimates which was derived in Section 5.4. These results are presented for each of the shape classes alongside the experimental results in Tables 6.1–2 to 6.1–5. The agreement between the experimental results and the Cramer-Rao lower bound is good for small amounts of obscuration, but decreases as the probability of obsuration increases. This indicates that the rate at which the covariance of the estimates approaches the Cramer-Rao lower bound decreases with increasing amounts of obscuration.

The rate of convergence also depends upon the stationarity of the CAR process associated with the shape class. In Section 3.3 it was established that the stationarity of a CAR process decreased as the poles associated with it moved closer to the unit circle. These results indicate that the rate of convergence between the experimental results and the Cramer-Rao lower bound decreases with the stationarity of the underlying CAR process. This relationship will be examined further in the analysis of the classification results presented in Section 7.2. Several other observations can also be

TABLE 6.1–2. COVARIANCE MATRICES OF SHAPE CLASS 1

EXPERIMENTAL RESULTS	CRAMER-RAO LOWER BOUND
$\begin{pmatrix} .452 & -.736 & .338 \\ -.736 & 1.37 & -.714 \\ .338 & -.714 & .422 \end{pmatrix} \times 10^{-2}$ q = 0.	$\begin{pmatrix} .371 & -.610 & .267 \\ -.610 & 1.18 & -.610 \\ .267 & -.610 & .371 \end{pmatrix} \times 10^{-2}$ q = 0.
$\begin{pmatrix} 1.54 & -2.79 & 1.40 \\ -2.79 & 5.53 & -2.97 \\ 1.40 & -2.97 & 16.9 \end{pmatrix} \times 10^{-2}$ q = .10	$\begin{pmatrix} .759 & -1.58 & .838 \\ -1.58 & 3.49 & -1.94 \\ .838 & -1.94 & 1.14 \end{pmatrix} \times 10^{-2}$ q = .10
$\begin{pmatrix} 2.42 & -4.87 & 2.57 \\ -4.87 & 10.2 & -5.56 \\ 2.57 & -5.56 & 3.12 \end{pmatrix} \times 10^{-2}$ q = .20	$\begin{pmatrix} 1.15 & -2.48 & 1.33 \\ -2.48 & 5.51 & -3.07 \\ 1.33 & -3.07 & 1.78 \end{pmatrix} \times 10^{-2}$ q = .20
$\begin{pmatrix} 3.03 & -6.19 & 3.27 \\ -6.19 & 13.1 & -7.12 \\ 3.27 & -7.12 & 3.98 \end{pmatrix} \times 10^{-2}$ q = .30	$\begin{pmatrix} 1.70 & -3.69 & 2.00 \\ -3.69 & 8.17 & -4.54 \\ 2.00 & -4.54 & 2.60 \end{pmatrix} \times 10^{-2}$ q = .30
$\begin{pmatrix} 4.54 & -9.53 & 5.15 \\ -9.53 & 20.4 & -11.2 \\ 5.15 & -11.2 & 6.33 \end{pmatrix} \times 10^{-2}$ q = .40	$\begin{pmatrix} 2.49 & -5.40 & 2.92 \\ -5.40 & 11.9 & -6.57 \\ 2.92 & -6.57 & 3.71 \end{pmatrix} \times 10^{-2}$ q = .40
$\begin{pmatrix} 6.40 & -13.4 & 7.24 \\ -13.4 & 28.7 & -15.6 \\ 7.24 & -15.6 & 8.66 \end{pmatrix} \times 10^{-2}$ q = .50	$\begin{pmatrix} 3.69 & -7.98 & 4.31 \\ -7.98 & 17.4 & -9.58 \\ 4.31 & -9.58 & 5.35 \end{pmatrix} \times 10^{-2}$ q = .50
$\begin{pmatrix} 14.0 & -29.4 & 15.6 \\ -29.4 & 62.2 & -33.3 \\ 15.6 & -33.3 & 18.0 \end{pmatrix} \times 10^{-2}$ q = .60	$\begin{pmatrix} 5.68 & -12.2 & 6.58 \\ -12.2 & 26.6 & -14.4 \\ 6.58 & -14.4 & 8.00 \end{pmatrix} \times 10^{-2}$ q = .60
$\begin{pmatrix} 20.1 & -42.1 & 22.3 \\ -42.1 & 89.3 & -47.8 \\ 22.3 & -47.8 & 25.9 \end{pmatrix} \times 10^{-2}$ q = .70	$\begin{pmatrix} 9.45 & -20.2 & 10.8 \\ -20.2 & 43.7 & -23.6 \\ 10.8 & -23.6 & 12.9 \end{pmatrix} \times 10^{-2}$ q = .70

TABLE 6.1–3. COVARIANCE MATRICES OF SHAPE CLASS 2

EXPERIMENTAL RESULTS	CRAMER-RAO LOWER BOUND
$\begin{pmatrix} .411 & -.729 & .343 \\ -.729 & 1.38 & -.695 \\ .343 & -.695 & .374 \end{pmatrix} \times 10^{-2}$ $q = 0.$	$\begin{pmatrix} .345 & -.625 & .295 \\ -.625 & 1.22 & -.625 \\ .295 & -.625 & .345 \end{pmatrix} \times 10^{-2}$ $q = 0.$
$\begin{pmatrix} 1.59 & -3.06 & 1.55 \\ -3.06 & 6.12 & -3.19 \\ 1.55 & -3.19 & 1.71 \end{pmatrix} \times 10^{-2}$ $q = .10$	$\begin{pmatrix} .700 & -1.47 & .787 \\ -1.47 & 3.18 & -1.73 \\ .787 & -1.73 & .970 \end{pmatrix} \times 10^{-2}$ $q = .10$
$\begin{pmatrix} 3.56 & -7.26 & 3.79 \\ -7.26 & 14.9 & -7.91 \\ 3.79 & -7.91 & 4.22 \end{pmatrix} \times 10^{-2}$ $q = .20$	$\begin{pmatrix} 1.02 & -2.18 & 1.17 \\ -2.18 & 4.72 & -2.57 \\ 1.17 & -2.57 & 1.42 \end{pmatrix} \times 10^{-2}$ $q = .20$
$\begin{pmatrix} 4.14 & -8.47 & 4.40 \\ -8.47 & 17.5 & -9.19 \\ 4.40 & -9.19 & 4.87 \end{pmatrix} \times 10^{-2}$ $q = .30$	$\begin{pmatrix} 1.43 & -3.06 & 1.64 \\ -3.06 & 6.59 & -3.57 \\ 1.64 & -3.57 & 1.96 \end{pmatrix} \times 10^{-2}$ $q = .30$
$\begin{pmatrix} 4.97 & -10.1 & 5.28 \\ -10.1 & 21.0 & -11.0 \\ 5.28 & -11.0 & 5.82 \end{pmatrix} \times 10^{-2}$ $q = .40$	$\begin{pmatrix} 1.98 & -4.22 & 2.25 \\ -4.22 & 9.06 & -4.89 \\ 2.25 & -4.89 & 2.67 \end{pmatrix} \times 10^{-2}$ $q = .40$
$\begin{pmatrix} 5.78 & -11.9 & 6.25 \\ -11.9 & 24.9 & -13.1 \\ 6.25 & -13.1 & 7.02 \end{pmatrix} \times 10^{-2}$ $q = .50$	$\begin{pmatrix} 2.77 & -5.88 & 3.14 \\ -5.88 & 12.5 & -6.76 \\ 3.14 & -6.76 & 3.66 \end{pmatrix} \times 10^{-2}$ $q = .50$
$\begin{pmatrix} 9.52 & -19.7 & 10.3 \\ -19.7 & 41.3 & -21.6 \\ 10.3 & -21.6 & 11.4 \end{pmatrix} \times 10^{-2}$ $q = .60$	$\begin{pmatrix} 4.01 & -8.50 & 4.51 \\ -8.50 & 18.1 & -9.67 \\ 4.51 & -9.67 & 5.21 \end{pmatrix} \times 10^{-2}$ $q = .60$
$\begin{pmatrix} 45.0 & -91.4 & 46.5 \\ -91.4 & 186. & -94.9 \\ 46.5 & -94.9 & 48.6 \end{pmatrix} \times 10^{-2}$ $q = .70$	$\begin{pmatrix} 6.26 & -13.2 & 6.99 \\ -13.2 & 28.0 & -14.8 \\ 6.99 & -14.8 & 7.95 \end{pmatrix} \times 10^{-2}$ $q = .70$

TABLE 6.1–4. COVARIANCE MATRICES OF SHAPE CLASS 3

EXPERIMENTAL RESULTS	CRAMER-RAO LOWER BOUND
$\begin{pmatrix} .328 & -.612 & .292 \\ -.612 & 1.17 & -.574 \\ .292 & -.574 & .289 \end{pmatrix} \times 10^{-2}$ $q = 0.$	$\begin{pmatrix} .289 & -.555 & .271 \\ -.555 & 1.09 & -.555 \\ .271 & -.555 & .289 \end{pmatrix} \times 10^{-2}$ $q = 0.$
$\begin{pmatrix} 1.03 & -2.04 & 1.03 \\ -2.04 & 4.10 & -2.09 \\ 1.03 & -2.09 & 1.08 \end{pmatrix} \times 10^{-2}$ $q = .10$	$\begin{pmatrix} .560 & -1.17 & .614 \\ -1.17 & 2.46 & -1.30 \\ .614 & -1.30 & .696 \end{pmatrix} \times 10^{-2}$ $q = .10$
$\begin{pmatrix} 1.44 & -2.94 & 1.51 \\ -2.94 & 6.03 & -3.12 \\ 1.51 & -3.12 & 1.63 \end{pmatrix} \times 10^{-2}$ $q = .20$	$\begin{pmatrix} .781 & -1.63 & .859 \\ -1.63 & 3.43 & -1.81 \\ .859 & -1.81 & .968 \end{pmatrix} \times 10^{-2}$ $q = .20$
$\begin{pmatrix} 3.29 & -6.71 & 3.45 \\ -6.71 & 13.7 & -7.10 \\ 3.45 & -7.10 & 3.68 \end{pmatrix} \times 10^{-2}$ $q = .30$	$\begin{pmatrix} 1.03 & -2.16 & 1.13 \\ -2.16 & 4.55 & -2.40 \\ 1.13 & -2.40 & 1.27 \end{pmatrix} \times 10^{-2}$ $q = .30$
$\begin{pmatrix} 8.82 & -18.0 & 9.29 \\ -19.0 & 37.0 & -19.0 \\ 9.29 & -19.0 & 9.84 \end{pmatrix} \times 10^{-2}$ $q = .40$	$\begin{pmatrix} 1.36 & -2.84 & 1.48 \\ -2.84 & 5.95 & -3.13 \\ 1.48 & -3.13 & 1.65 \end{pmatrix} \times 10^{-2}$ $q = .40$
$\begin{pmatrix} 11.3 & -23.0 & 11.7 \\ -23.0 & 46.9 & -24.0 \\ 11.7 & -24.0 & 12.3 \end{pmatrix} \times 10^{-2}$ $q = .50$	$\begin{pmatrix} 1.80 & -3.76 & 1.96 \\ -3.76 & 7.86 & -4.12 \\ 1.96 & -4.12 & 2.17 \end{pmatrix} \times 10^{-2}$ $q = .50$
$\begin{pmatrix} 17.0 & -34.7 & 17.8 \\ -34.7 & 71.2 & -36.6 \\ 17.8 & -36.6 & 18.8 \end{pmatrix} \times 10^{-2}$ $q = .60$	$\begin{pmatrix} 2.47 & -5.14 & 2.68 \\ -5.14 & 10.7 & -5.61 \\ 2.68 & -5.61 & 2.94 \end{pmatrix} \times 10^{-2}$ $q = .60$
$\begin{pmatrix} 62.0 & -125. & 63.6 \\ -125. & 253. & -128. \\ 63.6 & -128. & 65.4 \end{pmatrix} \times 10^{-2}$ $q = .70$	$\begin{pmatrix} 3.63 & -7.53 & 3.91 \\ -7.53 & 15.6 & -8.16 \\ 3.91 & -8.16 & 4.26 \end{pmatrix} \times 10^{-2}$ $q = .70$

TABLE 6.1–5. COVARIANCE MATRICES OF SHAPE CLASS 4

EXPERIMENTAL RESULTS	CRAMER-RAO LOWER BOUND
$\begin{pmatrix} .194 & -.380 & .187 \\ -.380 & .750 & -.371 \\ .187 & -.371 & .185 \end{pmatrix} \times 10^{-2}$ $q = 0.$	$\begin{pmatrix} .183 & -.362 & .180 \\ -.362 & .724 & -.362 \\ .180 & -.362 & .183 \end{pmatrix} \times 10^{-2}$ $q = 0.$
$\begin{pmatrix} .682 & -1.38 & .707 \\ -1.38 & 2.82 & -1.44 \\ .707 & -1.44 & .741 \end{pmatrix} \times 10^{-2}$ $q = .10$	$\begin{pmatrix} .356 & -.728 & .372 \\ -.728 & 1.49 & -.764 \\ .372 & -.764 & .392 \end{pmatrix} \times 10^{-2}$ $q = .10$
$\begin{pmatrix} .941 & -1.91 & .979 \\ -1.91 & 3.91 & -2.00 \\ .979 & -2.00 & 1.02 \end{pmatrix} \times 10^{-2}$ $q = .20$	$\begin{pmatrix} .483 & -.987 & .505 \\ -.987 & 2.02 & -1.03 \\ .505 & -1.03 & .532 \end{pmatrix} \times 10^{-2}$ $q = .20$
$\begin{pmatrix} 2.18 & -4.43 & 2.25 \\ -4.43 & 9.02 & -4.59 \\ 2.25 & -4.59 & 2.34 \end{pmatrix} \times 10^{-2}$ $q = .30$	$\begin{pmatrix} .624 & -1.27 & .652 \\ -1.27 & 2.61 & -1.33 \\ .652 & -1.33 & .685 \end{pmatrix} \times 10^{-2}$ $q = .30$
$\begin{pmatrix} 4.02 & -8.15 & 4.13 \\ -8.15 & 16.5 & -8.37 \\ 4.13 & -8.37 & 4.24 \end{pmatrix} \times 10^{-2}$ $q = .40$	$\begin{pmatrix} .799 & -1.63 & 8.33 \\ -1.63 & 3.33 & -1.70 \\ .833 & -1.70 & .874 \end{pmatrix} \times 10^{-2}$ $q = .40$
$\begin{pmatrix} 2.90 & -5.89 & 2.99 \\ -5.89 & 11.9 & -6.08 \\ 2.99 & -6.08 & 3.09 \end{pmatrix} \times 10^{-2}$ $q = .50$	$\begin{pmatrix} 1.03 & -2.10 & 1.07 \\ -2.10 & 4.30 & -2.19 \\ 1.07 & -2.19 & 1.12 \end{pmatrix} \times 10^{-2}$ $q = .50$
$\begin{pmatrix} 8.48 & -17.1 & 8.67 \\ -17.1 & 34.6 & -17.6 \\ 8.67 & -17.6 & 8.93 \end{pmatrix} \times 10^{-2}$ $q = .60$	$\begin{pmatrix} 1.37 & -2.80 & 1.43 \\ -2.80 & 5.72 & -2.92 \\ 1.43 & -2.92 & 1.49 \end{pmatrix} \times 10^{-2}$ $q = .60$
$\begin{pmatrix} 12.2 & -24.7 & 12.5 \\ -24.7 & 50.0 & -25.3 \\ 12.5 & -25.3 & 12.8 \end{pmatrix} \times 10^{-2}$ $q = .70$	$\begin{pmatrix} 1.95 & -3.98 & 2.02 \\ -3.98 & 8.10 & -4.12 \\ 2.02 & -4.12 & 2.10 \end{pmatrix} \times 10^{-2}$ $q = .70$

made. The variance of the estimates generally increases as the amount of obscuration increases. The variances of $\hat{a}_1$ and $\hat{a}_3$ are approximately equal and the variance of $\hat{a}_2$ is about four times the variances of $\hat{a}_1$ and $\hat{a}_3$. The covariance of $\hat{a}_1$ and $\hat{a}_3$ is positive, but the covariance of $\hat{a}_2$ and either $\hat{a}_1$ or $\hat{a}_3$ is negative. This is an interesting result, especially in light of the negative sign which appears in (3.3–7).

All of the experimental results obtained in this section were within reasonable limits and encourage the further testing of the extended ML estimator. In the next section the estimator is tested on real boundary data under less favorable conditions.

6.2 EXTENDED ML ESTIMATES USING REAL BOUNDARY DATA

The extended ML estimator was tested on real aircraft boundary data. Aircraft boundaries have traditionally been chosen as a source of real data on which to test shape descriptors [6, 13, 14, 15] because they possess interesting shapes which include both concavities and sharp corners. The conditions under which these tests were performed were significantly more severe than those found in the synthetic data experiments of the previous section. The boundary was again modeled as a third order ($m = 3$) CAR process, but this time the model fit was not perfect. Also, the same Bernoulli obscuring process was used so that the form of the estimator would be the same, but the obscuration parameter q was assumed to be unknown. The tests were repeated as the amount of obscuration q increased from zero to 40% in 10% increments. Additionally, all of the parameters, including q, were *unknown* and had to be estimated from the observed boundary sequence using the estimators derived in Section 5.3

The extended ML estimator was tested on the classes of swept-wing and straight-wing aircraft. The class of swept wing aircraft, shape class A, consist of the aircraft types A1 and A2 shown in Figures 6.2–1 and 6.2–2. Shape class B represents the two straight wing aircraft B1 and B2 shown in Figures 6.2–3 and 6.2–4. Each shape class contains more than one aircraft type so that the insensitivity of the CAR descriptors to within class variations could be demonstrated. Another source of within class variation is segmentation error. This was modeled by adding plus or minus one pixel of uniformly distributed white noise to the boundary samples. The number of

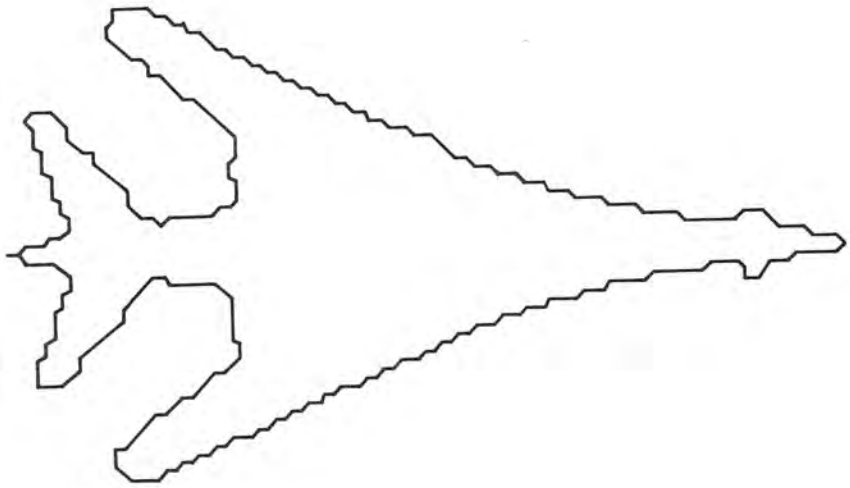

Figure 6.2–1. Swept Wing Aircraft Type A1

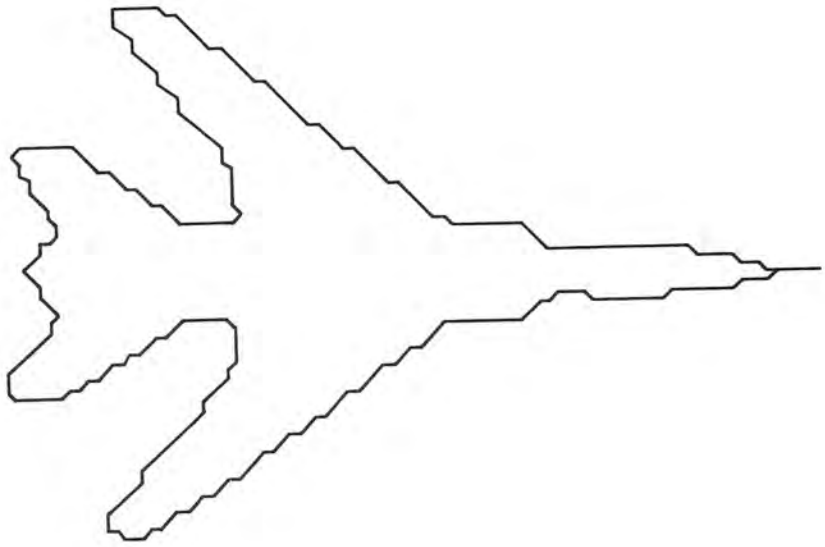

Figure 6.2–2. Swept Wing Aircraft Type A2

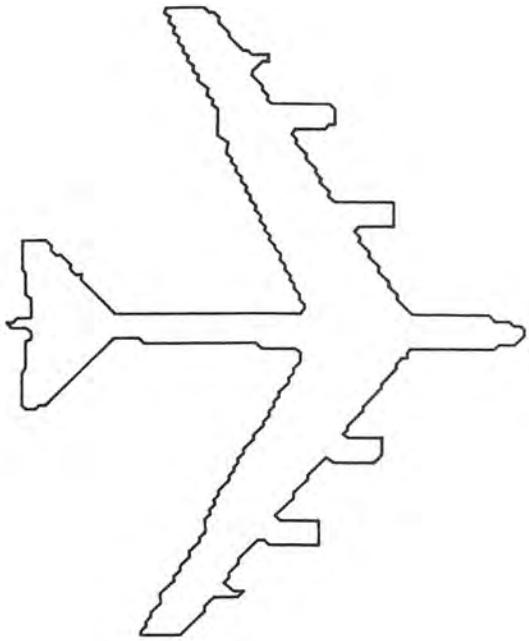

Figure 6.2–3. Straight Wing Aircraft Type B1

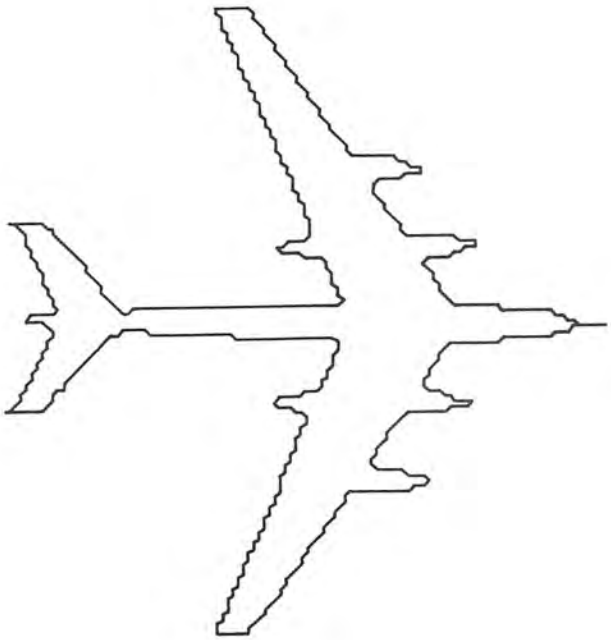

Figure 6.2–4. Straight Wing Aircraft Type B2

boundary samples was chosen as 256 again in order to take advantage of the computational efficiencies of the FTT algorithm and to maintain consistency with the previous section.

The extended ML estimates were computed from 200 sample boundary sequences of each shape class. These sample boundary sequences were equally distributed among the members of the shape classes. The extended ML estimates of the CAR descriptors computed from the complete boundary sequences ($q = 0$) of each aircraft type (e.g., A1) were used to construct the CAR diagrams shown in Figures 6.2-5, 6.2-6, 6.2-7, and 6.2-8. Notice that for both shape classes A and B the pole locations of the two members within a shape class are very close, yet there are distinct differences between the CAR diagrams of the two shape classes. For example, the poles of shape class A are all real, whereas shape class B has a complex conjugate pair of poles. These results are important because they show that the CAR descriptors are tolerant of within class variations. If this were not the case, then the similarity of the CAR diagrams of A1 and A2 or of B1 and B2 would indicate that the CAR descriptors are merely describing a generic plane shape. But since the CAR diagrams of shape class A and B are distinctly different, they must be describing the shape of swept and straight-wing aircraft respectively.

The contention that the CAR descriptors are tolerant of within class variations is further supported by the sample covariance matrices computed for each shape class and reported in Tables 6.2-1 and 6.2-2. If the CAR descriptors were at all sensitive to within class variations it would be expected that the covariance values would be larger. The insensitivity of the CAR descriptors to within class variation has application in the perception of three-dimensional objects. The CAR descriptors are expected to be insensitive to minor rotations of the object out of the image plane. This reduces the number of different perspective classes which must be defined for each shape class.

The observations made about the covariance of the estimates in the previous section are further substantiated by the results of these tests. The variance of the estimates generally increases with increasing amounts of obscuration. The variance of $\hat{a}_1$ and $\hat{a}_3$ are approximately equal and the variance of $\hat{a}_2$ is about four times the variance of $\hat{a}_1$, or $\hat{a}_3$. The covariance of $\hat{a}_2$ and either $\hat{a}_1$ or $\hat{a}_3$ is negative; all other covariances are positive.

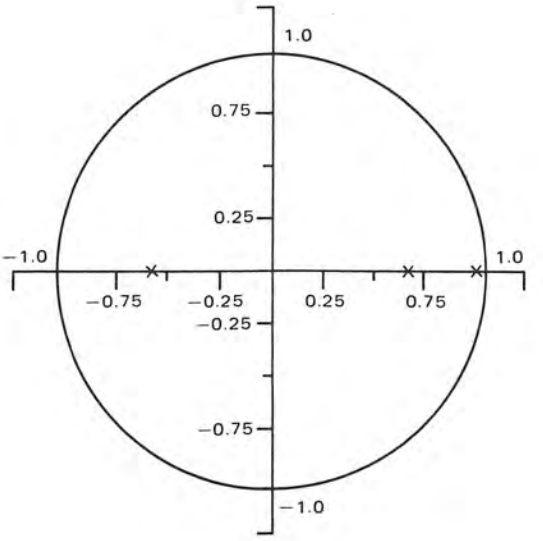

Figure 6.2–5. CAR Diagram of Aircraft Type A1

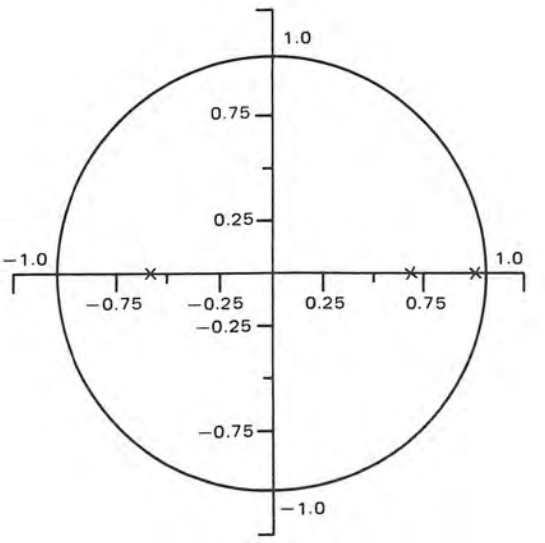

Figure 6.2–6. CAR Diagram of Aircraft Type A2

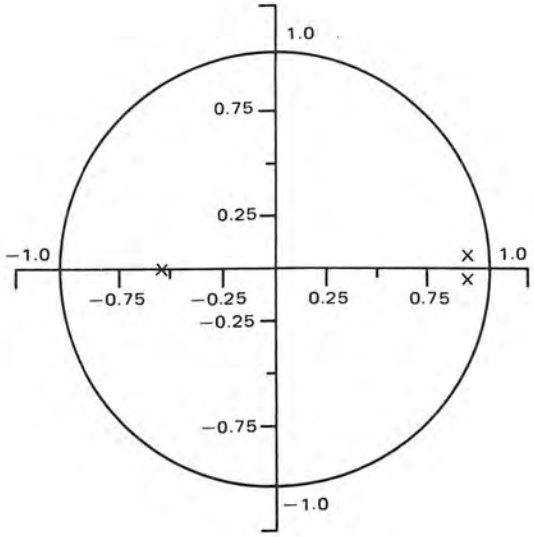

Figure 6.2–7. CAR Diagram of Aircraft Type B1

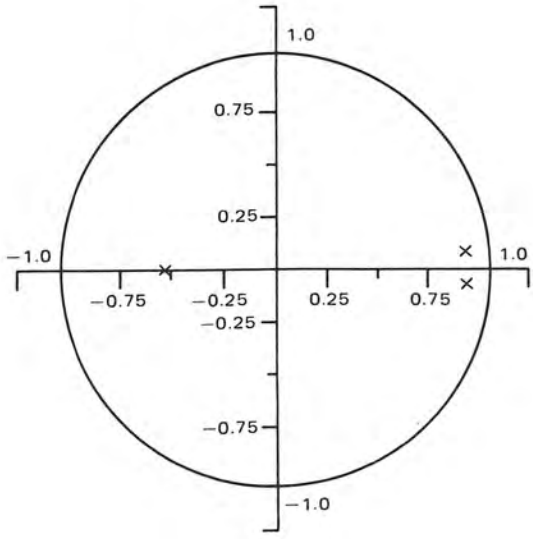

Figure 6.2–8. CAR Diagram of Aircraft Type B2

TABLE 6.2–1 SAMPLE COVARIANCE MATRICES OF REAL SHAPE CLASS A

$$q = 0. \qquad \begin{pmatrix} 1.2 & -2.2 & .9 \\ -2.2 & 5.5 & -3.3 \\ .9 & -3.3 & 2.3 \end{pmatrix} \times 10^{-3}$$

$$q = .10 \qquad \begin{pmatrix} 1.2 & -2.0 & .8 \\ -2.0 & 4.6 & -2.6 \\ .8 & -2.6 & 1.8 \end{pmatrix} \times 10^{-3}$$

$$q = .20 \qquad \begin{pmatrix} 2.1 & -3.8 & 1.6 \\ -3.8 & 7.8 & -4.1 \\ 1.6 & -4.1 & 2.4 \end{pmatrix} \times 10^{-3}$$

$$q = .30 \qquad \begin{pmatrix} 2.7 & -4.4 & 1.6 \\ -4.4 & 8.1 & -3.7 \\ 1.6 & -3.7 & 2.1 \end{pmatrix} \times 10^{-3}$$

$$q = .40 \qquad \begin{pmatrix} 3.2 & -5.3 & 2.1 \\ -5.3 & 10.1 & -4.8 \\ 2.1 & -4.8 & 2.7 \end{pmatrix} \times 10^{-3}$$

TABLE 6.2–2 SAMPLE COVARIANCE MATRICES OF REAL SHAPE CLASS B

q = 0.	$\begin{pmatrix} 1.5 & -3.0 & 1.4 \\ -3.0 & 6.4 & -3.4 \\ 1.4 & -3.4 & 1.9 \end{pmatrix} \times 10^{-3}$
q = .10	$\begin{pmatrix} 1.4 & -2.8 & 1.3 \\ -2.8 & 5.9 & -3.1 \\ 1.3 & -3.1 & 1.8 \end{pmatrix} \times 10^{-3}$
q = .20	$\begin{pmatrix} 2.5 & -4.8 & 2.3 \\ -4.8 & 9.6 & -4.8 \\ 2.3 & -4.8 & 2.5 \end{pmatrix} \times 10^{-3}$
q = .30	$\begin{pmatrix} 2.6 & -4.8 & 2.2 \\ -4.8 & 9.3 & -4.5 \\ 2.2 & -4.5 & 2.3 \end{pmatrix} \times 10^{-3}$
q = .40	$\begin{pmatrix} 3.4 & -6.5 & 3.0 \\ -6.5 & 12.5 & -6.1 \\ 3.0 & -6.1 & 3.1 \end{pmatrix} \times 10^{-3}$

7.0 CLASSIFICATION OF PARTIALLY SPECIFIED PLANAR SHAPES

Bayesian decision theory is used to derive a classifier from the asymptotic Gaussian property of the extended ML estimates. The result is a set of Gaussian discriminate functions which are separately trained for use in two classification experiments. The first classification experiment uses synthetically generated shapes. The second experiment demonstrates the classification performance of the extended ML estimator on real aircraft shapes.

The classification of the synthetic boundaries is performed under ideal conditions in which the model fit is perfect and all parameters are known. The dependence of the classification results upon the degree of stationarity of the CAR processes is examined in this experiment. The classification performance of the LS estimates computed from interpolated boundaries is also tested.

The second experiment tests the classification abilities of the extended ML estimates on real aircraft shapes. In this experiment the model fit is imperfect and all parameters are estimated from the observed real boundary sequence. The classification results are analyzed and general conclusions are drawn about the classification of real shapes.

A tight analytic upper bound on the probability of correct classification is derived from the asymptotic properties of the extended ML estimator of the CAR descriptors. This bound is a function of the CAR descriptors which identify the shape classes and parameters related to the performance of the segmentor.

7.1 THE CLASSIFIER

The CAR descriptors form a feature space of dimension m equal to the order of the CAR model associated with the boundary process. The use of a CAR model suggests an alternative means of representing a shape class in feature space. Traditionally, a shape class has been represented by a unique distribution of the features in feature space. In Section 3.2 all members of a shape class were represented by a single set of CAR descriptors $\vec{a}$ and the within class variations were contained in the error process of the CAR model. Using this definition, a shape class is represented by a single point $\vec{a}$ in feature space. A shape is easily classified using this representation if its CAR descriptors are known.

If the CAR descriptors of a shape which is to be classified are unknown, then they must be estimated from the observed sample sequence of the boundary. If the estimator used is consistent, it will converge in probability to the point $\vec{a}$ in feature space which represents the shape class. Due to estimation error the resulting estimates $\hat{a}$ of the CAR descriptors will be distributed about the representative point $\vec{a}$. Given the distribution of the estimates $\hat{a}$, classical Bayesian decision theory can be used to classify the shape. In Section 5.4 the asymptotic consistency of the extended ML estimator of the CAR descriptors was established along with the fact that the estimation error is asymptotically Gaussian distributed with zero mean. Consequently, the extended ML estimates $\hat{a}$ of the CAR descriptors are asymptotically Gaussian distributed about the point $\vec{a}$ which represents the shape class. By assuming that this Gaussian property extends to a finite number of boundary samples a Bayesian discriminant function classifier can be designed.

Let the set of possible shape classes C_i be represented in feature space by the points $\vec{a}_i$ respectively. The extended ML estimates $\hat{a}$ of the CAR descriptors associated with shape class C_i have the following Gaussian probability density function $p_i(\hat{a})$

$$p_i(\hat{a}) = \frac{1}{(2\pi)^{m/2}\,|\Sigma_i|^{1/2}}\, e^{-1/2\,(\hat{a}-\vec{a}_i)^t\,\Sigma_i^{-1}(\hat{a}-\vec{a}_i)} \tag{7.1-1}$$

where Σ_i is the covariance matrix of the estimates associated with shape class C_i. If all of the classes C_i have equal a priori probabilities, then the Bayesian classification rule is: assign $\hat{a} \in C_i$ if

$$p_i(\hat{a}) > p_j(\hat{a}) \qquad \forall\, j \neq i. \tag{7.1-2}$$

Substitution of the densities given in (7.1-1) into (7.1-2) produces the following inequality.

$$\frac{e^{-1/2\,(\hat{a}-\vec{a}_i)^t\,\Sigma_i^{-1}(\hat{a}-\vec{a}_i)}}{(2\pi)^{m/2}\,|\Sigma_i|^{1/2}} > \frac{e^{-1/2\,(\hat{a}-\vec{a}_j)^t\,\Sigma_j^{-1}(\hat{a}-\vec{a}_j)}}{(2\pi)^{m/2}\,|\Sigma_j|^{1/2}} \tag{7.1-3}$$

This inequality can be simplified by using the natural logarithm and subtracting off the common terms.

$$-\frac{1}{2}(\hat{a}-\dot{a}_i)^t\,\Sigma_i^{-1}(\hat{a}-\dot{a}_i)-\frac{1}{2}\ln|\Sigma_i| > -\frac{1}{2}(\hat{a}-\dot{a}_j)^t\,\Sigma_j^{-1}(\hat{a}-\dot{a}_j)-\frac{1}{2}\ln|\Sigma_j| \qquad (7.1\text{-}4)$$

Multiplication by minus one-half reverses the inequality and changes the classification rule to: assign $\hat{a} \in C_i$ if

$$g_i(\hat{a}) < g_j(\hat{a}) \qquad \forall\, j \neq i \qquad (7.1\text{-}5)$$

where the discriminant function $g_i(\hat{a})$ is given by the following.

$$g_i(\hat{a}) = (\hat{a}-\dot{a}_i)^t\,\Sigma_i^{-1}(\hat{a}-\dot{a}_i) + \ln|\Sigma_i| \qquad (7.1\text{-}6)$$

It is very unlikely that the CAR descriptors $\dot{a}_i$ and the covariance matrices Σ_i will be known for all of the classes C_i. If this is the case, then the sample estimates of $\dot{a}_i$ and Σ_i can be computed from a training set T_i. The training set T_i contains N_T extended ML estimates $\hat{a}_k$ of the CAR descriptors obtained from sample boundary sequences belonging to the shape class C_i. The sample mean $\bar{a}_i$ of the CAR descriptors $\dot{a}_i$ which represent the shape class C_i is given by the following.

$$\bar{a}_i = \frac{1}{N_T}\sum_{k=1}^{N_T}\hat{a}_k \qquad (7.1\text{-}7)$$

Similarily the unbiased sample covariance matrix $\bar{\Sigma}_i$ is given by the following.

$$\bar{\Sigma}_i = \frac{1}{N_T-1}\sum_{k=1}^{N_T}(\hat{a}_k-\bar{a}_i)(\hat{a}_k-\bar{a}_i)^t \qquad (7.1\text{-}8)$$

The resulting discriminant function denoted $\bar{g}_i(\hat{a})$ is defined below.

$$\bar{g}_i(\hat{a}) = (\hat{a}-\bar{a}_i)^t\,\bar{\Sigma}_i^{-1}(\hat{a}-\bar{a}_i) + \ln|\bar{\Sigma}_i| \qquad (7.1\text{-}9)$$

The derivation of the above classifier was based upon the asymptotic Gaussian distribution of the estimates of the CAR descriptors. The set of poles associated with each estimate of the CAR descriptors do not share this Gaussian property with the CAR descriptors. This is due to the nonlinear relationship between the CAR descriptors and their associated poles which was derived in Section 3.3. The absence of this Gaussian property is the primary reason the poles were not proposed as a set of shape descriptors.

7.2 CLASSIFICATION OF SYNTHETIC SHAPES

This experiment evaluates the classification performance of both the extended ML estimates and the interpolated LS estimates as the CAR model of the boundary process becomes less stationary. Less stationary means that the poles associated with the CAR models are located successively closer to the unit circle in the CAR diagram. The stationarity of the CAR models which define the four shape classes used in Section 6.1 steadily decreases, as can be seen from the CAR diagrams in Figures 6.1-1 through 6.1-4. For this reason, the same four classes were used in this classification experiment. The results of the estimation experiment conducted in Section 6.1 were used to train the Gaussian discriminant function classifier derived in Section 7.1. It was demonstrated in [35] that a Gaussian discriminant function classifier is also appropriate for use with the LS estimates. This classifier was separately trained on 100 sample boundary sequences of each shape class. An additional 100 sample boundary sequences were generated for each shape class to form the test set. These sample boundary sequences were generated using the same parameter values chosen in Section 6.1. A sample boundary sequence of each shape class is shown in Figures 7.2-1 through 7.2-4. The classification experiment was repeated eight times. Each time the experiment was repeated the amount of boundary obscuration was increased by 10% beginning with an unobscured boundary. A plot of the resulting experimental probability of correct classification is presented for each of the four shape classes in Figures 7.2-5 through 7.2-8.

The extended ML estimates and the interpolated LS estimates both provided good classification results for shape classes 1 and 2 even when large amounts ($>30\%$) of obscuration are present. Shape classes 1 and 2 also represent very stationary CAR processes as shown by the location of the poles well within the unit circle in the CAR diagrams of Figures 6.1-1 and 6.1-2 respectively. Shape class 3 represents a moderately stationary CAR process as shown by the location of its poles in the CAR diagram of Figure 6.1-3. Even with this decrease in stationarity the extended ML estimates result in good classification performance for up to 30% obscuration. The interpolated LS estimates show a marked decline in classification accuracy for this shape class. The location of the poles in the CAR diagram of shape class 4 in Figure 6.1-4 show that this shape class represents a CAR process which is only marginally stationary.

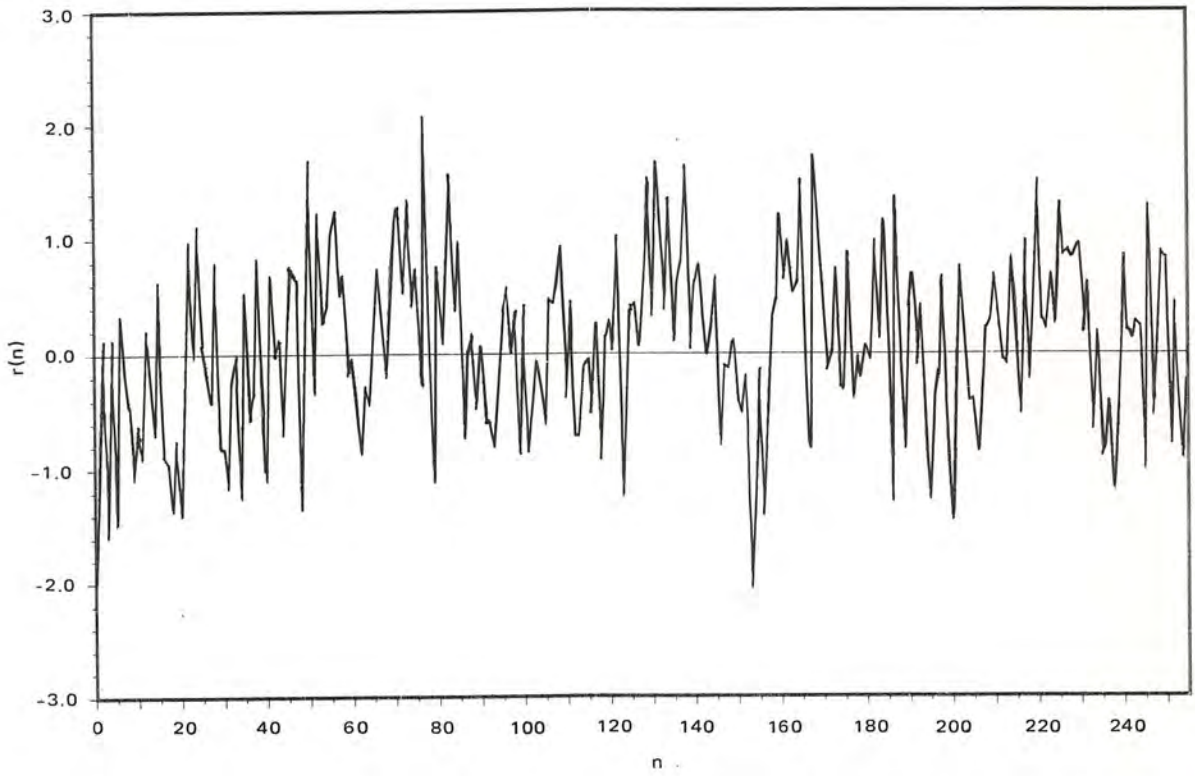

Figure 7.2–1. Sample Boundary Sequence of Shape Class 1

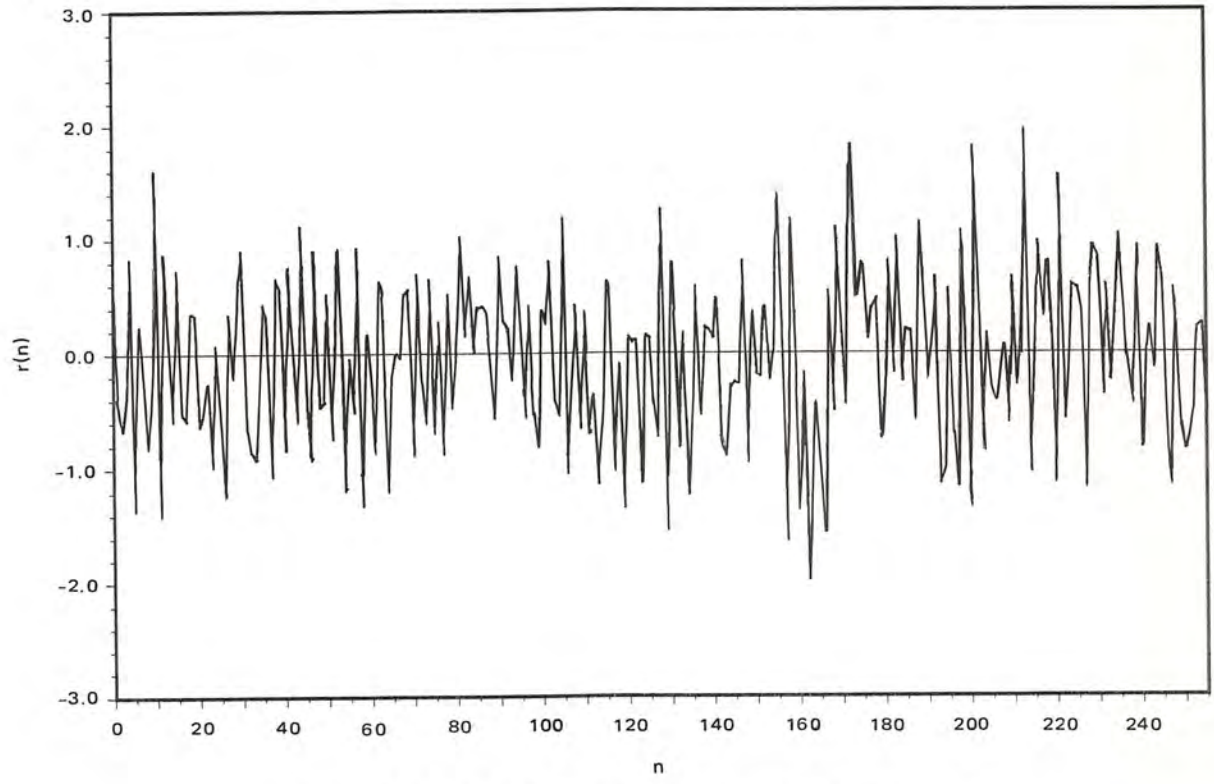

Figure 7.2–2. Sample Boundary Sequence of Shape Class 2

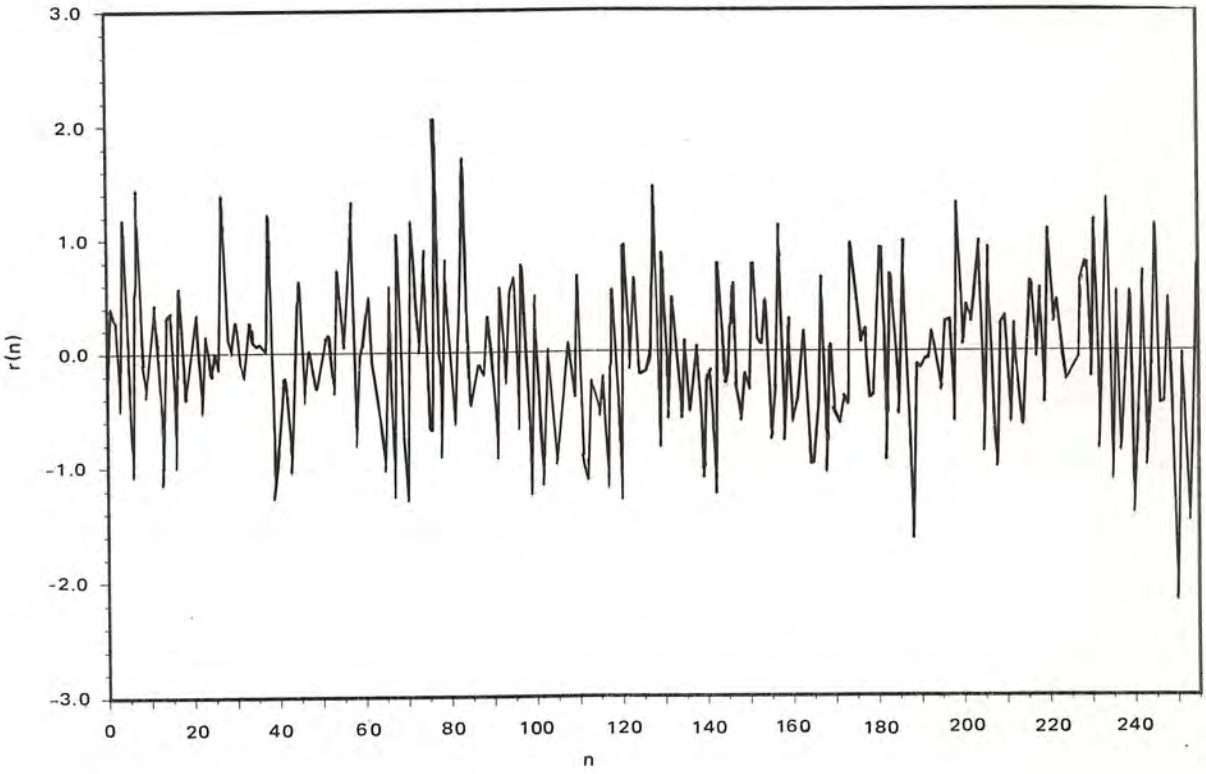

Figure 7.2–3. Sample Boundary Sequence of Shape Class 3

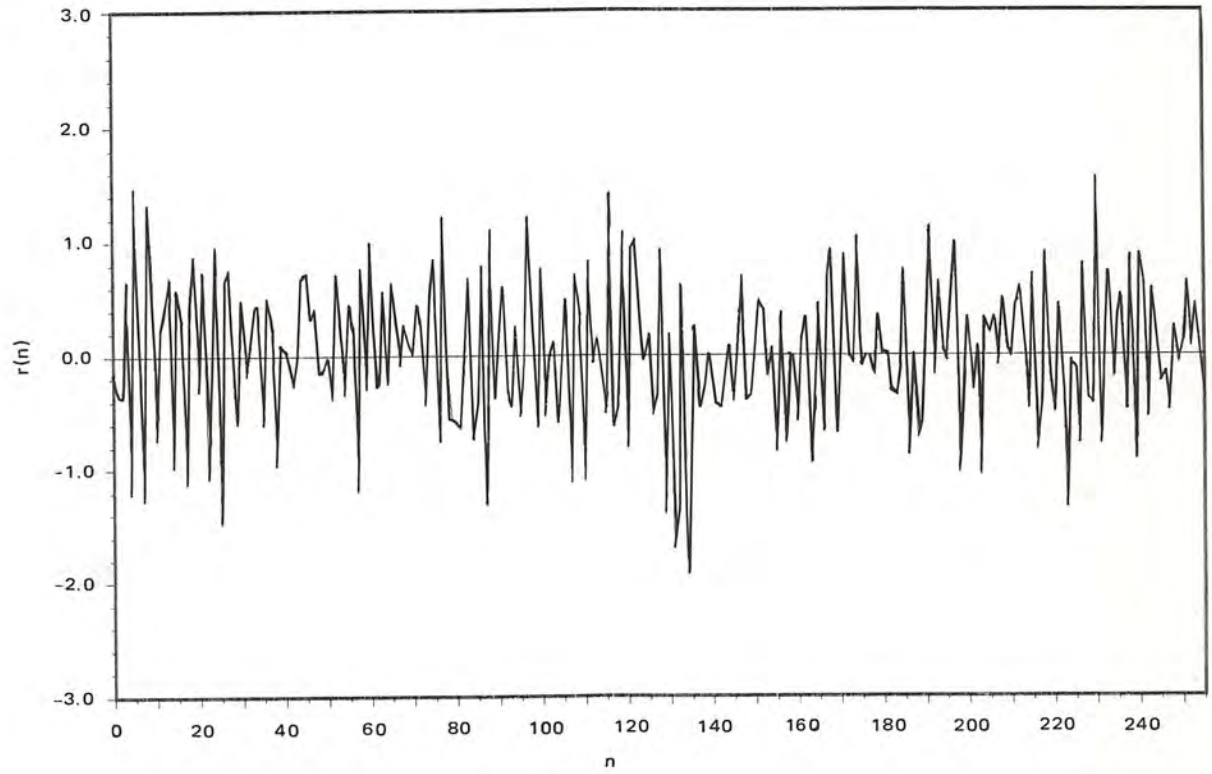

Figure 7.2–4. Sample Boundary Sequence of Shape Class 4

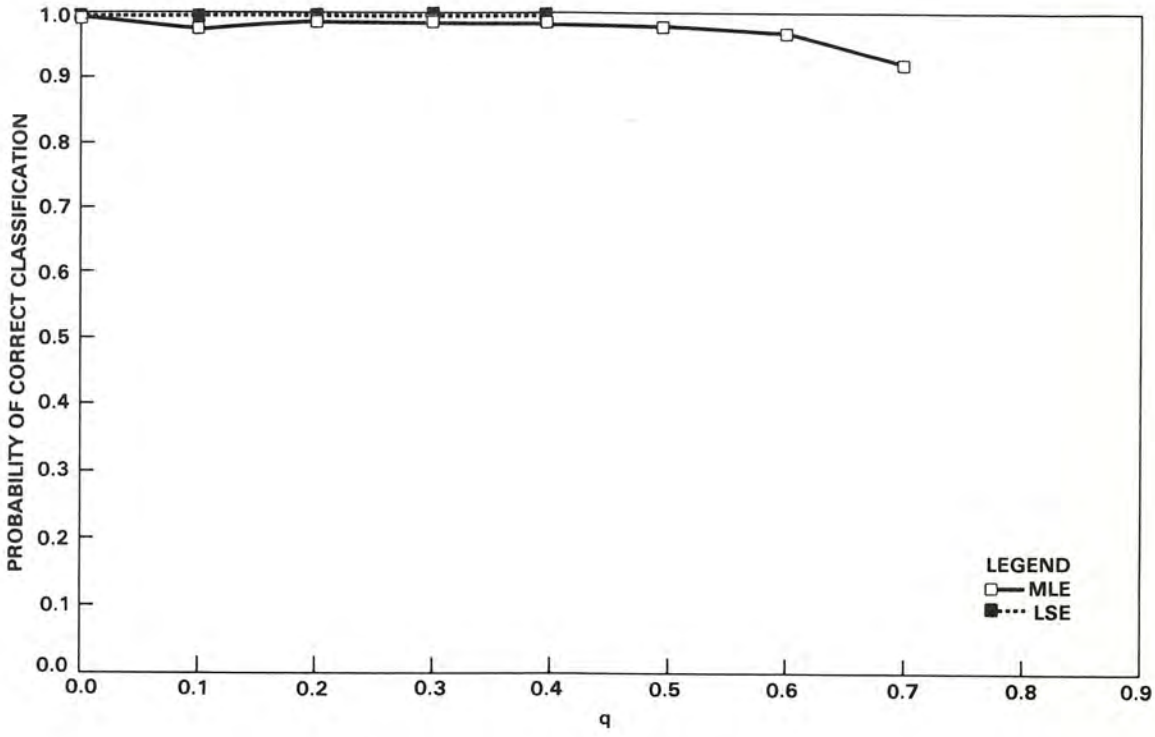

Figure 7.2–5. Experimental Results for Shape Class 1

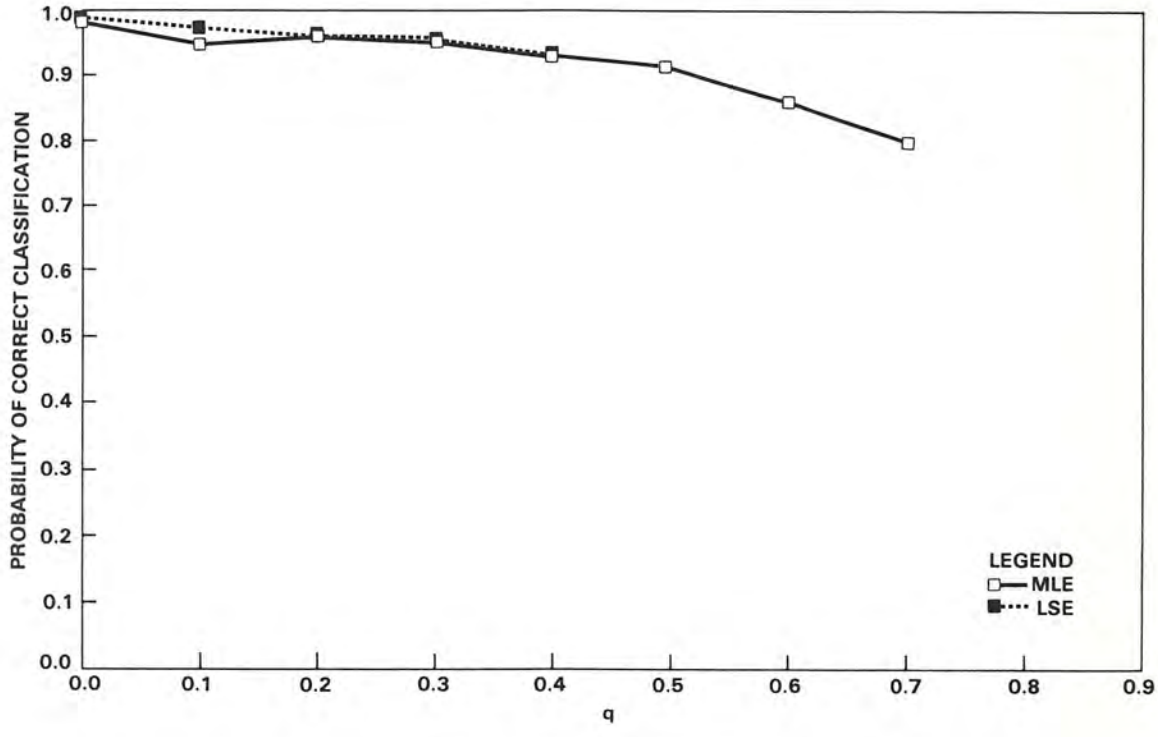

Figure 7.2–6. Experimental Results for Shape Class 2

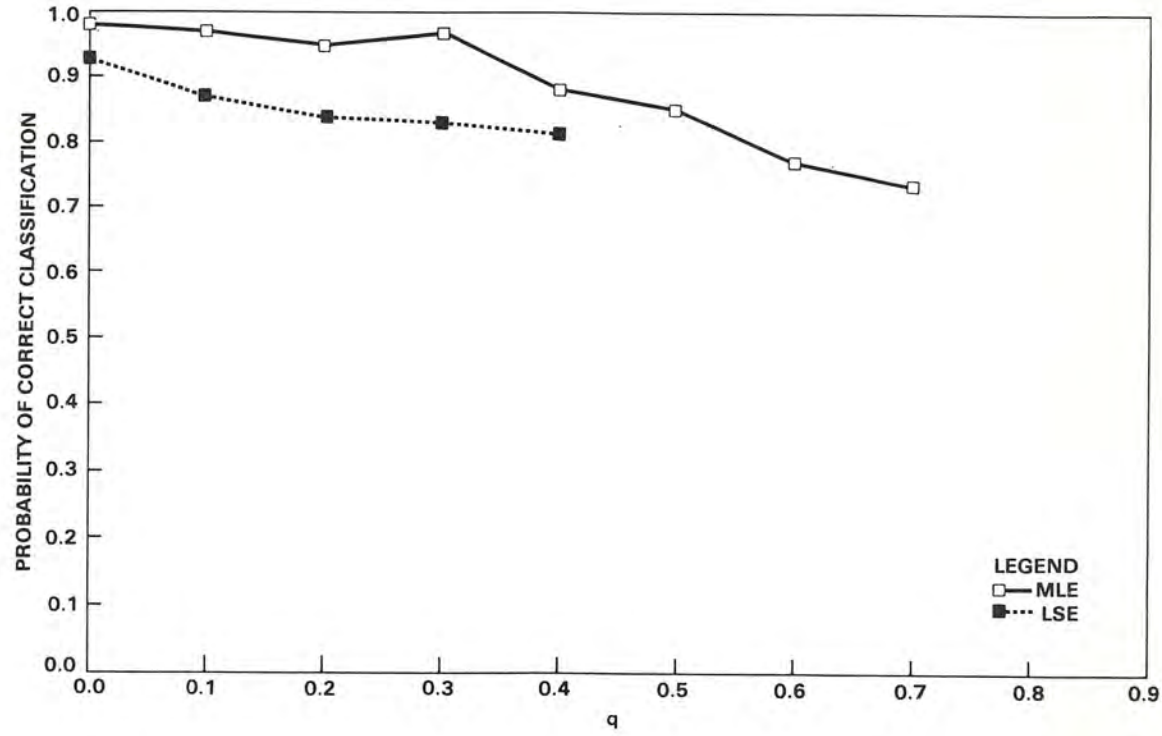

Figure 7.2–7. Experimental Results for Shape Class 3

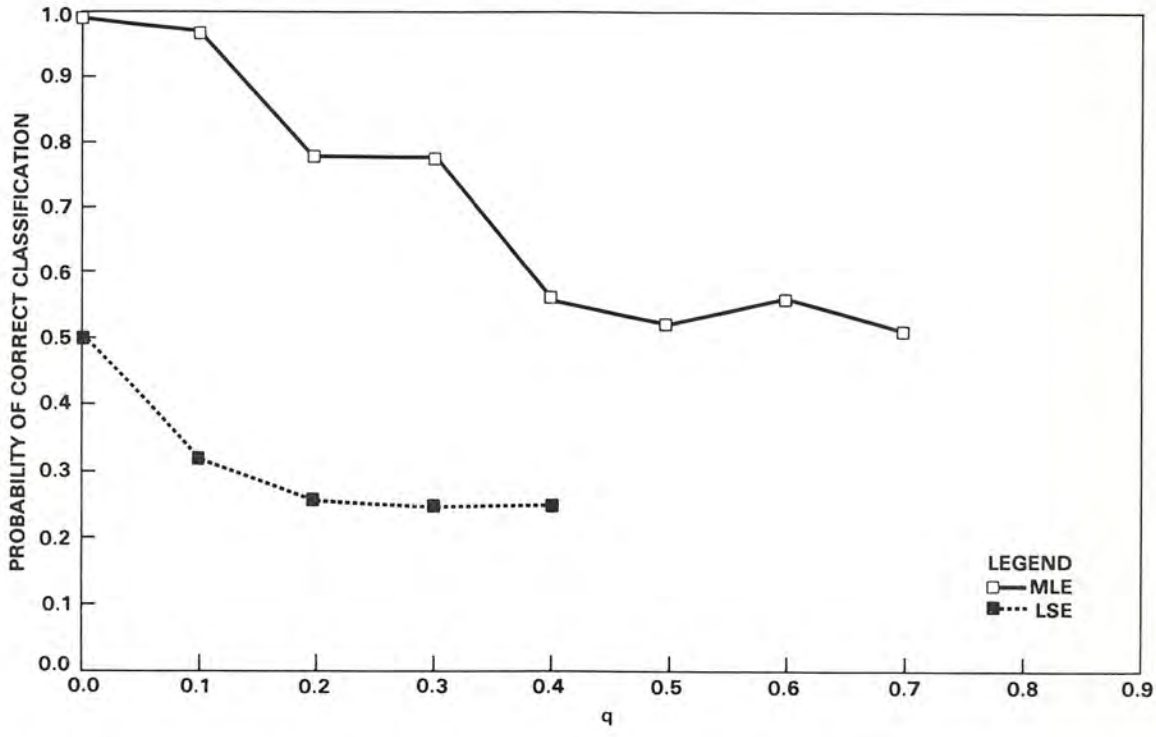

Figure 7.2–8. Experimental Results for Shape Class 4

This fact is reflected in the classification results of shape class 4. The extended ML estimates still provide good classification accuracy out to 10% obscuration. In comparison, the interpolated LS estimates are bad even when no obscuration is present and the results quickly decay to the a priori probability of occurrence (25%) as the amount of obscuration is increased. These experimental results show that classification performance is linked to the degree of stationarity of the boundary process. Whenever the boundary processes are anything less than very stationary, the extended ML estimator should be used. This is true even if no obscuration is present. Recall that for this case the extended ML estimator reduces to the ML estimator derived in Section 4.1.

The poor performance of the interpolated LS estimator can be explained as follows. The LS estimator is not consistent in any sense, therefore it does not converge in probability to the point $\vec{a}$ in feature space which represents the shape class. This is especially true if obscuration is present. If obscuration is present and the boundary is reconstructed using an interpolation scheme which is not based upon the underlying CAR process, the correlation structure of the boundary process will be disturbed. Since the CAR descriptors essentially identify the correlation structure of the boundary process their values will also be disturbed. Disturbing the values of the CAR descriptors results in decreased classification performance. The importance of preserving the correlation structure of the boundary process is evident in the results of Dunsmuir and Robinson [32]. They showed that if the sequence formed by replacing missing data points with zeros is substituted for the complete data sequence in an ML estimator derived under the assumption of complete data, the resulting estimator will be inconsistent. This is because the zeros upset the correlation structure of the data. The inclusion of an obscuration model in the derivation of the ML estimator, as was done in Section 5.2, preserves the correlation structure and produces an asymptotically consistent estimator.

7.3 CLASSIFICATION OF REAL SHAPES

This experiment tests the classification performance of the extended ML estimates of the CAR descriptors on the partially obscured aircraft boundaries introduced in Section 6.2. The amount of obscuration was varied from zero through 40% in 10%

increments. Sample boundaries of each aircraft type are shown in Figures 7.3-1 through 7.3-4 for the various amounts of obscuration. All model parameters, including those of the obscuring process, were assumed *unknown* and were estimated from the observed sample boundary sequence using the estimates derived in Section 5.3. The separation of the aircraft shape classes in the feature space was the criterion used to select the order of the CAR model. The CAR diagrams presented in Figures 6.2-5 to 6.2-8 provide a convenient means of evaluating this criterion. Since the classes of swept and straight wing aircraft are adequately separated in these CAR diagrams, a third order (m=3) CAR model was used in this experiment. The results of the estimation experiment performed in Section 6.2 were used to train the Gaussian discriminant function classifier derived in Section 7.1. Testing was done using a separate set of 200 sample boundary sequences of each aircraft class. The test set of each aircraft class was equally distributed within that class.

The classification results are presented as confusion matrices in Table 7.3-1. An attempt was made to classify the partially obscured aircraft using the LS estimates obtained from the linearly interpolated boundary, but these results were extremely poor. The disparity between the results of these two estimators can be explained in terms of the stationarity of the CAR processes. The CAR diagrams of the aircraft shape classes in Figures 6.2-5 to 6.2-8 show poles which lie very close to the boundary of nonstationarity (the unit circle). Shape class B (straight-wing aircraft) is worse than shape class A (swept-wing aircraft) in this respect, since it has two poles (a conjugate pair) located near the unit circle. This observation is substantiated by the slightly poorer results reported for shape class B in the confusion matrices of Table 7.3-1. The stationarity of the two aircraft shape classes relative to the synthetic boundary classes is between that of synthetic shape classes 3 and 4. Recall that the classification results of synthetic shape class 4 (Figure 7.2-8) also showed a large disparity between the performance of the extended ML estimates and the interpolated LS estimates. Notice also from the confusion matrices in Table 7.3-1 that the performance of the extended ML estimator decreases markedly when more than 30% of the boundary is obscured. This behavior is also present in the classification results of synthetic shape class 3 (Figure 7.2-7).

Some general conclusions regarding the classification of real shape boundaries can be made from the results of this and the synthetic boundary experiments. Notice

TABLE 7.3–1. CONFUSION MATRICES OF REAL BOUNDARY CLASSIFICATION EXPERIMENT

q = 0	A	B
A	.99	.01
B	.02	.98

q = .10	A	B
A	.97	.03
B	.05	.95

q = .20	A	B
A	.96	.04
B	.06	.94

q = .30	A	B
A	.91	.09
B	.13	.87

q = .40	A	B
A	.74	.26
B	.32	.68

first that the boundaries of real shapes are typically low frequency processes. This is evident in the sample boundary sequence plots of the four different aircraft type shown in Figures 7.3–5 to 7.3–8. The sample boundary sequences are relatively smooth, there are no discontinuities, and the structures within the boundary have relatively long periods. Consequently, the transfer functions associated with the CAR models of such processes also have a predominately low frequency characteristic. Now

consider the power spectrums of the transfer functions associated with the four synthetic shape classes. Their normalized plots are shown in Figures 7.3-9 to 7.3-12. Notice that the low frequency portion of the spectrum becomes more pronounced in the progression from shape class 1 to shape class 4. Shape class 4 has the strongest low frequency characteristic of the four shape classes and is also the least stationary. The following general observation may be made in this regard. If a transfer function of the form associated with CAR models is to have a predominately low frequency characteristic, then at least one pole must be located near the point $z=1$ in the CAR diagram. Since the point $z=1$ is on the unit circle, any CAR process associated with a pole near this point will be moderately stationary. Therefore, typical real shape boundaries will tend to be modeled by moderately stationary CAR processes. It can then be concluded that if allowance is made for variations in class separation, these experimental results are typical for many real shape classes.

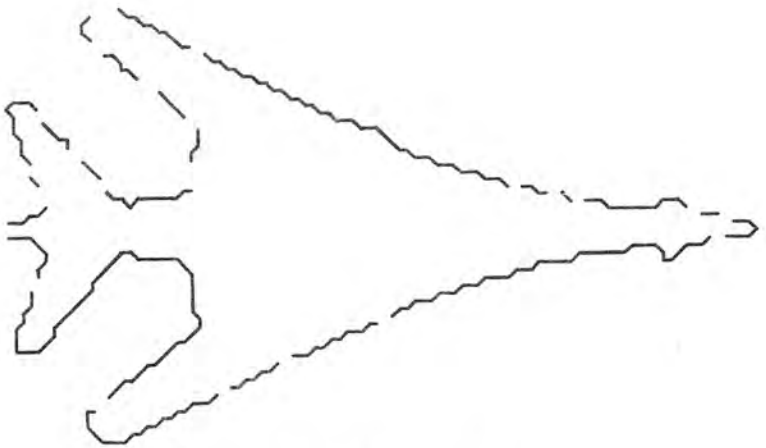

a. 10% obscuration

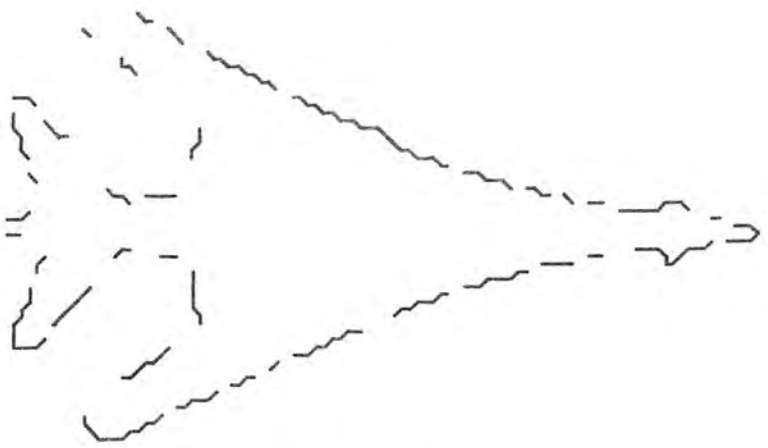

b. 20% obscuration

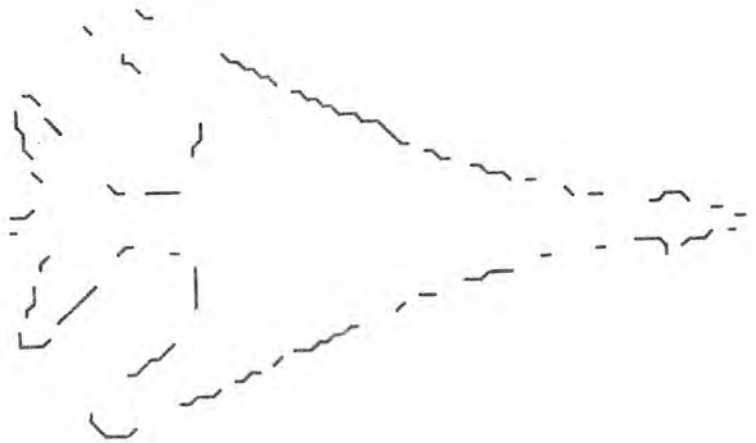

c. 30% obscuration

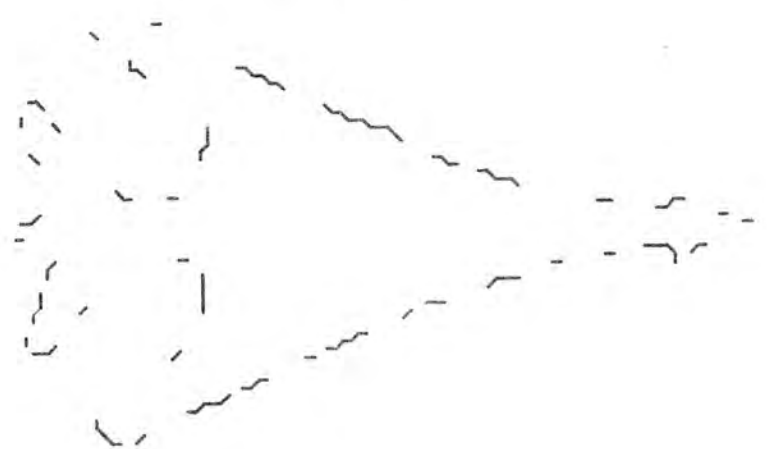

d. 40% obscuration

Figure 7.3–1. Sample Boundary of Aircraft Type A1

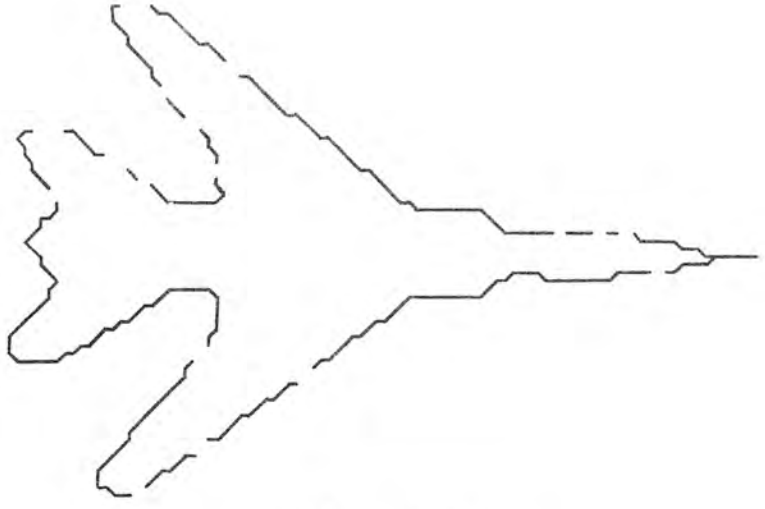

a. 10% obscuration

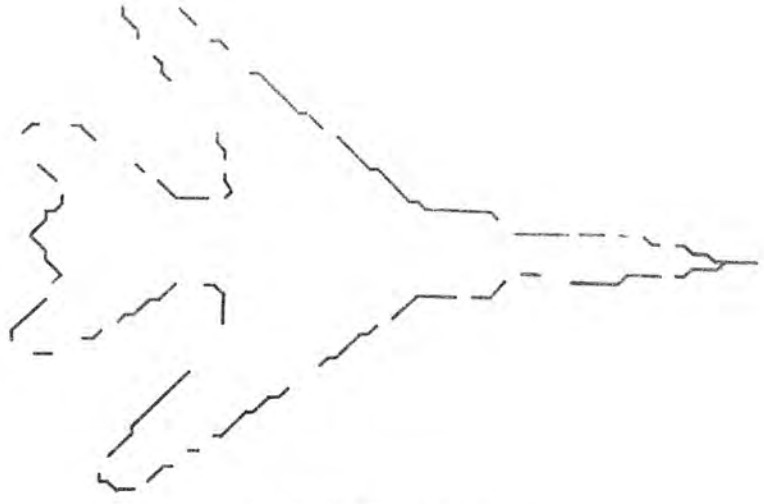

b. 20% obscuration

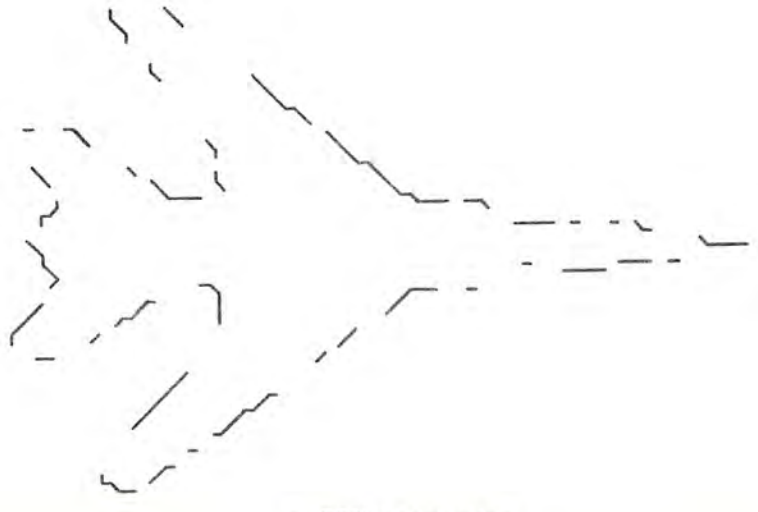

c. 30% obscuration

d. 40% obscuration

Figure 7.3–2. Sample Boundary of Aircraft Type A2

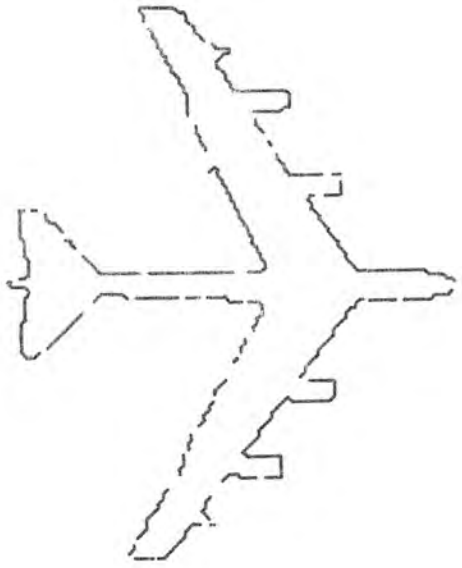

a. 10% obscuration

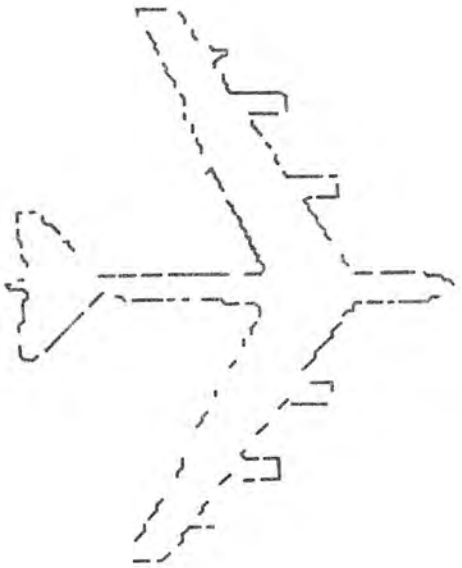

b. 20% obscuration

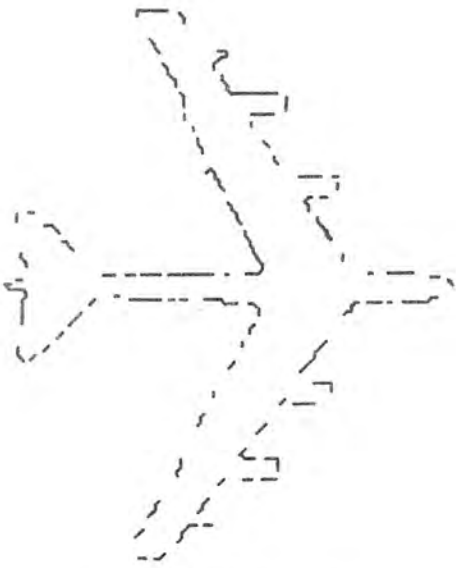

c. 30% obscuration

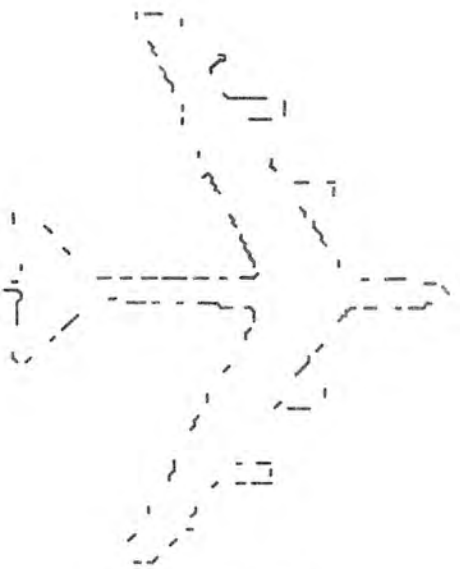

d. 40% obscuration

Figure 7.3–3. Sample Boundary of Aircraft Type B1

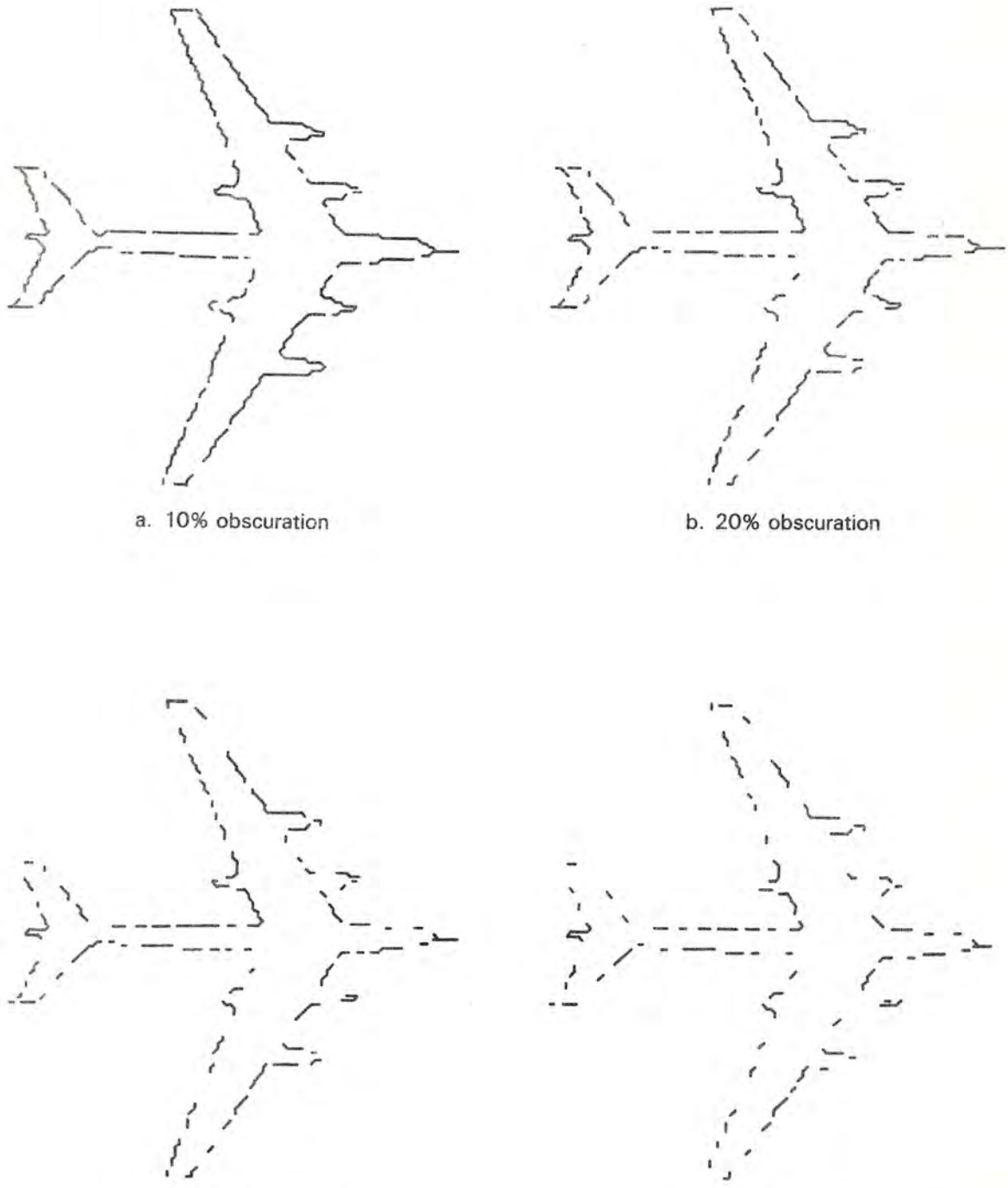

a. 10% obscuration

b. 20% obscuration

c. 30% obscuration

d. 40% obscuration

Figure 7.3–4. Sample Boundary of Aircraft Type B2

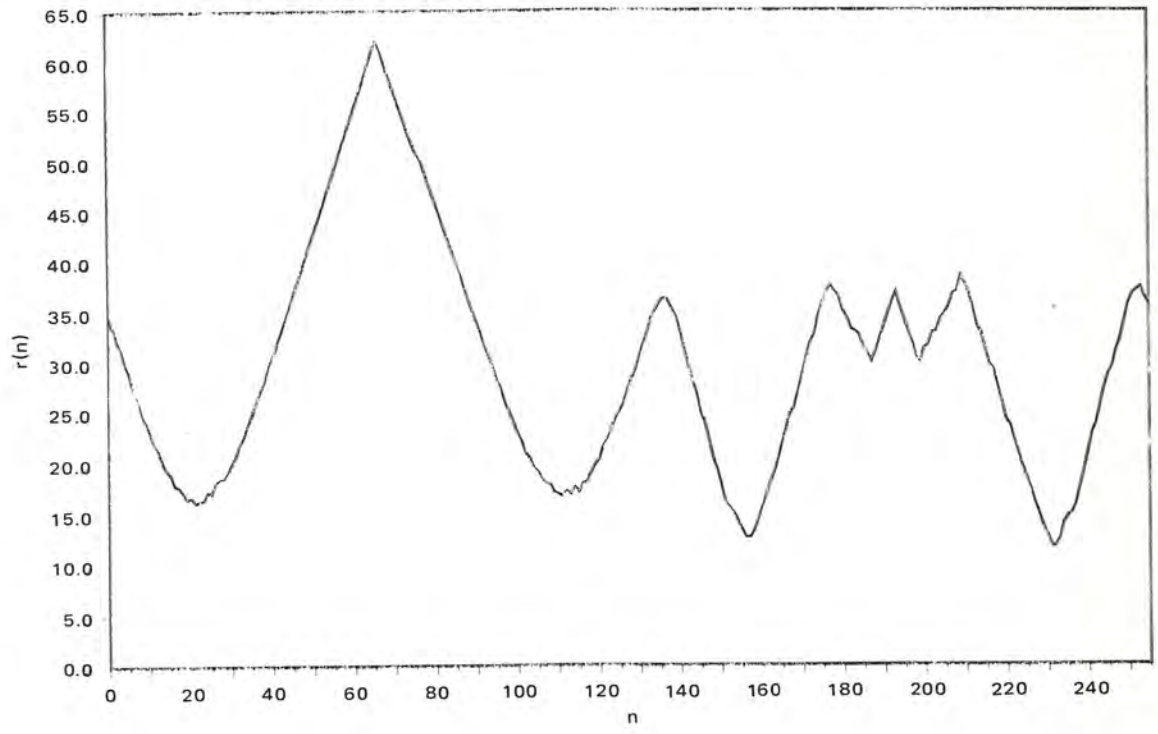

Figure 7.3–5. Sample Boundary Sequence of Aircraft Type A1

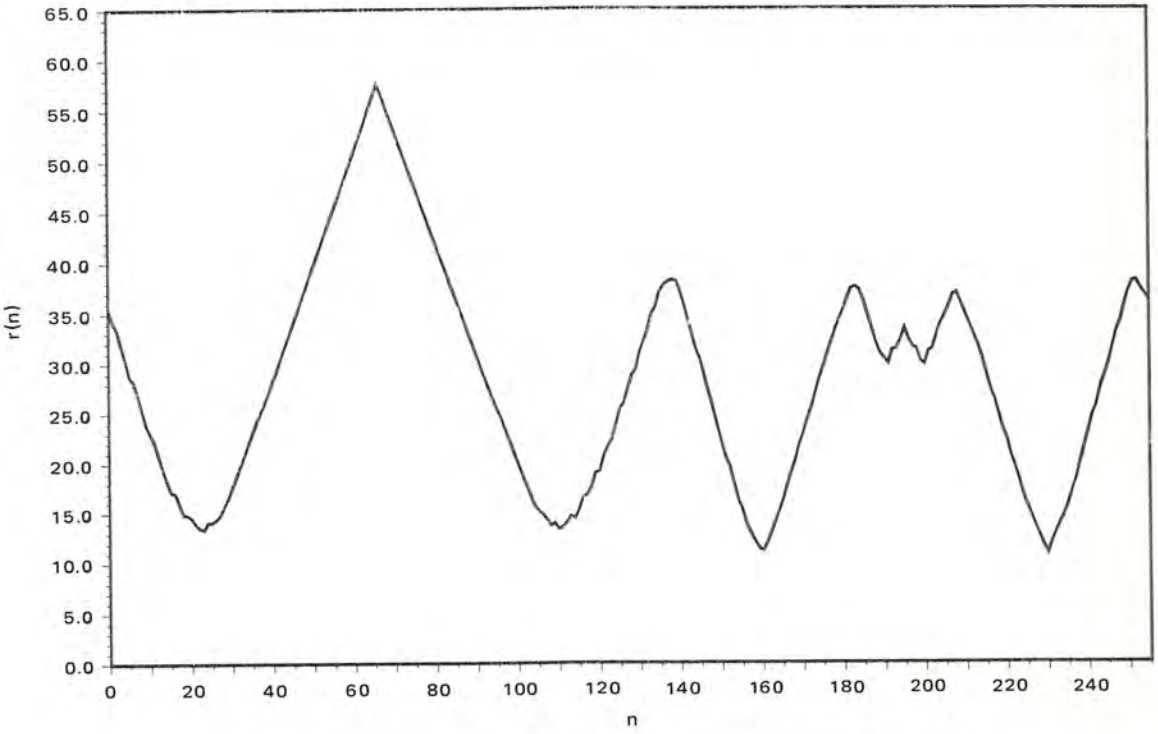

Figure 7.3–6. Sample Boundary Sequence of Aircraft Type A2

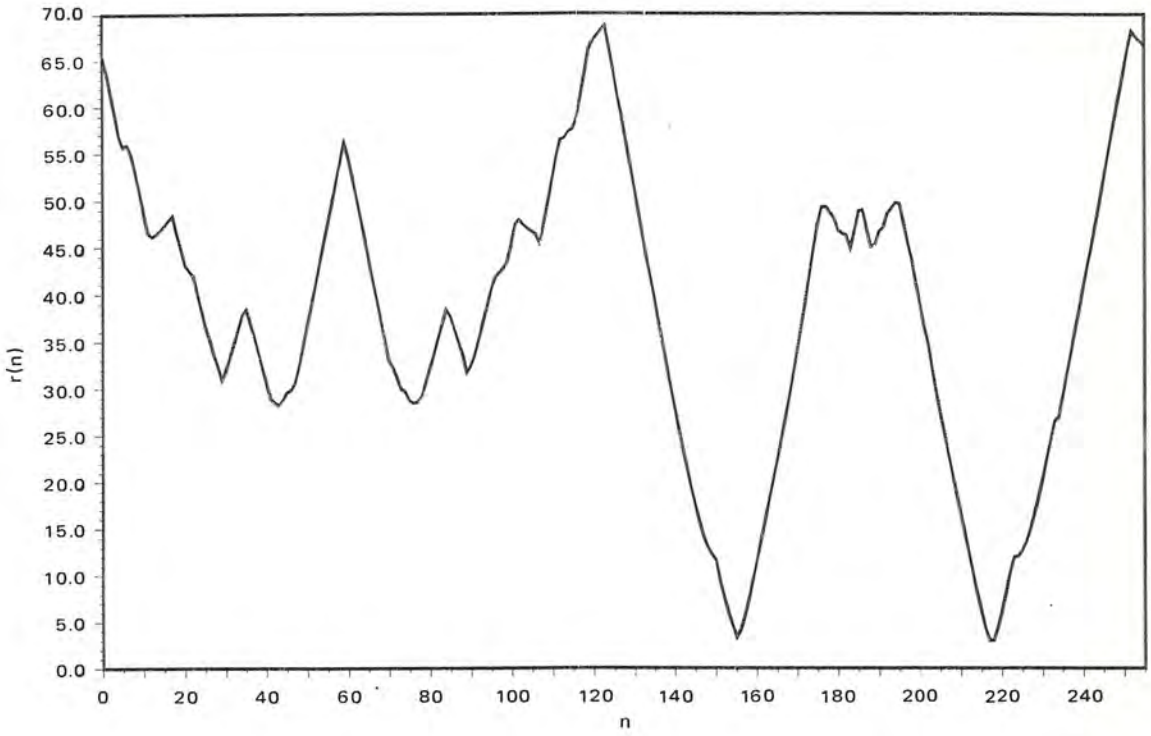

Figure 7.3–7. Sample Boundary Sequence of Aircraft Type B1

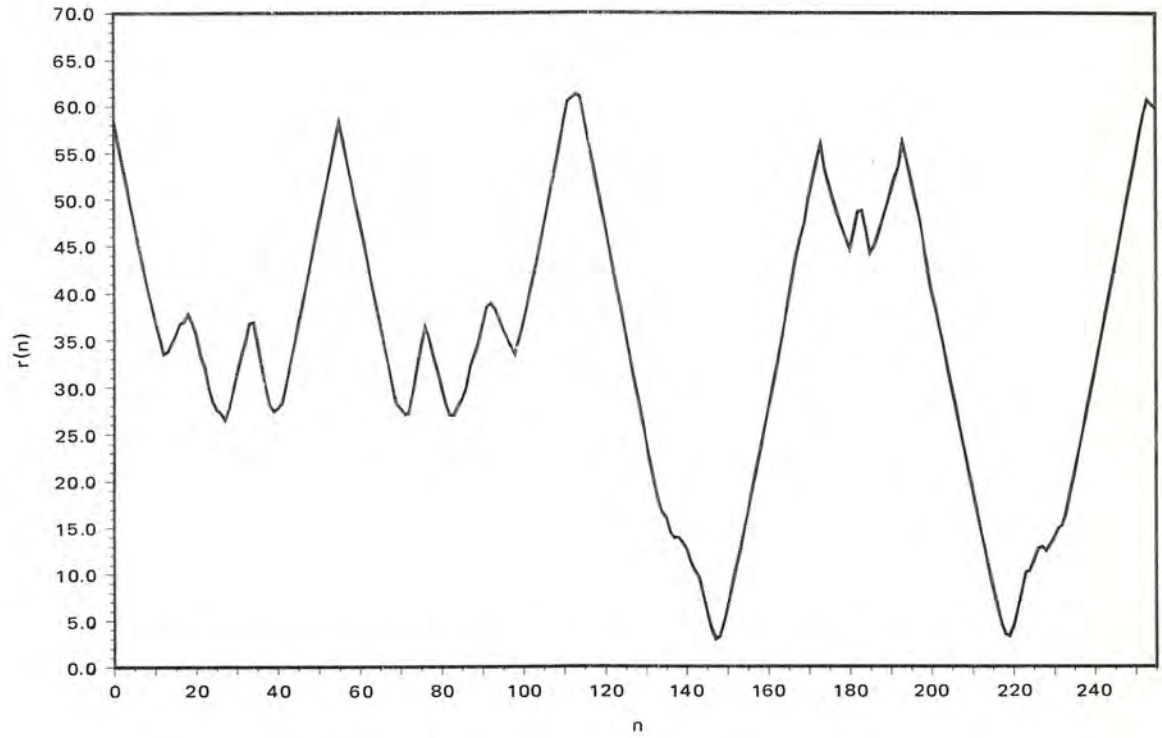

Figure 7.3–8. Sample Boundary Sequence of Aircraft Type B2

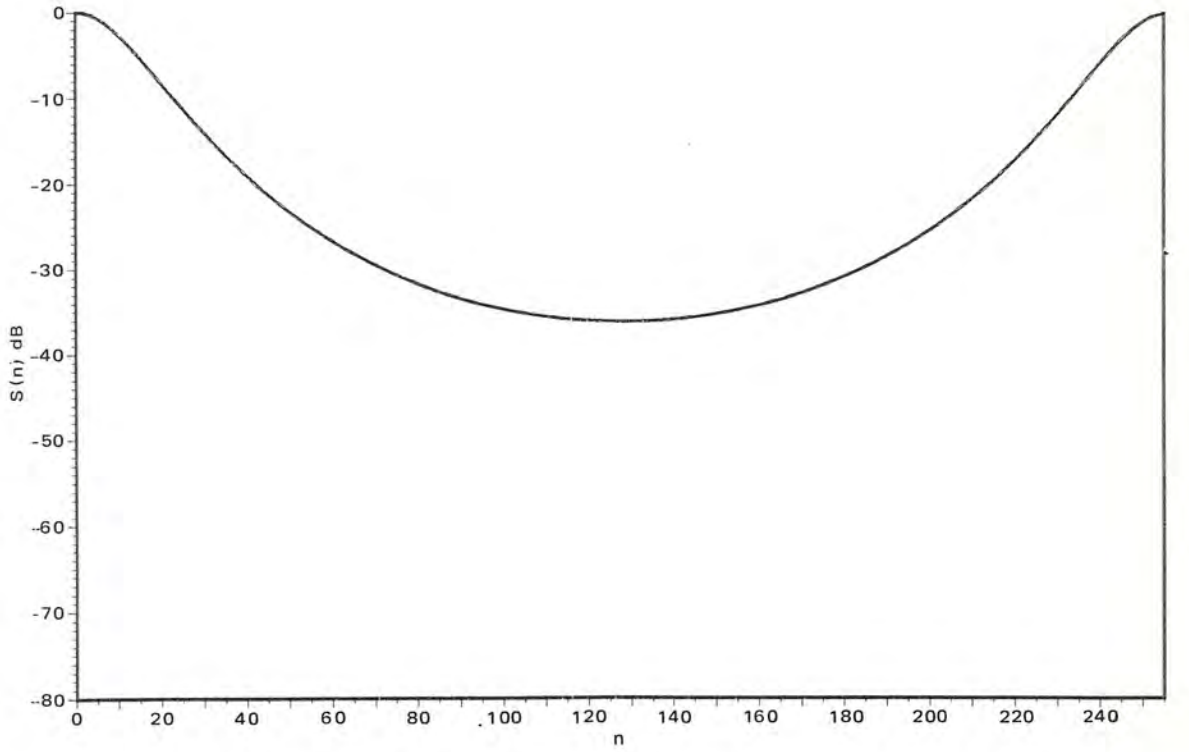

Figure 7.3–9. Normalized Power Spectrum of Shape Class 1

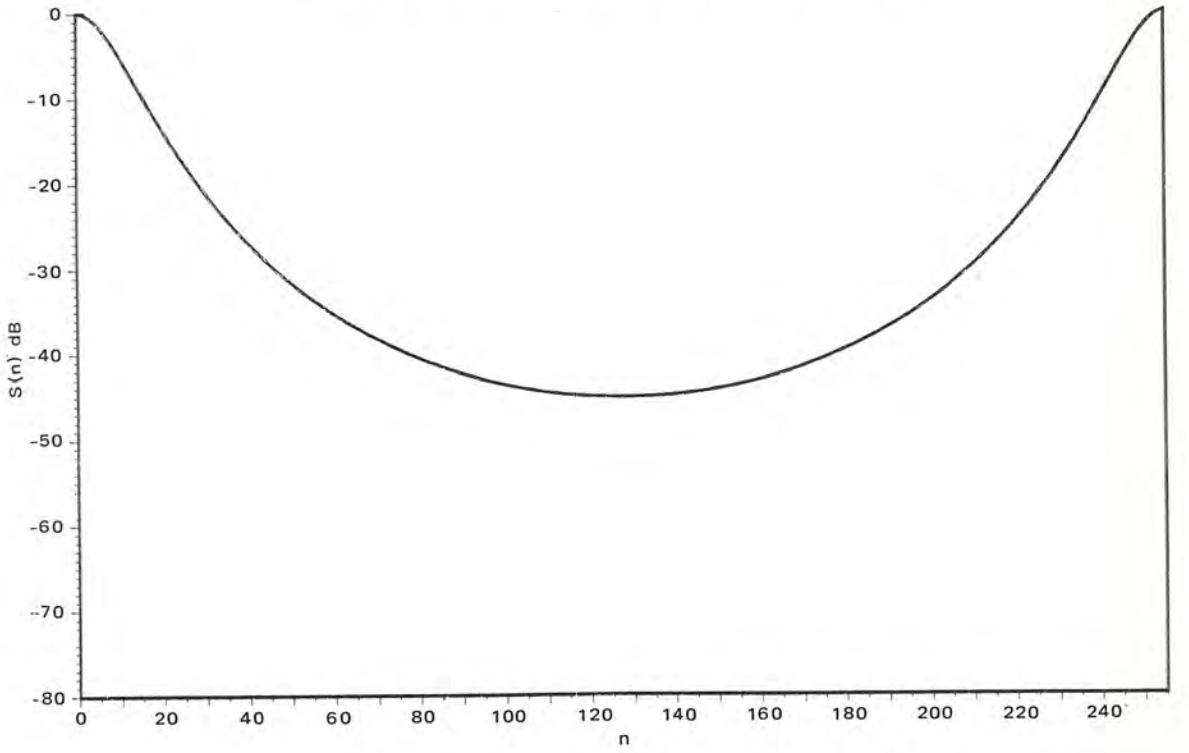

Figure 7.3–10. Normalized Power Spectrum of Shape Class 2

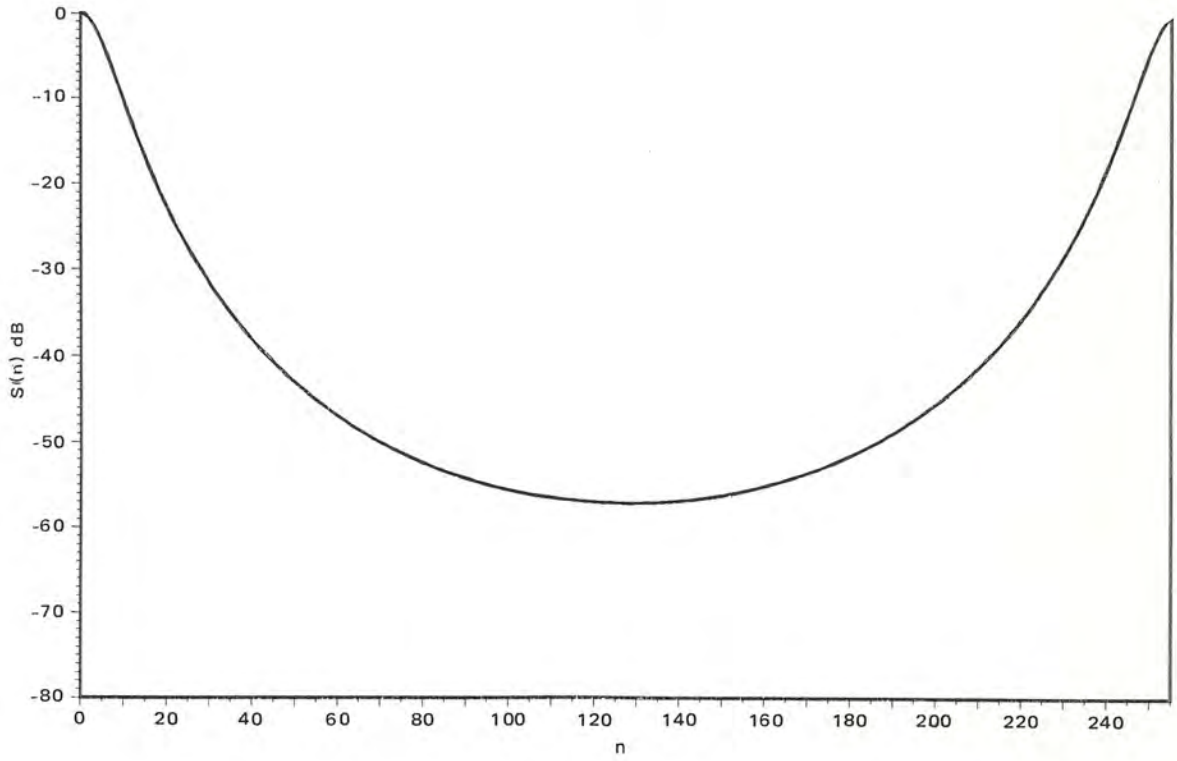

Figure 7.3–11. Normalized Power Spectrum of Shape Class 3

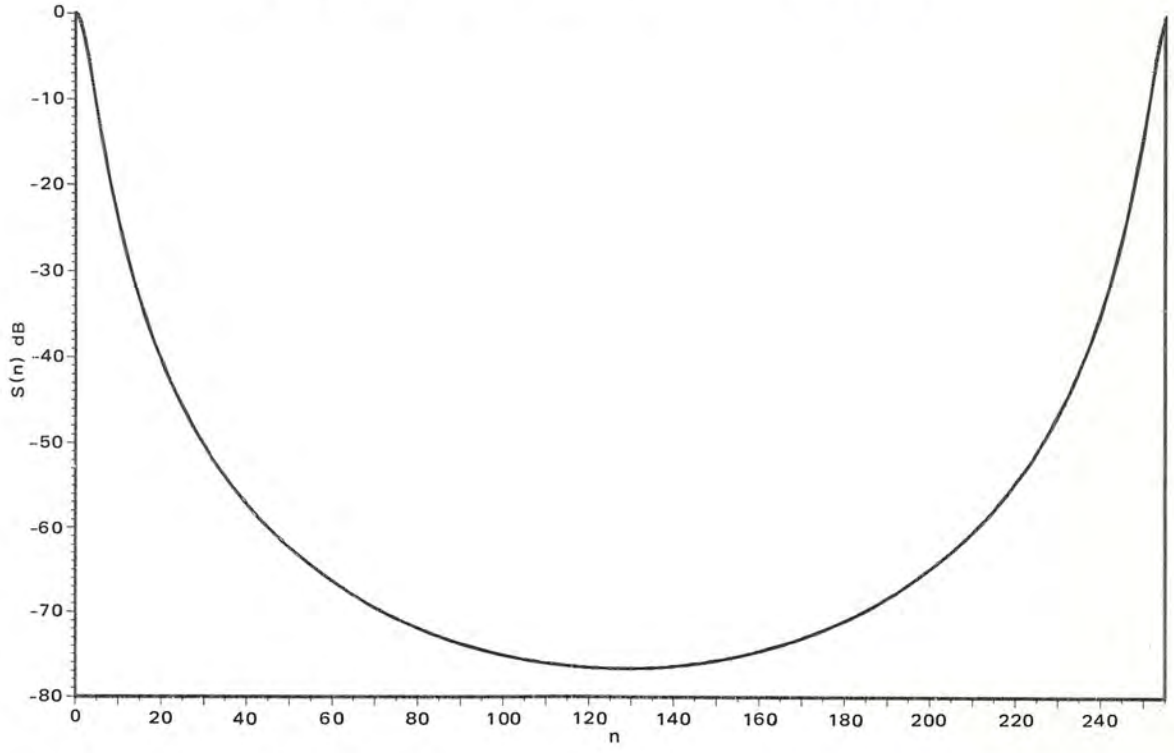

Figure 7.3–12. Normalized Power Spectrum of Shape Class 4

7.4 AN ANALYTIC UPPER BOUND ON CLASSIFICATION PERFORMANCE

The asymptotic properties of the extended ML estimator and its estimates which were established in Section 5.4 will be used in this section to derive a tight analytic upper bound on the probability of correct classification. First, the asymptotic probability density function of the extended ML estimates will be derived. The asymptotically optimal classifier will then be derived from this probability density function using Bayesian decision theory. The decision boundaries between the shape classes are then determined from the asymptotically optimal classifier. The upper bound on the probability of correct classification is then expressed in terms of the regions defined by these decision boundaries and the asymptotic probability density function of the estimates.

Let $\vec{a}_i$ denote the CAR descriptors which specify the shape class C_i, then, from Section 5.4, it is known that the extended ML estimates computed from sample boundary sequences belonging to shape class C_i are asymptotically Gaussian distributed about $\vec{a}_i$. The lower bound on the covariance of these estimates is given by the Cramer-Rao lower bound Σ_{a_i} which was derived in Section 5.4. Since the extended ML estimates are asymptotically efficient, the covariance matrix of the extended ML estimates is asymptotically equal to the Cramer-Rao lower bound Σ_{a_i}. The asymptotic probability density function $p_i(\hat{a})$ of the extended ML estimates $\hat{a}$ of shape class C_i is therefore completely specified, as given below.

$$p_i(\hat{a}) = \frac{1}{(2\pi)^{m/2} |\Sigma_{a_i}|^{1/2}} e^{-1/2 (\hat{a} - \vec{a}_i)^t \Sigma_{a_i}^{-1} (\hat{a} - \vec{a})} \tag{7.4-1}$$

The asymptotic minimum error rate classifier can be derived from the above probability density function using Bayesian decision theory. This derivation was presented in Section 7.1 under the assumption that the extended ML estimates were Gaussian distributed. The result was a set of discriminant functions which depend upon the mean and covariance of the estimates. The same results would be obtained if (7.4-1) were used, except that the mean and covariance would be $\vec{a}_i$ and Σ_{a_i} respectively. These discriminant functions, specifying the asymptotically optimal classifier, are given below.

$$g_i(\hat{a}) = (\hat{a} - \vec{a}_i)^t \Sigma_{a_i}^{-1} (\hat{a} - \vec{a}_i) + \ln |\Sigma_{a_i}| \tag{7.4-2}$$

The corresponding classification rule is: assign $\hat{\vec{a}} \in C_i$ if

$$g_i(\hat{\vec{a}}) < g_j(\hat{\vec{a}}) \qquad \forall\, j \neq i. \tag{7.4-3}$$

The decision boundary between shape classes C_i and C_j is given by the solution of the following equation.

$$g_i(\hat{\vec{a}}) = g_j(\hat{\vec{a}}) \tag{7.4-4}$$

All of the points on one side of this boundary are assigned to shape class C_i, those on the other side are assigned to shape class C_j.

The probability of correct classification associated with the asymptotic distribution of the estimates and these discriminant functions is given below [36].

$$P\,(\text{correct}) = \sum_{i=1}^{N_c} \int_{R_i} p_i(\hat{\vec{a}})\, d\hat{\vec{a}} \tag{7.4-5}$$

The region R_i contains all of the points $\vec{a}$ in the feature space of the CAR descriptors which are assigned by the asymptotically optimal classifier to shape class C_i. This region is contained within the decision boundaries specified by 7.4–4 for all $j \neq i$. The number of shape classes being considered is N_c. Since the extended ML estimator of the CAR descriptors is asymptotically efficient, the use of the Cramer-Rao lower bound on the covariance of the estimates in specifying the probability density function and in the design of classifier results in (7.4–5) being a tight upper bound on the probability of correct classification.

The integrals in (7.4–5) were evaluated using the covariance matrices computed from the Cramer-Rao lower bound in Section 6.1 for the four shape classes without obscuration. The resulting upper bound on the probability of correct classification for each shape class was 99%. This is in good agreement with the experimental results attained in Section 7.2. This bound may also be evaluated when obscuration is present.

This bound is useful since it may be evaluated without performing a classification experiment which requires a database of sample boundary sequences for each shape class. Since the definition of the obscuring process was general enough to include segmentation errors, the parameters of the obscuring process may be used to

characterize the performance of the segmentor. The performance of the segmentor is partially dependent upon the characteristics of the scene (e.g., contrast) and the sensor (e.g., resolution, SNR, etc.). If, for example, the relationship between the SNR of the sensor and the model parameters of the obscuring process is established, then the probability of correct classification can be studied as a function of sensor SNR. This bound on classification accuracy therefore provides a useful analysis technique for performing system engineering tradeoff studies for the design of machine perception systems.

8.0 SUMMARY AND CONCLUSIONS

A technique has been derived and demonstrated for machine perception of partially specified planar shapes. The recognition of shapes from their complete boundary sequences was considered first and the results were then extended to include partially specified boundaries. The boundaries were modeled as CAR processes. A new set of shape descriptors were defined from the coefficients of this model. They were named CAR descriptors. The CAR descriptors were shown to preserve class shape information and to be insensitive to within class variations. The probability density function of the boundary process was determined from its CAR model. This density function and a sample sequence of the boundary process were used to derive the negative log-likelihood function of the CAR descriptors. The ML estimates of the CAR descriptors were obtained by numerically minimizing the negative log-likelihood function. Several iterative algorithms for function minimization were presented and discussed. The LS estimator of the CAR descriptors was derived to provide the initial values of the CAR descriptors required by the function minimization algorithm. An estimator for the model parameter β was also developed which could be updated at each iteration of the minimization algorithm.

The ML estimator of the CAR descriptors was then extended to include the case where the observed sample boundary sequence is only partially specified. The observed boundary process was expressed as the product of the complete boundary process and a binary valued (0, 1) obscuring process. The obscuring process can be used to model both obscurations and segmentation errors. The form of the negative log-likelihood function was retained. The observed sample boundary sequence was substituted for the complete one and the eigenvalues were rederived using a statistical model of the obscuring process. This derivation was based upon the asymptotic stationarity of the observed boundary process. The resulting extended negative log-likelihood function contained both the CAR model of the boundary and the statistical model of the obscuring process. The extended ML estimates were obtained using the same minimization algorithm previously used. The LS estimates used to initialize the algorithms were computed from linearly interpolated sample boundary sequences. The asymptotic properties of the extended ML estimator were established. An

approximation to the extended ML estimator was developed which can be used when the statistics of the obscuring process are unknown.

The extended ML estimator was demonstrated on both synthetic data and real aircraft boundaries containing varying amounts of obscuration. The synthetic boundary data tested the extended ML estimator under ideal conditions and good results were obtained. The use of real aircraft boundaries resulted in an imperfect fit of the CAR model and *all* parameters were estimated from the observed boundary sequence. These results were equally as good and demonstrated the insensitivity of the CAR descriptors to within class variations.

A Bayesian classifier was derived from the asymptotic Gaussian distribution of the extended ML estimates. The resulting discriminant functions were trained on four synthetic shape classes. The experimental classification results were compared to the results obtained by using the LS estimates computed from linearly interpolated boundaries. Analysis of these results established a link between classification performance and the stationarity of the boundary being classified. The extended ML estimates produced good results for all four of the shape classes, but the amount of obscuration which could be tolerated decreased as the stationarity of the boundary process decreased. The LS estimates performed well only on the two most stationary shape classes. The classification performance of the extended ML estimates was then demonstrated on the real aircraft boundaries. In this experiment all parameters were *unknown* and had to be estimated from the observed boundary sequence. A classification accuracy of 91% was observed with 30% obscuration of the boundary.

The asymptotic properties of the extended ML estimator and its estimates were used to derive a tight analytic upper bound on the probability of correct classification. This bound depends only upon the CAR descriptors which represent the shape classes and the model parameters of the obscuring process. Since the obscuring process is general enough to model segmentation errors, the effects of these errors on the probability of classification can be studied analytically without the need to perform repeated classification experiments.

During the derivation of the statistics of the CAR process, the CAR model was analyzed as an all pole linear filter. A one-to-one onto mapping was established

between the points in the m dimensional feature space of the CAR descriptors and the set of poles in the complex plane which represent the CAR model. This mapping was used as a tool for viewing the relative locations of the shape classes. The stationarity of the CAR processes was determined by the location of the poles relative to the unit circle. This tool was called a CAR diagram and was used to analyze the experimental results previously discussed.

8.1 RELATED FUTURE RESEARCH TOPICS

The insensitivity of the CAR descriptors to within class variations may be exploited in the recognition of three-dimensional shapes. Small rotations out of the image plane generally produce only minor changes in the boundary. The expected insensitivity of the CAR descriptors to these changes will reduce the number of perspectives which must be considered for each shape class.

The development of the extended ML estimator of the CAR descriptors presented here could also be done for the Fourier descriptors and possibly the method of moments. The key step in extending the ML estimator of the CAR descriptors was the use of an asymptotically stationary model of the observed boundary process. Consequently, this model should be retained.

It would also be of interest to develop the relationships between the characteristics of a segmentor and the model of the obscuring process. The obscuring process could also be allowed to assume values other than zero or one. Most of the results presented here easily extend to that case.

REFERENCES

[1] L. Zusne, Visual Perception of Form. New York: Academic Press, 1970.

[2] A. Oosterlink, et al., "Evaluation of different profile description and decomposition methods for banded chromosomes," Proc. 3rd Int. Joint Conf. on Pattern Recognition, pp. 334–338, Nov. 1976.

[3] H. Wechsler and J. Sklansky, "Finding the rib cage in chest radiographs," Pattern Recognition, vol. 9, pp. 21–30, Jan. 1977.

[4] A. Ambler, et al., "A versatile system for computer controlled assembly," Artificial Intelligence, vol. 6, pp. 129–156, 1975.

[5] C. Rosen et al., "Exploratory research in advanced automation," Stanford Res. Inst., Tech. Rep. Aug. 1984.

[6] S.A. Dudani, et al., "Aircraft identification by moment invariants," IEEE Trans. Comput., vol. C–26, pp. 39–46, Jan. 1977.

[7] T. Pavlidis, "A review of algorithms for shape analysis," Comput. Graphics and Image Processing, vol. 7, pp. 243–258, 1978.

[8] M.K. Hu, "Visual pattern recognition by moment invariants," IEEE Trans. Inform. Theory, vol. 8, pp. 179–187, Feb. 1962.

[9] G.H. Granlund, "Fourier preprocessing for hand print character recognition," IEEE Trans. Comput., vol. C–21, pp. 195–201, Feb. 1972.

[10] C.T. Zahn and R.Z. Roskies, "Fourier descriptors for plane closed curves," IEEE Trans. Comput., vol. C–21, pp. 269–281, Mar. 1972.

[11] E. Persoon and K.S. Fu, "Shape discrimination using Fourier descriptors," IEEE Trans. Syst., Man and Cybern., vol. SMC–7, pp. 170–179, Mar. 1977.

[12] J.H. Munson, "Experiments in the recognition of handprinted text: Part I—Character recognition," 1968 Fall Joint Comput. Conf. AFIPS Conf. Proc., vol. 33, pp. 1125–1138, 1968.

[13] C.W. Richard, Jr. and H. Hemami, "Identification of three dimensional objects using Fourier descriptors of the boundary curve," IEEE Trans. Syst., Man and Cybern., vol. SMC–4, pp. 371–378, July 1974.

[14] T.P. Wallace and O.R. Mitchell, "Local and global shape description of two-and three-dimensional objects," Purdue Univ., School of Elec. Engr., TR–EE 79–43, Sept. 1977.

[15] T. Grogan, "Shape recognition and description: A comparative study," Purdue Univ., School of Elec. Engr., Ph.D. dissertation, 1983.

[16] K.S. Fu, Syntactic Methods in Pattern Recognition. New York: Academic Press, 1974.

[17] T. Pavlidis and F. Ali, "A hierarchical syntactic shape analyzer," IEEE Trans. Pattern Anal. Machine Intell., vol. PAMI-1, pp. 2-9, Jan. 1979.

[18] K.C. You and K.S. Fu, "A syntactic approach to shape recognition using attributed grammars," IEEE Trans. Syst., Man and Cybern., vol. SMC-9, pp. 334-345, June 1979.

[19] W.H. Tsai and K.S. Fu, "Attributed grammar—A tool for combining syntactic and statistical approaches to pattern recognition," IEEE Trans. Syst., Man and Cybern., vol. SMC-10, pp. 873-885, Dec. 1980.

[20] L.S. Davis, "Shape matching using relaxation techniques," IEEE Trans. Pattern Anal. Machine Intell., vol. PAMI-1, pp. 60-72, Jan. 1979.

[21] B. Bhanu and O.D. Faugeras, "Shape matching of two-dimensional objects," IEEE Trans. Pattern Anal. Machine Intell., vol. PAMI-6, pp. 137-156, Mar. 1984.

[22] H. Freeman, "On the encoding of arbitrary geometric configurations," IRE Trans. Elec. Comput., vol. EC-10, pp. 260-268, June 1961.

[23] A.V. Oppenheim and R.W. Schafer, Digital Signal Processing. New Jersey: Prentice-Hall, 1975.

[24] R.L. Kashyap and R. Chellappa, "Stochastic models for closed boundary analysis: representation and reconstruction," IEEE Trans. Inform. Theory, vol. IT-27, pp. 627-637 Sept. 1981.

[25] R.L. Kashyap and M.C. Mittal, "Recognition of spoken words and phrases in multitalker environment using syntactic methods," IEEE Trans. Comput., vol. 27, pp. 442-451, May 1978.

[26] A. Papoulis, Probability, Random Variables, and Stochastic Processes. New York: McGraw-Hill, 1965.

[27] R.M. Gray, "Toeplitz and circulant matrices: a review," Stanfort Elec. Lab., Tech. Rep. No. 6502-1, June 1971.

[28] N.E. Nahi, Estimation Theory and Applications. New York: R.E. Krieger, 1976.

[29] M.S. Bazaraa and C.M. Shetty, Nonlinear Programming Theory and Algorithms. New York: John Wiley and Sons, 1979.

[30] W.C. Davidon, "Variable metric method for minimization," AEC Res. Dev. Rep., ANL-5990, 1959.

[31] R. Fletcher and M. Powell, "A rapidly convergent decent method for minimization," Comput. Journal, vol. 6, pp. 163-168, 1963.

[32] W. Dunsmuir and P.M. Robinson, "Parametric estimators for stationary time series with missing observations," Adv. Appl. Prob., vol. 13, pp 129-146, 1981.

[33] E. Parzen, "On spectral analysis with missing observations and amplitude modulation," Sankhya: Series A, vol. 25, pp 383-292, 1963.

[34] A. Papoulis, Signal Analysis. New York: McGraw-Hill, 1977.

[35] P.F. Singer and R. Chellappa, "Classification of boundaries on the plane using stochastic models," Proc. Comput. Vision and Pattern Recognition 1983, pp. 146-147, June 1983.

[36] R.O. Duda and P.E. Hart, Pattern Classification and Scene Analysis. New York: John Wiley and Sons, 1973.

APPENDIX A. THE GRADIENT OF THE NEGATIVE LOG–LIKELIHOOD FUNCTION

$$\left(\vec{\nabla}_a \bar{L}(\vec{a})\right)_i = \frac{1}{\lambda_0}\frac{\partial\lambda_0}{\partial a_i} + \sum_{n=1}^{N-1}\left(1 - \frac{|P_\rho(n)|^2}{N}\frac{1}{\lambda_n}\right)\frac{1}{\lambda_n}\frac{\partial\lambda_n}{\partial a_i}$$

$$\frac{\partial\lambda_n}{\partial a_i} = p^2\beta\frac{\partial}{\partial a_i}|H(n)|^2 + pq\left[\alpha^2\frac{\partial}{\partial a_i}|H(0)|^2 + \frac{\beta}{N}\sum_{k=0}^{N-1}\frac{\partial}{\partial a_i}|H(k)|^2\right]$$

$$\frac{\partial}{\partial a_i}|H(n)|^2 = 2\,\mathrm{Re}\left\{H(n)\frac{\partial H^*(n)}{\partial a_i}\right\}$$

$$\frac{\partial H(n)}{\partial a_i} = H^2(n)\,e^{-j2\pi/N\,ni}$$

$$H(n) = \frac{1}{1 - \sum_{k=1}^{m} a_k\,e^{-j2\pi/N\,nk}}$$

APPENDIX B. THE HESSIAN OF THE NEGATIVE LOG–LIKELIHOOD FUNCTION

$$\left(H(\vec{a})\right)_{ij} = \frac{\partial^2 L^-(\vec{a})}{\partial a_i\, \partial a_j} = \frac{\partial}{\partial a_j}\left(\frac{\partial L^-(\vec{a})}{\partial a_i}\right) = \frac{\partial}{\partial a_j}\left(\vec{\nabla}_a L^-(\vec{a})\right)_i$$

$$= \frac{1}{\lambda_0}\frac{\partial^2 \lambda_0}{\partial a_i\, \partial a_j} - \frac{1}{\lambda_0^2}\frac{\partial \lambda_0}{\partial a_i}\frac{\partial \lambda_0}{\partial a_j} + \sum_{n=1}^{N-1}\left(1 - \frac{|P_\rho(n)|^2}{N}\frac{1}{\lambda_n}\right)\frac{1}{\lambda_n}\frac{\partial^2 \lambda_n}{\partial a_i \partial a_j}$$

$$- \left(1 - 2\frac{|P_\rho(n)|^2}{N}\frac{1}{\lambda_n}\right)\frac{1}{\lambda_n^2}\frac{\partial \lambda_n}{\partial a_i}\frac{\partial \lambda_n}{\partial a_j}$$

$$\frac{\partial^2 \lambda_n}{\partial a_i\, \partial a_j} = p^2\beta\frac{\partial^2}{\partial a_i\, \partial a_j}|H(n)|^2 + pq\left[\alpha^2\frac{\partial^2}{\partial a_i\, \partial a_j}|H(0)|^2 + \frac{\beta}{N}\sum_{k=0}^{N-1}\frac{\partial^2}{\partial a_i\, \partial a_j}|H(k)|^2\right]$$

$$\frac{\partial^2}{\partial a_i\, \partial a_j}|H(n)|^2 = 2\,\mathrm{Re}\left\{\frac{\partial H(n)}{\partial a_i}\frac{\partial H^*(n)}{\partial a_j}\right\} + 2\,\mathrm{Re}\left\{H(n)\frac{\partial^2 H^*(n)}{\partial a_i\, \partial a_j}\right\}$$

$$\frac{\partial^2}{\partial a_i\, \partial a_j}H(n) = 2\,H^3(n)\,e^{-j\,2\pi/N\,n\,(i\,+\,j)}$$